INEEL/EXT-04-01760

Development of New Geothermal Wellbore Holdup Correlations Using Flowing Well Data

Sabodh K. Garg
John W. Pritchett
James H. Alexander

March 2004

Idaho National Engineering and Environmental Laboratory
Bechtel BWXT Idaho, LLC

INEEL/EXT-04-01760

Development of New Geothermal Wellbore Holdup Correlations Using Flowing Well Data

Sabodh K. Garg
John W. Pritchett
James H. Alexander

March 2004

Science Application International Corporation
San Diego, California 92121

Prepared for the
U.S. Department of Energy
Office of Energy Efficiency and Renewable Energy
Under DOE Idaho Operations Office
Contract DE-AC07-99ID13727

TABLE OF CONTENTS

Section **Page**

LIST OF FIGURES

Figure **Page**

Figure **Page**

Figure **Page**

Figure **Page**

Figure **Page**

Figure **Page**

Figure **Page**

Figure **Page**

Figure **Page**

LIST OF TABLES

Table **Page**

1 INTRODUCTION

An ability to predict both the quantity of fluid that can be produced and its thermodynamic state (pressure, temperature, enthalpy, gas content, salinity, *etc*.) is essential for estimating the total usable energy of a geothermal resource. Numerical reservoir simulators can be utilized to calculate the thermodynamic state of the fluid at the underground feed-zone(s) at which the fluid enters the wellbore. The computation of the well-head fluid properties from a given underground state (or vice-versa) requires the use of a wellbore simulator.

The fluid flow in the wellbore is not amenable to strict analytical treatment. Depending upon the relative amounts of gas and liquid, a variety of flow patterns can occur in the pipe. At small gas loadings, bubble flow takes place. An increase in gas flow rate can result in slug, churn or annular flow. Existing methods for treating two-phase flow in a wellbore require use of empirical correlations for friction factor and for liquid hold-up.

Because of slip between the gas and liquid phases, the flowing gas quality Q_f is generally different from the *in situ* gas quality Q_s. The liquid hold-up correlation provides a relationship between Q_f and Q_s. Almost all of the existing holdup correlations (see *e.g.*, Ansari *et al*., 1994; Aziz *et al*., 1972; Beggs and Brill, 1973; Duns and Ros, 1963; Hagedorn and Brown, 1965; Hadgu, 1989; Hughmark, 1962; Hughmark and Pressburg, 1961; Orkiszewski, 1967) are based on flow in two-phase petroleum (oil and gas) systems. At present, there does not exist a sufficient basis for selecting one or another of these correlations to simulate two-phase flow in geothermal wellbores. Utilization of different correlations very often yields widely differing results (see *e.g.*, Finger, *et al*., 1999).

Recent availability of high quality downhole pressure/temperature/spinner logs from flowing geothermal wells suggests that it may be worthwhile to take a fresh look at the empirical correlations for liquid hold-up. The present research effort is designed to develop new hold-up correlations for geothermal applications using data from flowing geothermal wells. To support this research work, Unocal has agreed to release proprietary downhole logs and other required data from 42 wells. Data sets are also available from flowing wells from several Japanese geothermal fields; these data sets were previously supplied to SAIC (previously Maxwell Technologies) by various Japanese developers as part of a DOE/Sandia funded research program. In addition, Caithness has supplied data for one well. Because of programmatic reasons, this research effort is divided in to several phases.

During FY 2001, SAIC was asked by Bechtel to (1) evaluate the available well data for completeness and internal consistency, and (2) identify high quality well data for use in developing new correlations. As a result of a detailed examination of well data made available by Unocal and various Japanese developers, SAIC identified (see Garg and Pritchett, 2001) over 30 wells with high quality discharge (mass discharge rate and enthalpy)

and downhole pressure and temperature data. The data set encompasses a wide range of discharge enthalpies (*i.e.*, moderate enthalpy wells producing from liquid feedzones, and wells with enthalpies approaching the enthalpy of saturated steam), and casing diameters (ID's ranging from 100 mm to 384 mm). As far as fluid composition is concerned, the data set leaves something to be desired. The salinity and non-condensable gas content of most of the wells in the data set are less than 1.5% and 1% (mass fraction of the produced fluid), respectively. In any event, the present data set is eminently suitable for developing a new empirical liquid hold-up correlation for geothermal wells.

In FY 2002, Bechtel asked SAIC to use the above-mentioned well data to devise new liquid hold-up correlations for geothermal wells. To make the problem tractable, a two-stage research program was devised. During the first stage (FY 2002 and 2003), a new correlation was developed that is restricted to the cased section of geothermal wells. Obviously, the fluid flow in the cased section is much simpler than in the open hole or in the slotted/blank liner section. With the exception of the work by Hadgu (1989), all of the published papers treat two-phase flow in a pipe (*i.e.*, the cased section). The well data will be used in a second stage (FY 2004) to formulate a separate holdup correlation for the open hole/slotted liner section of geothermal wells.

The present report describes the work performed by SAIC during FY 2002 and FY 2003. Our methodology for developing a hold-up correlation is outlined in Section 2. The downhole pressure/temperature profiles were simulated using an existing wellbore code with an adjustable hold-up correlation. The results of these simulations were employed to generate a multi-parameter (flowing quality, static quality, flowing gas volume fraction, gas and liquid densities, gas and liquid viscosities *etc*.) data set. The latter data are used in Section 3 to relate flowing gas quality to other parameters. Finally, in Section 4, future work (FY 2004 and beyond) is described.

2 MATHEMATICAL MODELING OF FLUID FLOW IN GEOTHERMAL WELLS

2.1 GENERAL APPROACH

The pressure drop associated with two-phase fluid transport in a geothermal well represents the combined effects of friction, acceleration, and the loss of elevation. While the pressure drop due to acceleration is usually small in single-phase liquid flow in a pipe, it is very often the most important component in two-phase flow. The fluid flow in a geothermal well is not amenable to strict analytical treatment. For two-phase flow, it is necessary to supplement mass, momentum and energy balance relations by empirical correlations for (1) friction factor, and (2) liquid hold-up. In the following, a wellbore simulator, incorporating an existing friction factor correlation and an adjustable liquid hold-up correlation, is used to match the downhole pressure profiles in flowing wells. The simulation results are employed to generate a multi-parameter (flowing quality, static quality, *in situ* liquid and gas volume fractions, gas and liquid viscosities, *etc*.) data set. The data set forms the basis for the development of a new liquid hold-up correlation (Section 3).

2.2 SIMULATION OF FLUID FLOW

The downhole pressure (and temperature) profiles in the cased portion of flowing wells (see Garg and Pritchett, 2001, for a critical appraisal of the data set) have been simulated using a specially modified version (see below) of the wellbore computer simulation program WELBOR (Pritchett, 1985). The WELBOR code treats the steady flow of liquid water and steam up a borehole. The user provides parameters describing the well geometry (inside diameter and angle of deviation with respect to the vertical along the hole length), a stable formation temperature distribution with depth, and an "effective thermal conductivity" as a function of depth representing the effects of conductive heat transfer between the fluid in the wellbore and the surrounding formation. For boreholes with two-phase flow at the bottom of the cased portion, the fluid state is prescribed by specifying flowing pressure, flowing enthalpy, salinity, and gas content.

In two-phase water/steam flow, pressure and temperature are not independent of each other. For any reasonable value of effective thermal conductivity κ, the downhole flowing enthalpy may be adjusted to yield the appropriate pressure, and hence temperature, distribution in the wellbore, and flowing wellhead enthalpy. Matching the pressure/ temperature distribution in the wellbore and flowing wellhead enthalpy does not constrain the heat loss and downhole (*e.g.*, at the bottom of the cased section) enthalpy. Since the flowing downhole enthalpy is not a measured quantity, it is not possible to determine a unique value for heat loss in the presence of two-phase flow. It is, therefore, appropriate to eliminate

effective thermal conductivity as a free parameter, and use a constant value for κ. Except for slimhole KE1-4 (see below), κ was assumed to be 4 W/m-^{o}C.

In WELBOR, the frictional pressure gradient is computed using the Dukler I (or Dukler II) correlation (Dukler *et al*., 1964), and a user prescribed roughness factor, ε. The Dukler II correlation gives a much larger pressure drop than the Dukler I correlation. Numerical experiments (Garg and Combs, 2002; also present study) have shown that it is usually necessary to use the Dukler I correlation in order to match the reported discharge rate and enthalpy data from geothermal boreholes. It was, therefore, decided to use the Dukler I correlation (see Appendix A for a description of Dukler I correlation) for the present study. The roughness factor, ε, may vary with depth. For most of the pressure profiles considered herein, the roughness factor was assumed to be zero. In a few cases, it was found necessary to use a non-zero value for ε.

The relative slip between the liquid and gas phases is treated in WELBOR using a modified version of the Hughmark liquid holdup correlation (Hughmark, 1962). The slippage rate may vary between the value given by the Hughmark correlation and no slip at all, according to the value of a user specified parameter, η, which varies between zero (no slip) and unity (Hughmark). For the present application, the WELBOR code was modified to allow η to vary as a function of depth. For all of the pressure profiles considered herein, it was found that at most two values of η (and a small transition zone in between) were required to produce a satisfactory match between the measured and computed pressures.

Given the fluid state (pressure, enthalpy, salinity, gas content) at the bottom of the cased interval and the mass discharge rate, a wellbore simulator such as WELBOR can be used to compute the fluid state along the wellbore and at the wellhead. The principal parameters that may be varied to match the measured conditions along the wellbore (pressure and temperature) and at the wellhead (pressure, temperature, steam and liquid flow rates, liquid salinity, gas content of steam) are (1) flowing enthalpy, salinity and gas content at the bottom of the cased interval, (2) holdup parameter, η, and (3) interior roughness factor, ε.

2.3 AN EXAMPLE

To illustrate the computational procedure, it is useful to consider Unocal well A-4 (Garg and Pritchett, 2001). Well A-4 is cased and cemented to a depth of 888.5 mTVD (901.6 mMD). The following well geometry is assumed for the cased section of well A-1:

Measured Depth (meters)	Vertical Depth (meters)	Angle with Vertical (Degrees)	Internal Diameter (mm)
0–277.4	0–277.4	0.000	384
277.4–901.6	277.4–888.5	14.068	315

The measured pressures in the flowing well are in good agreement with the saturation pressure for pure water corresponding to the measured temperatures (Garg and Pritchett, 2001). A pressure of ~23.49 bars (taken as the average of measured and saturation pressures)

was recorded in the flowing well at 888.5 mTVD. The reported discharge rate and wellhead enthalpy were 135 (±3) kg/s and 1089 (±12) kJ/kg, respectively. Total dissolved solids content of the separated liquid was 14600 (±150) ppm; the non-condensable gas content of the steam was 0.68 (±0.1) %.

The stable formation temperature (Garg and Pritchett, 2001) was approximated by the following temperature distribution using linear interpolations between tabulated data.

Vertical Depth (meters)	Temperature (Degrees Celsius)
0	27
305	68
754	212
888.5	227

The best match to the downhole pressure profile and wellhead fluid state (pressure, enthalpy, salinity, gas content) was obtained using the following values for the unknown model parameters:

Flowing enthalpy at 888.5 mTVD = 1102 kJ/kg
Fluid (liquid + steam) salinity at 888.5 mTVD = 0.012 kg/kg
Fluid (liquid + steam) gas content at 888.5 mTVD = 0.0011 kg/kg
Hughmark parameter, η = 0.09 for depths < 350 m
= 0.09 + 0.0062 (depth – 350) for 350 m < depth < 400 m
= 0.40 for depths > 400 m
Roughness factor, ε = 0.00 mm for all depths

The computed pressure profile is compared with the measurements in Figure 2.1; the agreement is excellent. The computed fluid state at the wellhead (fluid enthalpy: 1089 kJ/kg, liquid phase salinity: 14,300 ppm; steam phase gas content: 0.67 %) is very close to the measurements.

2.4 SIMULATION RESULTS

An essentially identical procedure was used to fit the downhole pressure and wellhead fluid state measurements for all of the wells in the dataset. Parameters used to match downhole pressure and temperature profiles are given in Appendix B. The computed pressure profiles are compared with the measurements in Appendix C; the agreement is very good in most cases.

The data for the Unocal wells (A-, B- and C- wells, and presumably the single Caithness well) were obtained while these wells were discharging in a more or less stable manner. Available data for these wells include the NCG and salt content of the discharge

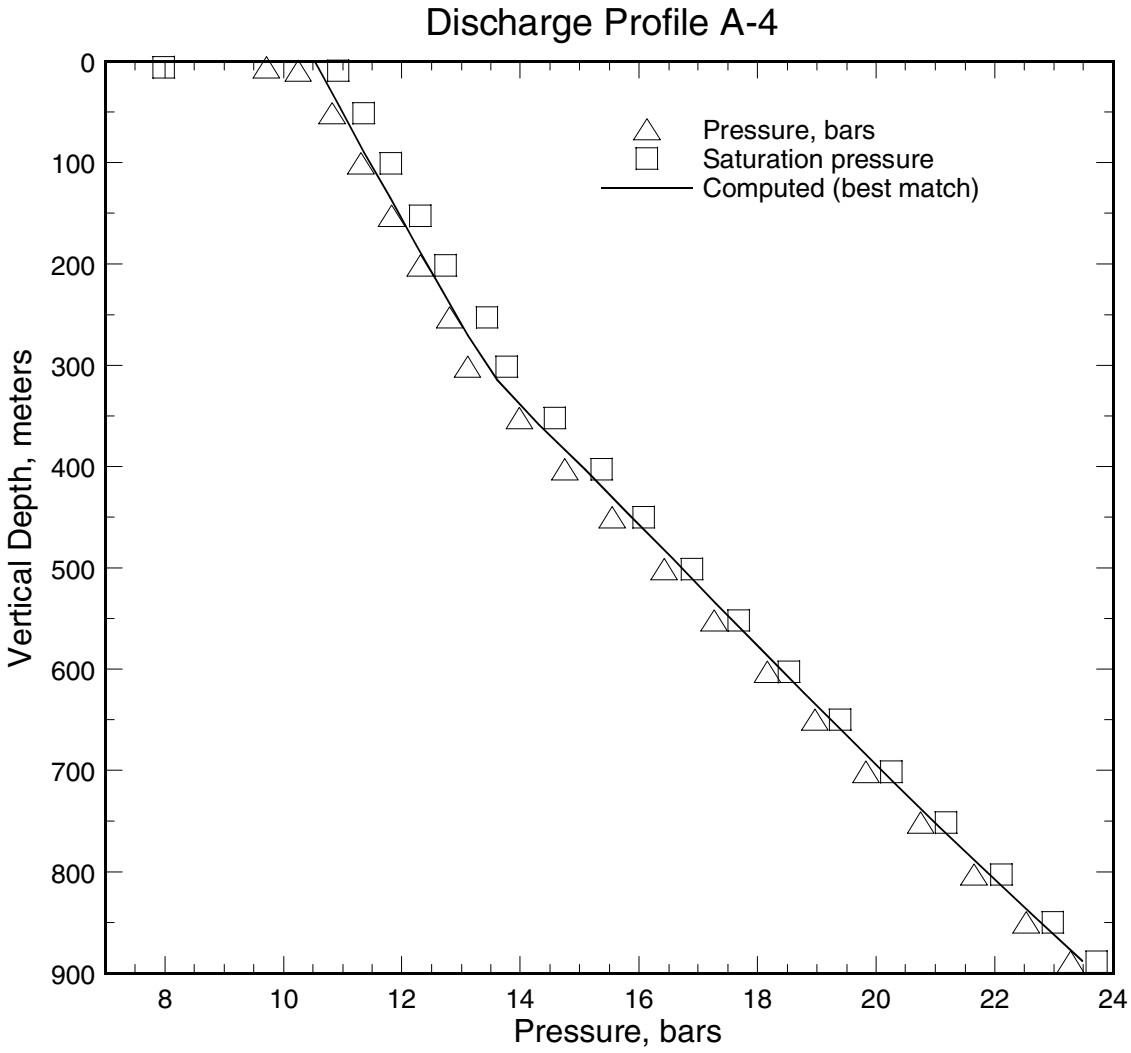

Figure 2.1. Pressure profile (triangle) recorded in discharging well A-4. The square indicates saturation pressure corresponding to local measured temperature. The solid line is the computed pressure profile.

stream in addition to an estimate of the error bounds for the discharge rate and wellhead enthalpy. By way of contrast, data for the Japanese wells (KE-, GH- and S- wells) were obtained during short term (from a few hours to a few days duration) discharge tests. No NCG and salinity measurements are available for the production fluid from these short term tests. Also, discharge rate and wellhead enthalpy measurements from the short term tests may not be very accurate; these errors are likely to be most problematical for wells with very low discharge rates (*e.g.*, KE1-4, KE1-9, KE1-11, S-2). To simulate the pressure profiles in KE1-4, an unusually low value for effective thermal conductivity had to be assumed. For well KE1-17, an unrealistically large value for the roughness factor was required to match the deeper part of the pressure profile; it is likely that the quoted discharge rate and wellhead enthalpy measurements for KE1-17 are in error. Although flow data for the Japanese wells in the dataset are liable to be less accurate than for the Unocal wells, it was decided to retain these data, since the Japanese well test data are typical of measurements taken during the exploration phase.

The results of these downhole pressure/temperature simulations (Appendices B and C) were used to define the fluid state and associated quantities (*e.g.*, liquid and gas velocities) in the cased section of all the wells in the dataset. Somewhat arbitrarily, it was decided to use 21 equally spaced points along each downhole profile to create a dataset (see Table 2.1 for an example) for formulating a new holdup correlation (Section 3).

Table 2.1. Flow parameters computed from a simulation of downhole pressure profile in well A-4 (see Figure 2.1). Row 1 (Row 21) corresponds to parameter values at the bottom (wellhead) of the simulated depth interval (Figure 2.1).

Flow Parameter (K)	Reynolds Number (Rn)	Froude Number (Fr)	Flowing Liquid Volume Fraction (Y_l)	Weber Number (We)	*In situ* Liquid Fraction (S_l)
0.944111E+00	0.154495E+08	0.402794E+02	0.124374E+00	0.138119E+05	0.173310E+00
0.944493E+00	0.158112E+08	0.442975E+02	0.115473E+00	0.144626E+05	0.164570E+00
0.944852E+00	0.161676E+08	0.486497E+02	0.107140E+00	0.151282E+05	0.156380E+00
0.945192E+00	0.165138E+08	0.532888E+02	0.994595E-01	0.157775E+05	0.148820E+00
0.945516E+00	0.168505E+08	0.582344E+02	0.923534E-01	0.164078E+05	0.141810E+00
0.945830E+00	0.171789E+08	0.635153E+02	0.857512E-01	0.170178E+05	0.135280E+00
0.946131E+00	0.174988E+08	0.691445E+02	0.796074E-01	0.176007E+05	0.129190E+00
0.946426E+00	0.178126E+08	0.751785E+02	0.738508E-01	0.181595E+05	0.123470E+00
0.946718E+00	0.181208E+08	0.816566E+02	0.684406E-01	0.186901E+05	0.118080E+00
0.947008E+00	0.184246E+08	0.886351E+02	0.633322E-01	0.191899E+05	0.112970E+00
0.947311E+00	0.187274E+08	0.962285E+02	0.584727E-01	0.196650E+05	0.108080E+00
0.947616E+00	0.190281E+08	0.104482E+03	0.538469E-01	0.201019E+05	0.103410E+00
0.969907E+00	0.213201E+08	0.175823E+03	0.492332E-01	0.316548E+05	0.778400E-01
0.976431E+00	0.223711E+08	0.225820E+03	0.453655E-01	0.382388E+05	0.678600E-01
0.972831E+00	0.182476E+08	0.806953E+02	0.426301E-01	0.197942E+05	0.686400E-01
0.974626E+00	0.186066E+08	0.899448E+02	0.403659E-01	0.211497E+05	0.647200E-01
0.976312E+00	0.189660E+08	0.100327E+03	0.382072E-01	0.226018E+05	0.609900E-01
0.977900E+00	0.193271E+08	0.112038E+03	0.361422E-01	0.241644E+05	0.574400E-01
0.979401E+00	0.196910E+08	0.125317E+03	0.341603E-01	0.258538E+05	0.540600E-01
0.980824E+00	0.200590E+08	0.140464E+03	0.322522E-01	0.276894E+05	0.508100E-01
0.982176E+00	0.204325E+08	0.157861E+03	0.304089E-01	0.296955E+05	0.476900E-01

3 DEVELOPMENT OF A HOLDUP CORRELATION

3.1 INTRODUCTION

Duns and Ros (1963) suggest that the various flow regimes that accompany two-phase flow in wells can be divided into three main regions depending on the gas throughput (Figure 3.1). The axes in Figure 3.1 denote the non-dimensional liquid and gas velocity numbers:

$$\text{Liquid velocity number, } N_l = S_l v_l \left(\frac{\rho_l g}{\sigma} \right)^{0.25}$$

$$\text{Gas velocity number, } N_g = S_g v_g \left(\frac{\rho_g g}{\sigma} \right)^{0.25}$$

Here $v_l (v_g)$ is the liquid (gas) velocity, $S_l (S_g)$ is the *in situ* liquid (gas) volume fraction, $\rho_l (\rho_g)$ is the liquid (gas) density, g is the acceleration due to gravity, and σ is the surface tension. Region I has a continuous liquid phase, and contains the bubble flow, plug flow and part of the froth-flow regimes. Liquid and gas phases alternate in region II covering the slug flow and the remainder of the froth-flow regimes. Region III is characterized by a continuous gas phase, and contains the mist-flow regime.

Data from two-phase geothermal wells (see Section 2) are shown as diamonds in Figure 3.1. Although the geothermal data lie in all the three regions, the bulk of these data are contained in Region II. It appears from Figure 3.1 that relatively high liquid velocities characterize geothermal wells such that only froth-flow (regions I and II) and mist-flow (region III) are encountered in geothermal wells. Once the geothermal fluid starts flashing in the wellbore, the gas (and hence liquid) velocity increases rapidly. Thus, bubble flow, plug flow and slug flow regimes, if present at all, are likely to be confined to a narrow depth range and difficult to observe. Because of the limited range of flow regimes, it should be possible to describe two-phase flow in geothermal wells by a single (or at most a two-part) holdup correlation.

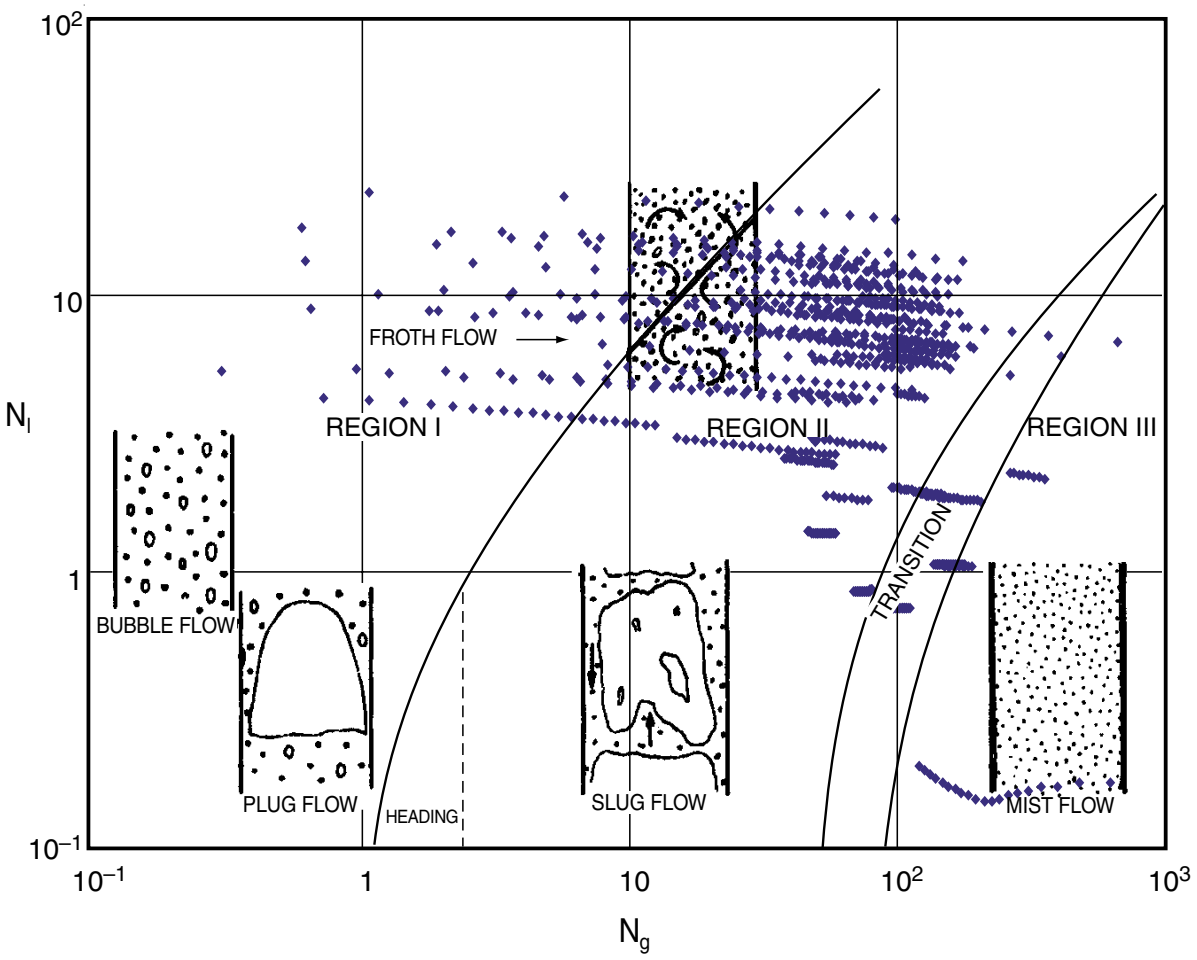

Figure 3.1. Two-phase fluid flow regimes according to Duns and Ros (1963). Also shown (as blue diamonds) are the data from geothermal boreholes (see Section 2).

3.2 HOLDUP CORRELATION PARAMETERS

The flowing quality Q_f (=gas flow rate/total flow rate) is defined as follows:

$$Q_f = \frac{AS_g\rho_g v_g}{M} \tag{3.1}$$

where A is the internal cross-sectional area of the pipe, and M is the total mass flow rate. Assuming a power law relationship for the velocity and *in situ* gas volume fraction, Bankoff (1960) derived a relation for flowing quality Q_f that is equivalent to:

$$Q_f = \frac{Q_s}{[1-Q_s]K + Q_s\left[1-\rho_l(1-K)/\rho_g\right]} \tag{3.2}$$

where Q_s *is* the *in situ* (or static) quality, ρ_m is the mixture (gas plus liquid) density, and K is a flow parameter (see below).

$$Q_s = \frac{S_g\rho_g}{\rho_m} \tag{3.3}$$

$$\rho_m = S_l\rho_l + S_g\rho_g \tag{3.4}$$

For the case of homogeneous (*i.e.*, no slip) flow, the *in situ* quality Q_s is equal to the flowing quality Q_f; furthermore, the flow parameter K is identically equal to unity. In general, one would expect the gas phase to rise more rapidly in the well than the liquid phase due to buoyancy; this implies that

$$Q_f \geq Q_s \tag{3.5a}$$

$$S_g \leq K \leq 1 \tag{3.5b}$$

The two-phase flow in a well is influenced by buoyancy, inertial, viscous and surface tension forces (Bankoff, 1960). Based on dimensional arguments, Hughmark (1962) concluded that the flow parameter K might be expected to depend on the flowing liquid volume fraction Y_l, and Reynolds (*Rn*), Froude (*Fr*), and Weber (*We*) numbers.

$$Y_l = \frac{S_l v_l}{\left(S_l v_l + S_g v_g\right)}$$
$$Rn = \frac{d_w M}{A\mu_m}$$
$$Fr = \frac{M^2}{\left(d_w A^2 g \rho_m^2\right)}$$
$$We = \frac{d_w^2 g \rho_g Fr}{\sigma} \qquad (3.6a–d)$$

Here d_w is the inside well diameter, σ is the liquid surface tension, and μ_m is the mixture viscosity.

$$\mu_m = S_l \mu_l + S_g \mu_g \qquad (3.7)$$

In Equation (3.7), μ_l (μ_g) denotes the liquid (gas) viscosity.

Mixture (liquid plus gas) density ρ_m and mixture viscosity μ_m can be defined in a number of ways (see *e.g.* Hughmark, 1962; Dukler, *et al.*, 1964); in the following, the expressions given by Hughmark, Equations (3.4) and (3.7), will be used. These definitions for ρ_m and μ_m are different than those used by Dukler, *et al.* (1964; see Appendix A). In a preliminary investigation (Garg *et al.*, 2003), the authors formulated a holdup correlation using Dukler *et al.*'s definitions for ρ_m and μ_m. Subsequent numerical experiments showed that the latter correlation constitutes a highly implicit and non-linear relation for flow parameter *K*, and a solution is not possible in many cases. It was therefore decided to adopt Hughmark's definitions for ρ_m and μ_m which result in a better-behaved relation for *K*.

3.3 HOLDUP CORRELATION

To find a correlation for *K*, it is assumed that *K* can be expressed as a function of a single variable *Z*:

$$K = K(Z(Rn, Fr, Y_l, We, S_l)) \qquad (3.8)$$

Hughmark (1962) investigated the dependence of *Z* on Rn, Fr, Y_l, and We, and found that *Z* (and hence *K*) did not appreciably depend on the Weber number (We). The authors have independently confirmed this result using data for geothermal wells (Section 2). Consequently, *Z* is assumed to depend on only four variables, *i.e.*, Rn, Fr, Y_l and S_l; note that Hughmark (1962) did not account for the dependence of *Z* on S_l. Following Hughmark (1962), we introduce a particularly simple relationship for *Z*:

$$Z = Rn^{\alpha} Fr^{\beta} Y_l^{\gamma} S_l^{\omega} \qquad (3.9)$$

where α,β,γ, and ω are as yet undetermined constants. Determination of the exponents in Equation (3.9) is straightforward when the functional relationship between K and Z is known; in this case, exponents can be estimated by minimizing the variance between the calculated (*i.e.*, from the functional relationship K-Z) and measured (*i.e.*, those derived from fitting the flow data) values for K. Unfortunately, the functional relationship $K(Z)$ is unknown, and must be determined from the dataset.

To determine the exponents in Equation (3.9), we introduce a nonparametric measure of variation. Given a candidate set of exponents, we calculate Z for each point in the dataset for geothermal wells (Section 2, and Figure 3.1). Next, we sort the dataset in order of increasing Z, and calculate a pseudo-variance $S.V.$ as follows:

$$S.V. = \sum_{i=1}^{n-1} (K_{i+1} - K_i)^2 \tag{3.10}$$

Here K_i denotes the value of K corresponding to Z_i, n is the number of points in the dataset, and Z_n is the largest value of Z. The exponents in Equation (3.9) are obtained by minimizing this pseudo-variance.

Since a set of exponents may be multiplied by an arbitrary non-zero constant without changing the order of the sequence of K's, only three (3) of the exponents need to be varied when minimizing the pseudo-variance. Note that very small changes in the exponents can leave the order of the sequence of K's unchanged and that when the order of the sequence is changed, the $S.V.$ jumps discontinuously. Such functional behavior rules out the use of gradient methods for finding a minimum. The *downhill simplex method* (Press, *et al.*, 1992) is a procedure for finding minima of multidimensional functions that does not make use of derivatives, making it well suited to the present effort. A set of exponents for starting the procedure was obtained by assuming that log (K) is a linear function of log (Z) (and hence of log Rn, log Fr, log Y_l, and log S_l), and using the least squares method to determine an initial set of coefficients (α,β,γ, and ω). The downhill simplex method finds smaller and smaller values for the $S.V.$ until a region is reached which appears to be a broad local minimum. Since there is no reason to believe that this procedure yields a global minimum, various other sets of starting exponents were tried. While the downhill simplex method failed for some starting sets, it worked for a number of others. The function $K(Z)$ was found to be monotonic in all cases, but with varying sign. By simply multiplying all the exponents in a set by –1, the order of the sequence of K's is inverted, giving the same $S.V.$ and a graph with a slope of the opposite sign.

Changing the sign of the various exponents as needed to ensure that the exponent of the flowing liquid volume fraction is negative, and plotting K versus Z, it was found that the graphs always looked like a hyperbola with $K = 1$ as an asymptote (see *e.g.* Figure 3.2). Although a hyperbola for $K(Z)$ can be made to yield a pseudo-variance that is close to the minimum, a more general functional form for $K(Z)$ is needed in order to improve the fit in regions of Z that make little contribution to the pseudo-variance.

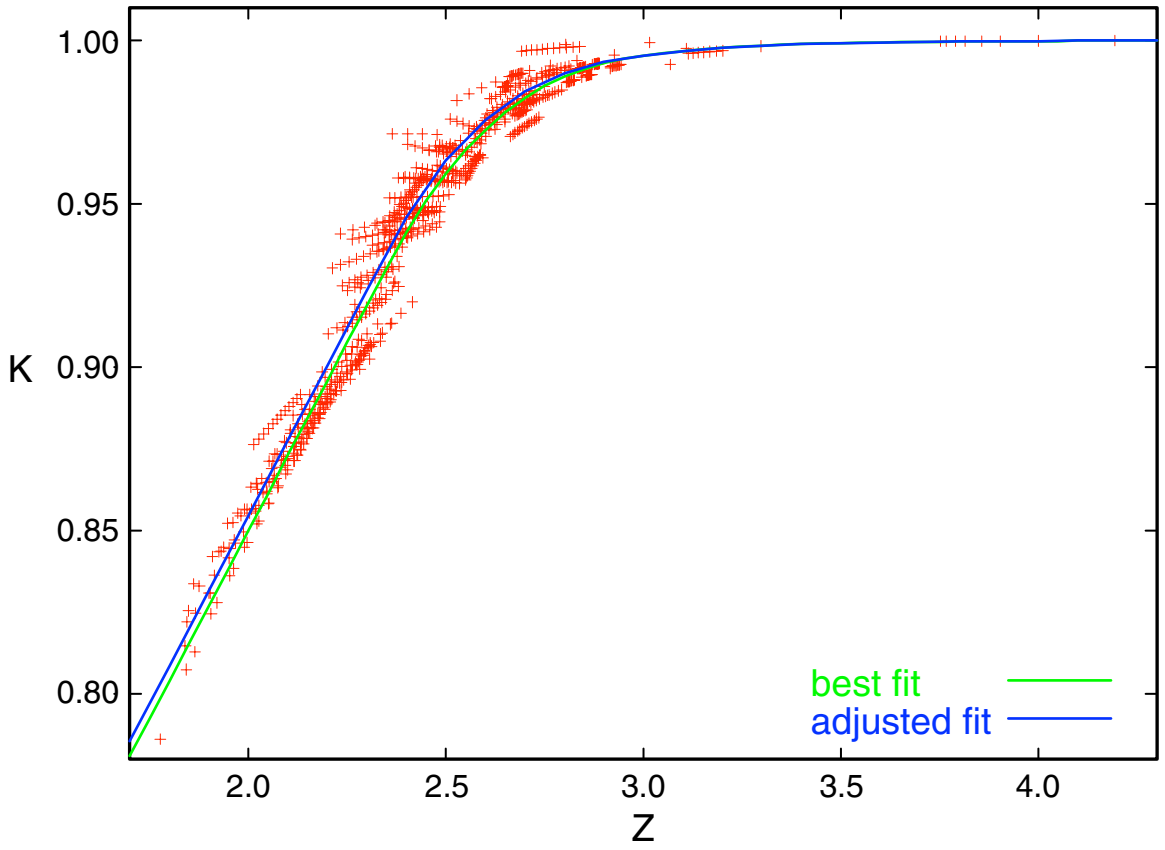

Figure 3.2. **A plot of *K* versus *Z*. Data points (+), *i.e.*, *K* versus *Z* values, in the figure were obtained by minimizing the pseudo-variance. *Z* is defined by Equation (3.9) with $\alpha = 0.0388887$, $\beta = 0.0065170$, $\gamma = -0.0002960$, and $\omega = -0.1$. The green line denotes the best fit to the *K*-*Z* data. The blue line was obtained by making slight modifications to the green line (see text).**

3.4 VALIDATION OF HOLDUP CORRELATION

To verify that the holdup correlation (*i.e.*, $K(Z)$ relationship) developed in the preceding section can be used to simulate two-phase flow in geothermal wells, a special version of WELBOR code was created; this version was configured to use the $K(Z)$ relation (green line) shown in Figure 3.2. The latter version of WELBOR was employed to simulate flow data for all the wells in the dataset. Except for the holdup correlation, these simulations utilized the parameters (Appendix B) used in the calculations described in Section 2.

The computed results for wellhead pressure for all the high mass velocity (mass velocity = total discharge rate / pipe cross-sectional area > 687 kg/s-m^2; the low mass velocity profiles are considered separately in Section 3.5) profiles are compared with data (*i.e.*, wellhead pressures computed by matching downhole pressure profiles in Section 2) in Table 3.1. The computed wellhead pressures using the best-fit relation for $K(Z)$ were found (on average) to be a little on the low side. The observation that the computed pressures are lower than the measured values suggests that the "best-fit" correlation for $K(Z)$ over-predicts the slip between the liquid and gas phases. Stated somewhat differently, the correlation yields too low values for K. It was, therefore, decided to modify the correlation for $K(Z)$; the modified correlation is shown as the blue curve in Figure 3.2. The modified $K(Z)$ fit yields satisfactory agreement between data and computed wellhead pressures (Table 3.1); the root-mean-square error is only 0.67 bars.

It is apparent from Table 3.1 that the above-derived correlation for $K(Z)$ leads to choking for three pressure profiles (KE1-4a, KE1-4b, KE1-19Sa). Well KE1-4 is a slim hole (internal diameter = 10.2 cm), and the downhole profiles were recorded during a short-term discharge test. As remarked in Section 2, the nominal discharge rates for KE1-4 (7.08 kg/s on November 12, 1983, and 8.44 kg/s on November 13, 1983) may be in substantial error. The modified $K(Z)$ fit implies that the maximum discharge rate for KE1-4 is around 6.9 kg/s, which is within the likely error band for the nominal discharge rate for KE1-4. For KE1-19Sa, the computed value for the maximum discharge rate (23.0 kg/s) is within 4% of the nominal discharge rate (23.9 kg/s). Thus, it can be concluded that the modified $K(Z)$ fit gives acceptable results for these three profiles as well.

As mentioned above, downhole pressure profiles for all the high mass velocity cases in the dataset (Table 3.1) were simulated using the modified correlation for $K(Z)$. The latter computed profiles are compared with (1) measurements, and (2) calculated profile (best-match) using an adjustable holdup correlation (Section 2). In most cases, the agreement is quite good (see Appendix C). A typical example (well A-4) is shown in Figure 3.3; the computed pressure profile for well A-4, shown as a dashed line in Figure 3.3, is in excellent agreement with the measurements.

Table 3.1. Comparison of wellhead pressures for high mass velocity profiles (mass velocity > 687 kg/s-m^2) computed using (1) best fit correlation for $K(Z)$, and (2) modified correlation for $K(Z)$ with data.

Well	*P*-data	*P*-comp (best fit)	*P*-comp (modified fit)	δ*P****
A-1	8.94	9.14	9.51	–0.57
A-2	8.78	8.83	9.22	–0.44
A-4	10.53	10.35	10.75	–0.22
A-6	14.70	14.74	15.15	–0.45
A-7	12.85	10.81	11.23	1.62
A-8	9.75	9.17	9.66	0.09
A-9	14.56	13.75	14.17	0.39
A-10	11.39	10.17	10.59	0.80
A-11	11.16	11.36	11.79	–0.63
A-12	12.14	11.72	12.12	0.02
A-13	12.18	11.42	11.79	0.39
A-14	10.98	10.44	10.86	0.12
A-16	10.36	10.39	10.89	–0.53
A-19	9.61	9.16	9.59	0.02
A-20	10.12	9.81	10.26	–0.14
A-21	10.52	9.31	9.77	0.75
B-5	10.97	9.64	10.26	0.71
C-6	9.55	6.81	7.68	1.87
KE1-4a	4.26	Choke @ 26.0 m	Choke @ 3.7m*	NA
KE1-4b	3.98	Choke @ 108.1 m	Choke @ 88.9m	NA
KE1-17a	6.64	6.67	7.11	–0.47
KE1-19Sa	3.53	Choke @ 30.3 m	Choke @7.6m**	NA
KE1-19Sb	6.37	6.18	6.61	–0.24
KE1-22b	7.37	7.79	8.15	–0.78
GH-11a	12.23	11.90	12.12	0.11
GH-11b	10.51	9.79	10.10	0.41
GH-20a	14.14	14.37	14.56	–0.42
GH-20b	13.02	13.38	13.59	–0.57
GH-20c	11.70	12.19	12.43	–0.73
			Total (26 profiles)	1.11

* At 6.9 kg/s, p = 2.31 bars; 6.8 kg/s, p = 2.66 bars; 6.5 kg/s, p = 3.28 bars

** At 23.0 kg/s, p = 3.66 bars.

*** δ*P* = *P*-data – *P*-comp (modified fit)

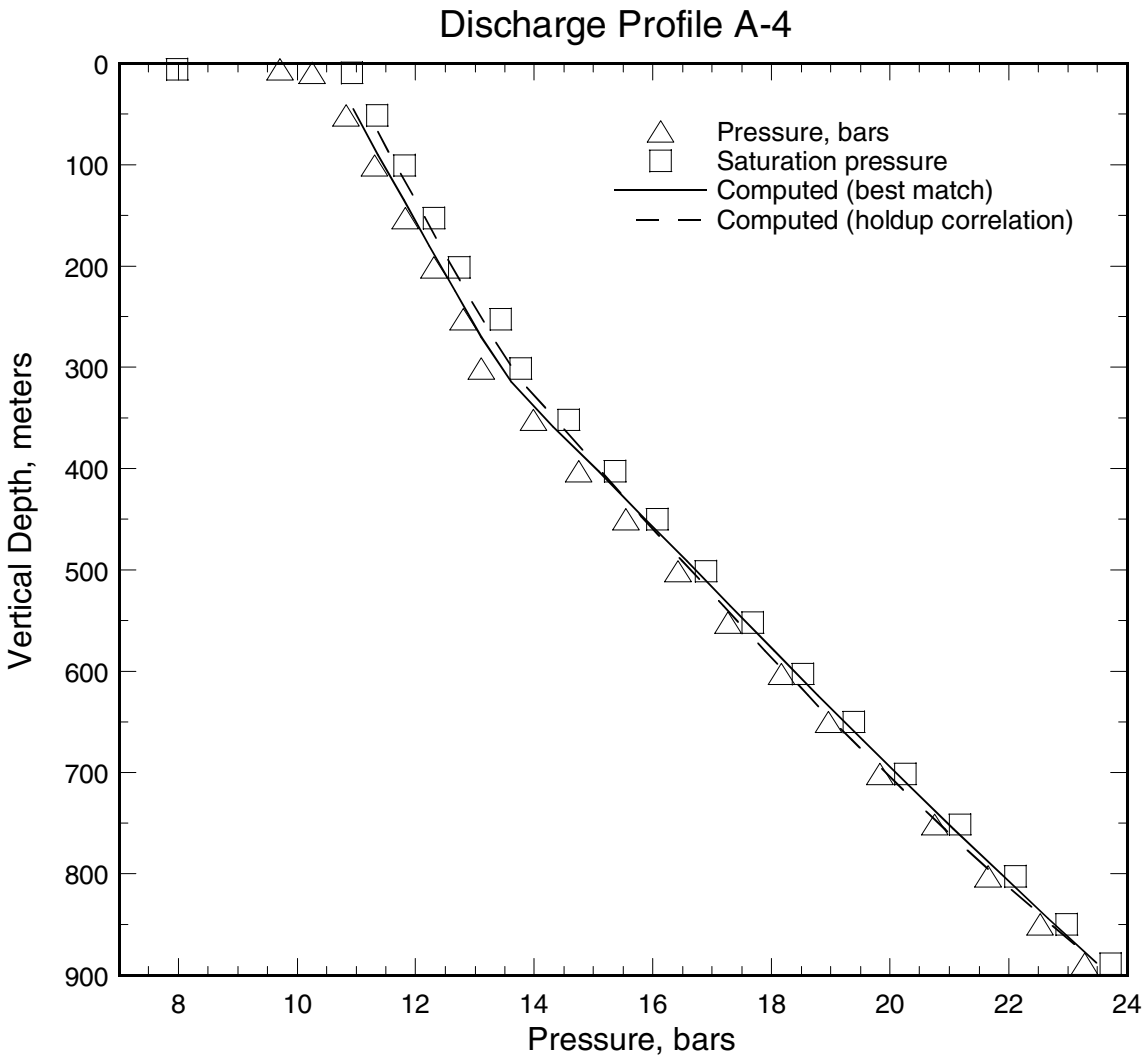

Figure 3.3. Pressure profile (triangle) recorded in discharging well A-4. The square indicates saturation pressure corresponding to the local measured temperature. The solid line is the computed pressure profile using an adjustable holdup correlation (see Section 2 for details). The computed pressure profile using the modified correlation for $K(Z)$ is shown as a dashed line.

3.5 HOLDUP CORRELATION FOR LOW MASS VELOCITY

The modified correlation was found to yield satisfactory results for all the high mass velocity (mass velocity > 687 kg/s-m^2) profiles in the dataset. The computed pressures for low mass velocity (mass velocity < 650 kg/s-m^2) profiles are, however, too high, and imply that the correlation for $K(Z)$ would need to further modified for low mass velocity. Attempts to develop a single correlation for both the high and low mass velocity cases by including an additional variable (*i.e.*, mass velocity) in the relation for Z (Equation 3.9) were unsuccessful. Accordingly, it was decided to consider the low mass velocity profiles separately. The $K(Z)$ correlation for the latter case is shown in Figure 3.4. To minimize the deviation between data and the computed wellhead pressures, it was found necessary to slightly adjust the best-fit correlation (see Figure 3.4).

The computed results for wellhead pressure for all the low mass velocity (mass velocity = total discharge rate / pipe cross-sectional area < 650 kg/s-m^2.) profiles are compared with data (*i.e.*, wellhead pressures computed by matching downhole pressure profiles in Section 2) in Table 3.2. The computed wellhead pressures using the best-fit relation for K (green line, Figure 3.4) were found (on average) to be a little on the low side. The modified $K(Z)$ fit (blue line, Figure 3.4), however, yields satisfactory agreement between data and computed wellhead pressures (Table 3.2); the root-mean-square error is 0.73 bars.

As for the high mass velocity cases, the downhole pressure profiles for all the low mass velocity cases in the dataset (Table 3.2) were simulated using the modified correlation for K (blue line, Figure 3.4). The latter computed profiles are compared with (1) measurements, and (2) calculated profile (best-match) using an adjustable holdup correlation (Section 2). In most cases, the agreement is good (see Appendix C).

3.6 COMPARISON WITH SPINNER DATA

The rotational speed of a spinner is proportional to the mass-averaged velocity of the fluid mixture passing through the spinner. Except for annular flow, the mass-averaged velocity indicated by the spinner should correspond closely to the mass-averaged velocity of the entire flow stream (Gang, *et al*., 1990). The spinner response f is related to mass-averaged fluid velocity v_m and cable speed v_c as follows:

$$f = m(v_m - v_c) + c \tag{3.11}$$

where m and c are the calibration constants. Note that the spinner does not rotate for a small range of relative fluid velocities, $v_m - v_c$, in either the upward or the downward logging direction. The smallest value of $|v_m - v_c|$ at which spinner rotation begins is called the threshold velocity v_{th}.

$$v_{th} = -\frac{c}{m} \tag{3.12}$$

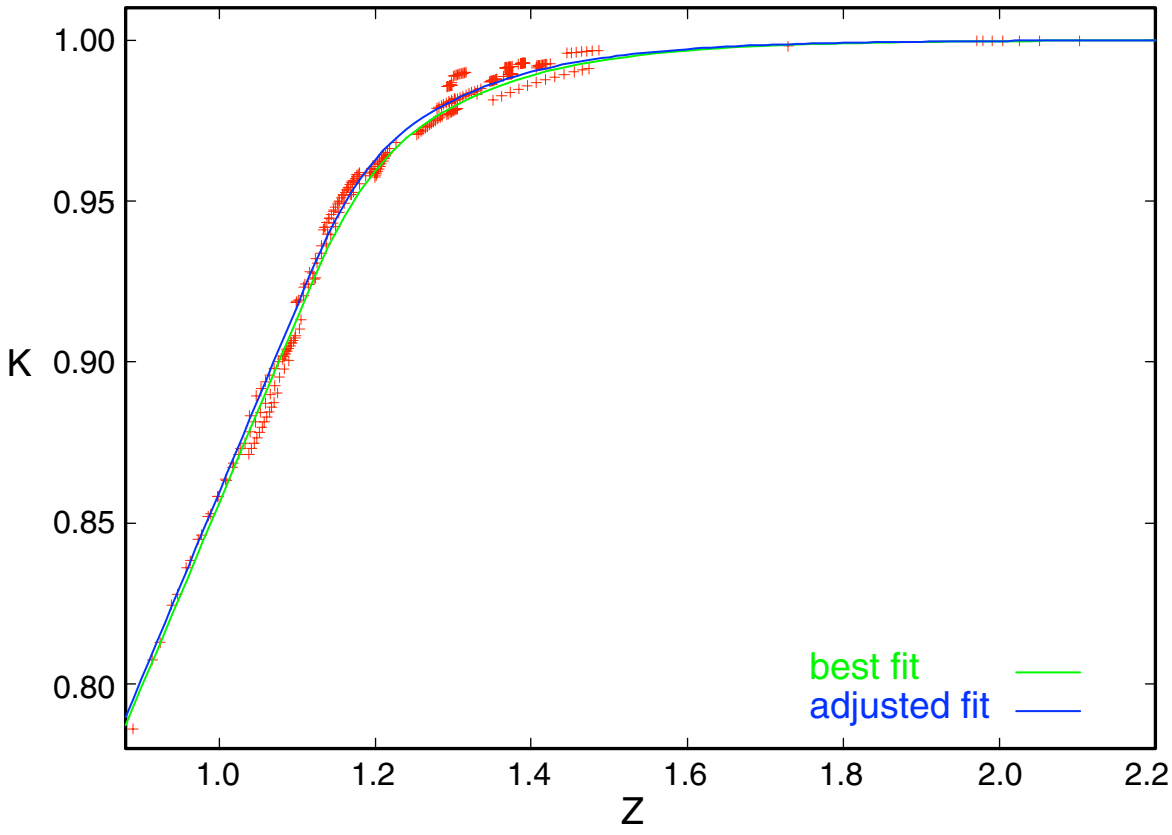

Figure 3.4. **A plot of *K* versus *Z* for low mass velocity (mass velocity < 650 kg/s-m^2) profiles. Data points (+), *i.e.*, *K* versus *Z* values, in the figure were obtained by minimizing the pseudo-variance. *Z* is defined by Equation (3.9) with α = –0.009546812, β = 0.00975959, γ = –0.000149868, and ω = –0.1.The green line denotes the best fit to the *K*-*Z* data. The blue line was obtained by making slight modifications to the green line (see text).**

Table 3.2. Comparison of wellhead pressures for low mass velocity profiles (mass velocity < 650 kg/s-m^2) computed using (1) best fit correlation for $K(Z)$, and (2) modified correlation for $K(Z)$ with data.

Well	P-data	P-comp (best fit)	P-comp (mod fit)	δP**
A-18	8.19	No Solution*	8.99	–0.80
C-1	10.35	9.89	10.35	0.00
C-2	11.58	11.41	11.69	–0.11
C-3	11.74	10.27	10.92	0.82
C-4	12.43	11.66	12.15	0.28
C-5	13.88	13.78	14.64	–0.76
B-3	16.27	16.04	16.70	–0.43
B-4	18.70	17.10	17.96	0.74
B-13	11.76	9.77	10.57	1.19
KE1-9	8.59	8.27	8.74	–0.15
KE1-11	18.66	17.10	17.29	1.37
KE1-17b	7.11	7.08	7.38	–0.27
KE1-22a	7.82	7.98	8.22	–0.40
S-2	1.15	2.45	2.50	–1.35
CS-1	3.97	3.31	4.06	–0.09
			Total (15 profiles)	0.04

** δP = P-data – P-comp (modified fit)

* No solution for discharge rate less than 45.1 kg/s. P-comp = 8.15 bar at 45.1 kg/s

The mass-averaged mixture velocity v_m can be computed from the *in situ* liquid and vapor saturations, densities, and velocities.

$$v_m = \frac{\left(\rho_l S_l v_l + \rho_g S_g v_g\right)}{\left(\rho_l S_l + \rho_g S_g\right)} \tag{3.13}$$

In geothermal wells, the liquid (*i.e.* water) density is much greater than the vapor (*i.e.* steam) density; this means that the mass-averaged mixture velocity is a strong function of the in situ liquid volume fraction S_l. Thus matching the spinner data can provide an independent check on the holdup correlations developed in Sections 3.3–3.5.

Comparison of spinner data with the computed fluid velocity requires a certain amount of care. Spinner data are often quite noisy in two-phase flow, and must be smoothed for a meaningful comparison. In this work, a rather simple procedure was adopted to smooth the spinner data. A running average of 11 (or 21 in the case of extremely noisy data) data points was used to compute the smoothed spinner response. Spinner surveys often display anomalous response (*e.g.* a decrease or no change in rotation rate as the spinner tool is traversed up or down the hole, or a less than commensurate change in rotation rate at a

discontinuous change in well diameter) due to improper centering of the tool in the well or a possible temporary flow obstruction in the spinner tool. Obviously, such spinner data must be discarded.

The smoothed spinner data for well A-4 are compared with the computed spinner response in Figure 3.5. The mass-averaged velocity was computed using the "high mass velocity" correlation developed in Section 3.4 (see also Figure 3.3 for a comparison of the computed pressure profile with the measurements). A least-squares procedure was employed to evaluate the calibration constants in Equation (3.11), and thereby relate the smoothed spinner response to the computed mass-averaged velocity. The spinner data for well A-4 (Figure 3.5) exhibit an anomalous response (decrease/no change in the rotation rate) in the depth range 0–150 m. As can be seen from Figure 3.5, except for the depth range 0–150 m, the smoothed spinner response shows a good agreement with the computed curve. Similar results for all the other wells with spinner data are displayed in Appendix D. Barring very few exceptions; the spinner measurements are in good agreement with the computed response (Appendix D and Table 3.3). Thus, taken as a whole, the spinner measurements tend to validate the holdup correlations developed in Sections 3.3–3.5.

3.7 FORTRAN SUBROUTINES

The holdup correlations described in Sections 3.3–3.5 have been incorporated into three Fortran subroutines (holdfk; hldfn1; hldfn2) listed in Appendix E Subroutine holdfk is designed to compute flow parameter K and its derivative with respect to the flowing quality Q_f; holdfk in turn calls subroutines hldfn1 (for mass velocities > 687 kg/s-m^2) and hldfn2 (for mass velocities < 650 kg/s-m^2). In the transition region (650 kg/s-m^2 < mass velocity < 687 kg/s-m^2), a linear interpolation is used to evaluate K and its derivative w.r.t. Q_f. The Fortran subroutines given in Appendix E may be used in conjunction with any wellbore simulator. The authors have included the latter subroutines in a special version of WELBOR code. To illustrate the use of the WELBOR code (including the holdup correlations developed herein) to simulate the downhole pressure/temperature surveys and the wellhead discharge data (*i.e.*, discharge rate versus wellhead pressure data), an example is given in the following subsection.

3.8 AN EXAMPLE

Slimhole SNLG87-29 (Finger *et al.*, 1999) is completed with a 4.5-inch casing (102 mm internal diameter) to a depth of 159.7 m; an open hole (99 mm internal diameter) completion is used below the latter depth. PTS surveys in the discharging borehole show that the principal feedzone is located at a depth of 248.4 m. Four (4) brief discharge tests were performed during August and September 1993. A pressure survey taken about an hour after the initiation of discharge on August 5, 1993 is shown in Figure 3.6. The saturation pressures corresponding to the temperature survey are also displayed in Figure 3.6. It is apparent from Figure 3.6 that liquid conditions prevail in the wellbore below a depth of ~100 meters. The

Continued on page 3-19

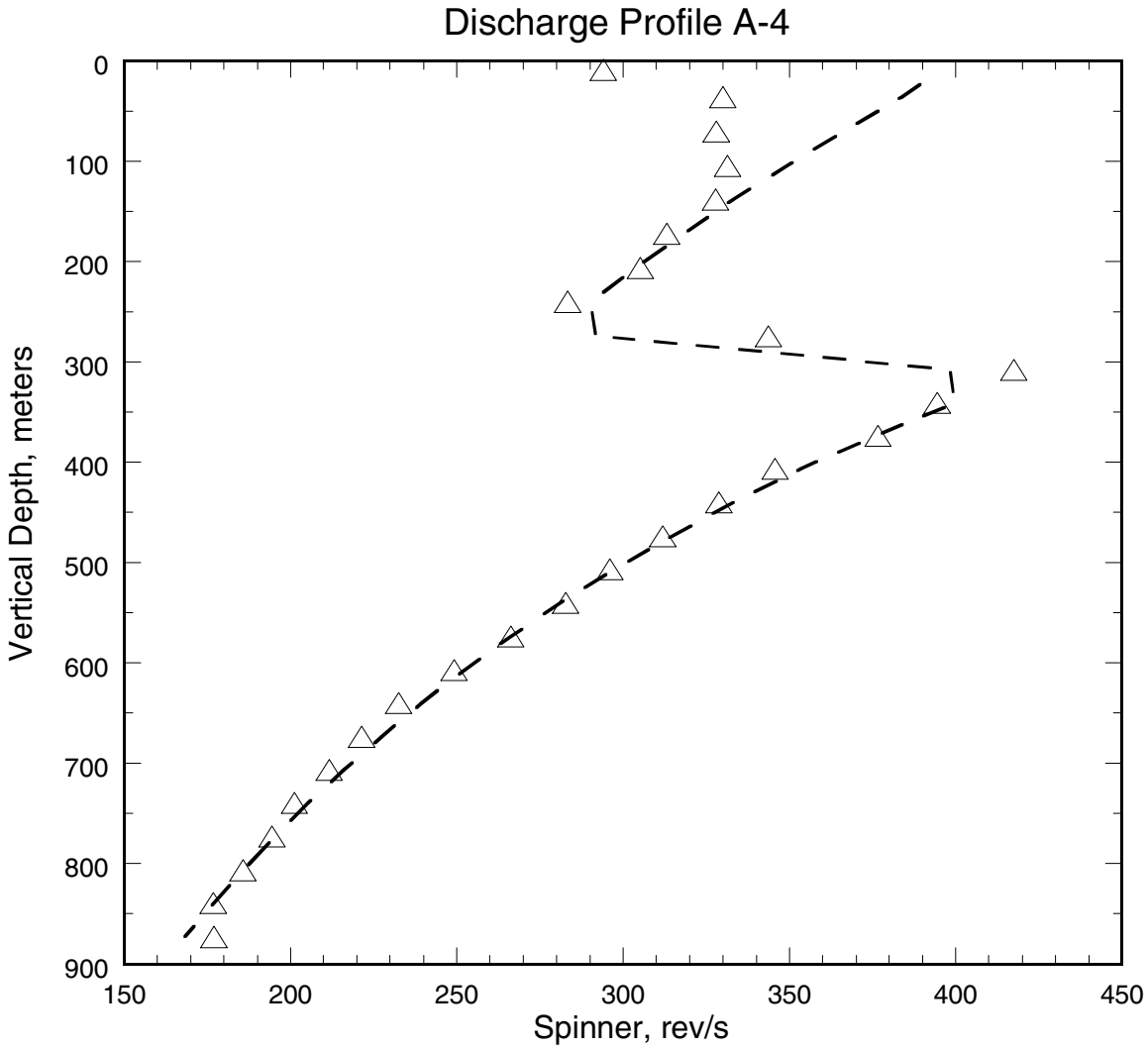

Figure 3.5. Comparison of the smoothed spinner response (triangles) with the computed spinner response (dashed line) for well A-4.

Table 3.3. Comparison of the smoothed spinner response with the computed response for wells in the dataset.

Well Name	Comments
A-1	Good fit
A-2	Good fit
A-4	Spinner data shows no change in spinner rotation rate in depth range 0–100m and is not reliable. Good fit to spinner data below 100 m.
A-6	Spinner data shows no change or decrease in rotation rate in depth range 0–200m and is not reliable. Good fit to spinner data below 200 m.
A-7	Spinner data shows no change in rotation rate in depth range 0–80 m. Good fit to spinner data below 80 m.
A-8	Spinner data shows no change in rotation rate in depth range 250–500 m. Good fit to other spinner data.
A-9	Spinner data unreliable in depth range 0–50 m. Good fit to spinner data below 50 m.
A-10	Good fit.
A-11	Spinner data shows a decrease in rotation rate in depth range 0–30m. Good fit to spinner data below 30 m.
A-12	Spinner data unreliable in depth range 0–10 m. Good fit to spinner data below 10 m.
A-13	Spinner data extremely noisy in depth range 360–430 m and below 970 m. Fair fit.
A-14	Spinner data unreliable in depth range 0–20 m. Good fit to spinner data below 20 m.
A-16	Good fit to spinner data in the upper large-diameter (384 mm) part of the well. Poor fit to spinner data in the 315 mm section.
A-18	Poor spinner data in depth range 0–100 m, and below 400 m (inconsistent change in rotation rate). Poor fit.
A-19	Good fit.
A-20	Good fit.
A-21	Spinner response anomalous in depth interval 450–520 m (no change in rotation rate). Fair fit to other spinner data.

Table 3.3. Comparison of the smoothed spinner response with the computed response for wells in the dataset (concl).

Well Name	Comments
B-3	Spinner response very noisy in 221 mm portion. Smoothed spinner data does not show much change in rotation rate between 221 mm and 315 mm sections. Good fit to spinner data in 315 mm section.
B-4	Good fit.
B-5	Spinner survey shows a reduction in gradient at ~500 m; no indication in corresponding pressure/temperature data. Good fit to spinner data above 500 m.
B-13	Spinner survey shows an offset at 500–600 m; no such indication in pressure/temperature data. Good fit to spinner data above 500 m.
C-1	Good fit.
C-2	Spinner data anomalous from 0–100 m and from 250–350 m. Good fit to other spinner data.
C-3	Good fit.
C-4	Spinner rotation rate anomalous (slow increase 0–300 m, fast increase 300–530 m, constant 530–650 m, fast increase below 650 m); no indication of such behavior in pressure/temperature data. Poor fit.
C-5	Spinner rotation rate anomalous below 400 m (fast increase 400–500 m, essentially constant 500–800 m); no indication of such behavior in pressure/temperature data. Good fit to spinner data above 400 m.
C-6	Spinner survey shows an increase in gradient at ~300 m; no such indication in pressure/temperature data. Good fit to spinner data below 300 m.
CS-1	Spinner data very noisy. Smoothed data show little variation in rotation rate below ~320 m; no such indication in pressure/temperature data. Good fit to data above 320 m.
GH-11	Spinner rotation rate shows a discontinuous jump at ~100 m. Good fit to spinner data below 100 m.

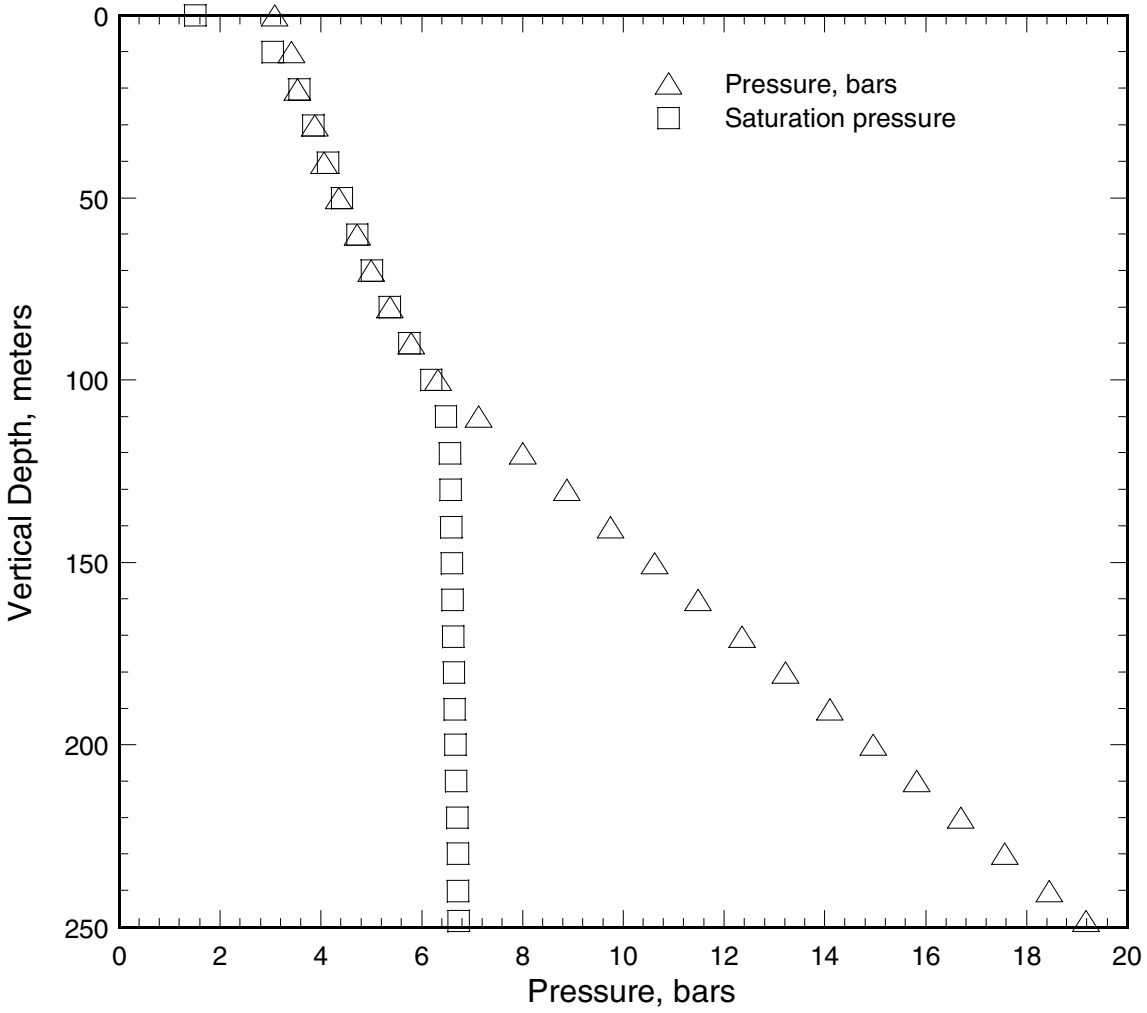

Figure 3.6. A pressure survey (triangle) recorded in slimhole SNLG87-29 on August 5, 1993. Also shown is the saturation pressure profile (square) corresponding to the temperature survey.

close agreement between the measured and saturation pressures over the depth interval 20 to 100 meters indicates that the downhole pressure/temperature data are consistent. Divergence between the measured and saturation pressures above 20 meters is believed to be due to a possible malfunctioning of the temperature gauge since the temperature (and hence saturation pressure) drop off above 20 meters observed on August 5, 1993 was not seen in any of the later temperature surveys. Based on downhole pressure measurements (Finger *et al.*, 1999), it can be concluded that the productivity index for SNLG87-29 is, for all practical purposes, infinite (> 400 kg/s-bar); this implies that the flowing feedzone pressure is essentially independent of the discharge rate.

To match the pressure and temperature profiles recorded on August 5, 1993, the following well geometry is assumed for slimhole SNLG87-29:

Measured Depth (meters)	Vertical Depth (meters)	Angle with Vertical (Degrees)	Internal Diameter (mm)
0–159.7	0–159.7	0.000	102
159.7–248.4	159.7–248.4	0.000	99

A pressure of ~19.18 bars was recorded in the flowing well at 248.4 mTVD; the corresponding temperature was 163.48^{o}C. The reported discharge rate was 7.1 kg/s. In the absence of data on the chemical composition of the produced fluids, the reservoir fluid is assumed to be pure water.

The stable formation temperature, as recorded in a downhole survey in the shut-in borehole, was approximated by the following temperature distribution using linear interpolations between tabulated data.

Vertical Depth (meters)	Temperature (Degrees Celsius)
0	22
25	76
100	149
200	162
250	163.5

To match the measured temperature distribution below 100 meters (*i.e.*, in the single phase liquid portion), it was found necessary to use a rather high value (30 W/m-^{o}C) for the effective thermal conductivity, *K*. This is really not surprising in that the temperature profile was taken about 1 hour after the initiation of discharge. Heat losses from the borehole to the formation are treated using a steady-flow model in the WELBOR code. The difficulty is that at early times, the steady-flow model is inappropriate, and the heat transfer is augmented. As remarked by Pritchett (1993), the transient case may be treated as a succession of states in which the effective thermal conductivity is a decreasing function of time, which reaches the steady-state value only at infinite time.

The computed pressure and temperature profiles are compared with the measurements in Figures 3.7 and 3.8, respectively. Simulated results (Figures 3.7 and 3.8) are shown for two different roughness factors:

(i) Roughness factor, ε = 0.000 mm for all depths

(ii) Roughness factor, ε = 0.125 mm for depths < 159.7 m

= 0.000 mm for depths > 159.7 m

It is apparent from Figures 3.7 and 3.8 that the pressure and temperature profiles computed using the smooth pipe assumption are indistinguishable from those for a rough pipe for depths greater than 80 meters. At shallower depths (depth < 80 m), a non-zero roughness factor is required to provide a good match between the measurements and the computed profiles.

The model parameters (effective thermal conductivity, roughness factor) inferred from a match to the downhole pressure and temperature surveys (Figures 3.7 and 3.8) were used to compute the characteristic curve (*i.e.*, mass discharge rate versus wellhead pressure) for SNLG87-29. The computed values are compared with the measurements in Figure 3.9; the agreement is very good. It is apparent from Figure 3.9 that the theoretical curve has a discontinuity in slope at about a discharge rate of 5 kg/s due to a change from the "low mass velocity" holdup correlation to the "high mass velocity" holdup correlation.

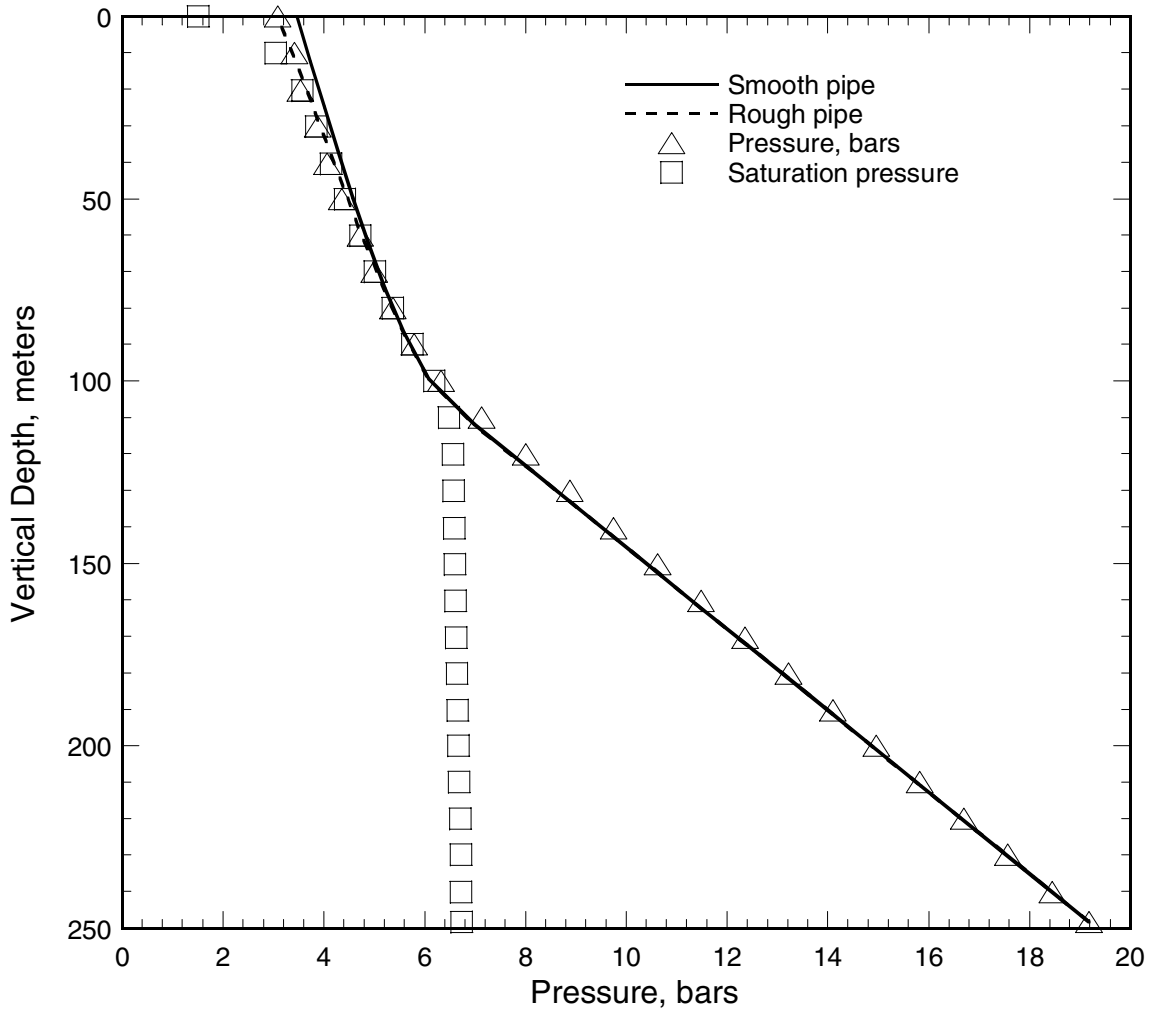

Figure 3.7. Pressure profile (triangle) recorded in the discharging slimhole. The square indicates saturation pressure corresponding to the local measured temperature. The solid (dashed line) line is the computed pressure profile assuming a smooth (rough) pipe.

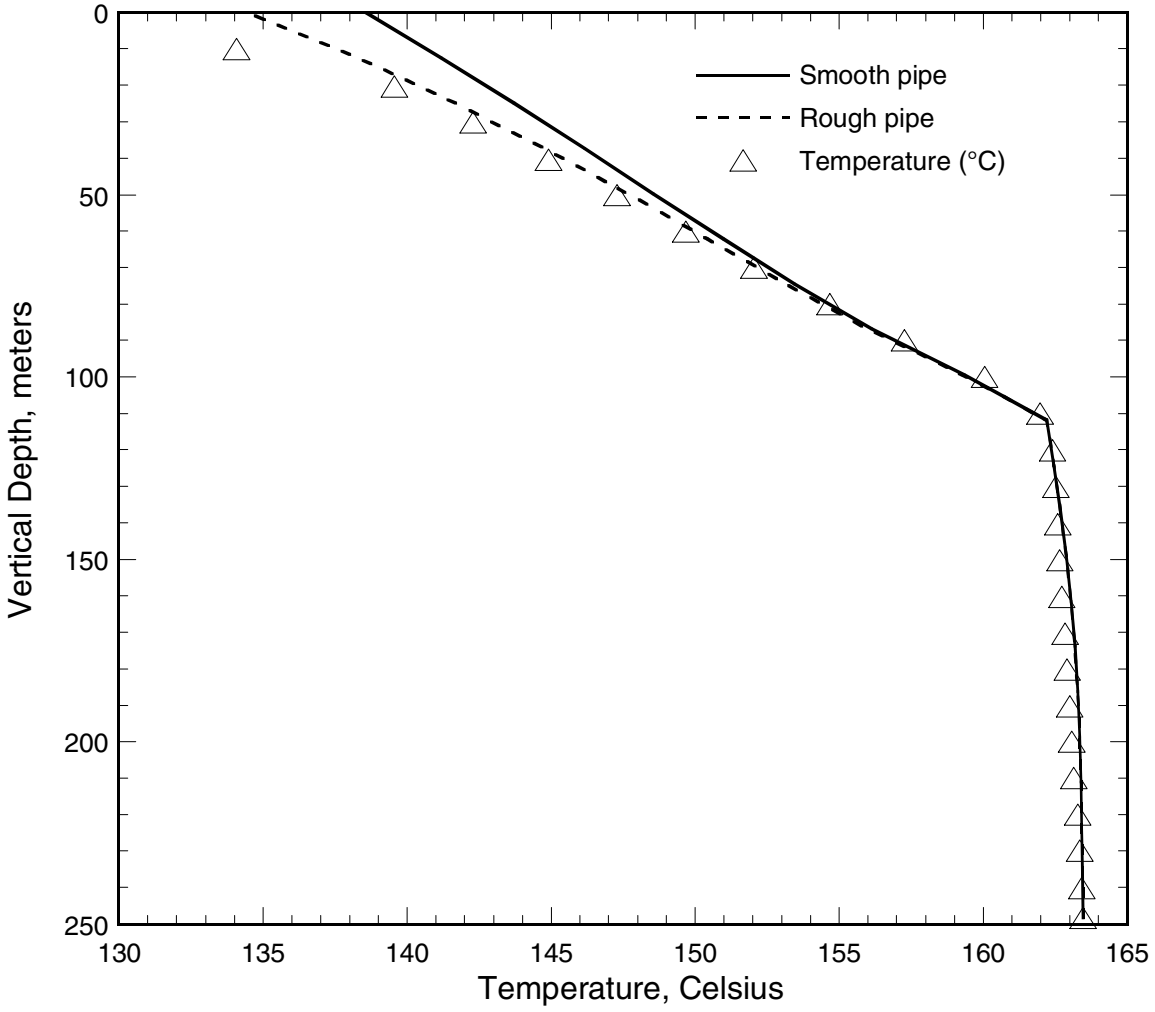

Figure 3.8. Temperature profile (triangle) recorded in the discharging slimhole. The solid (dashed line) line is the computed temperature profile assuming a smooth (rough) pipe.

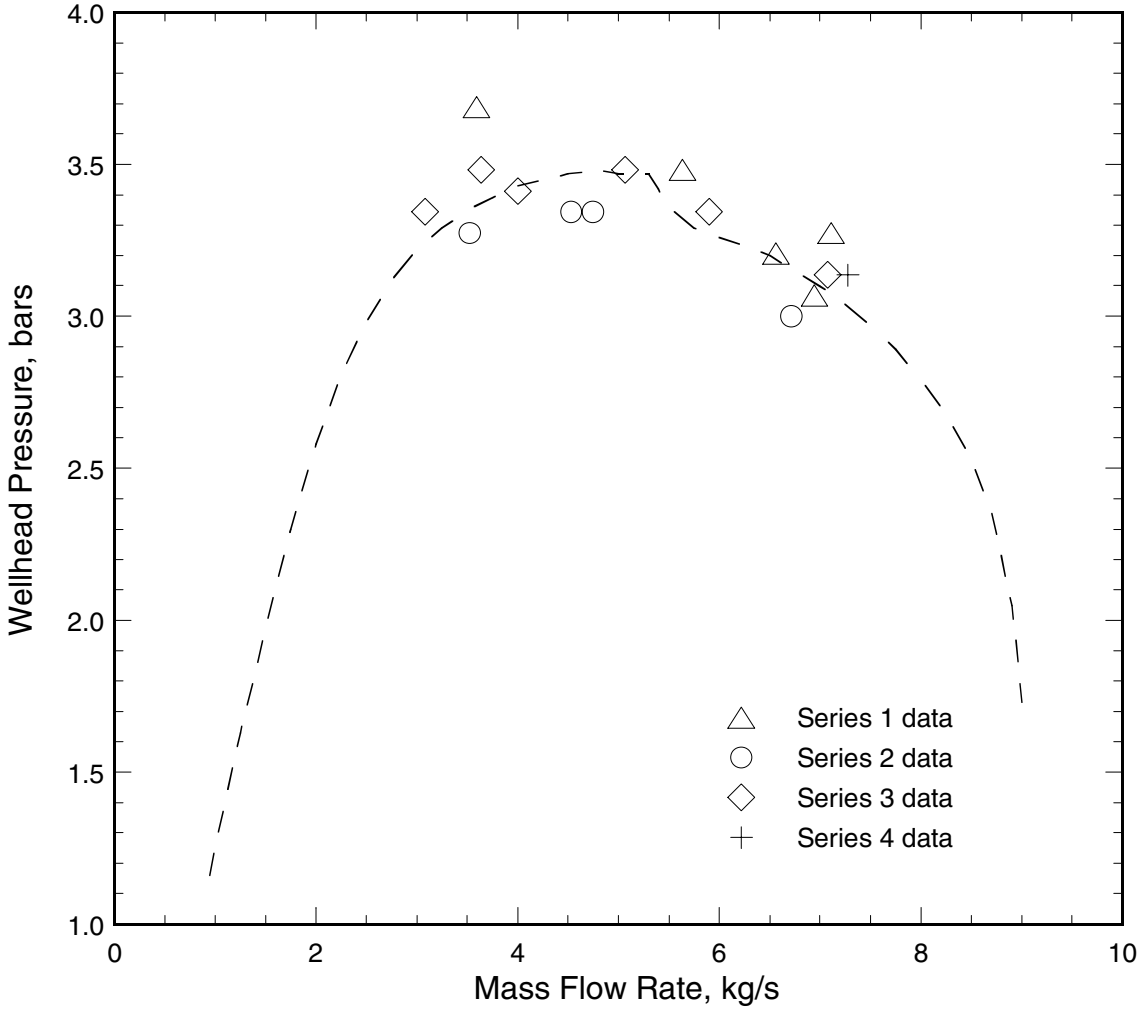

Figure 3.9. Wellhead pressure versus mass flow rate for slimhole SNLG87-29. Measurements (symbols) and computed values (dashed line).

4 FUTURE WORK

The principal goal of the present work is to use high quality data from flowing geothermal wells (Garg and Pritchett, 2001) to devise new liquid holdup correlations for geothermal applications. To make the problem tractable, it was decided to at first develop a holdup correlation restricted to the cased section of geothermal wells. Accordingly, a methodology was formulated for constructing a holdup correlation utilizing measurements in flowing wells. The holdup correlation developed during the current work period (Section 3) displays considerable promise for simulating two-phase flow in the cased section of geothermal wells.

Future plans call for the formulation of a holdup correlation for the open hole/slotted liner section of geothermal wells. The fluid flow in the open hole/slotted liner section is much more complicated than in the cased section. With a single exception (Hadgu, 1989), all of the published papers treat two-phase flow in a pipe (*i.e.*, cased section). Based on the work presented in this report, we believe that it should be possible to use the available well data to formulate a holdup correlation for the open hole/slotted liner section of geothermal wells.

5 REFERENCES

Ansari, A. M., Sylvester, N. D., Sarica, C., Shoham, O., and Brill, J. P. (1994), A Comprehensive Mechanistic Model for Upward Two-Phase Flow in Wellbores, SPE Production & Facilities, pp. 143–165, May.

Aziz, K., Govier, G., and Fogarasi, M. (1972), Pressure Drop in Wells Producing Oil and Gas, Journal Canadian Petroleum Technology, No. 4, pp. 38–48.

Bankoff, S. G. (1960), A variable density single-fluid model for two-phase flow with particular reference to steam-water flow, Journal of Heat Transfer, ASME Transactions, Series C, Vol. 82, pp. 265–272.

Beggs, H. D. and Brill, J. P. (1973), A Study of Two-Phase Flow in Inclined Pipes, Journal of Petroleum Technology, pp. 607–617, May.

Dukler, A. E., Wickes III, M., and Cleveland, R. G. (1964), Frictional Pressure Drop in Two-Phase Flow: B. An Approach Through Similarity Analysis, A.I.Ch.E. Journal, Vol. 10(1), pp. 44–51.

Duns, H., and Ros, N. C. J. (1963), Vertical Flow of Gas and Liquid Mixtures in Wells, Proceedings 6th World Petroleum Congress, Section II, Paper 22 – PD 6, pp. 451–465, Frankfurt Am Main, Germany.

Finger, J., Jacobsen, R., Hickox, C., Combs, J., Polk, G., and Goranson, C. (1999), Slimhole Handbook: Procedures and Recommendations for Slimhole Drilling and Testing in Geothermal Exploration, Report No. SAND99-1976, Sandia National Laboratories, Albuquerque, New Mexico, October.

Gang, X. Z., Golan, M., and Sveen, J. (1990), Determining Downhole Flow Rates of Oil and Gas in Oil Wells Using Pressure Drop and Spinner Response Measurements, Paper No. 20893, Society of Petroleum Engineers, Dallas, Texas.

Garg, S. K. and Combs, J. (2002), A Study of Production/Injection Data from Slim Holes and Large-Diameter Wells at the Okuaizu Geothermal Field, Tohoku, Japan, Report No. SAIC-02/2000, Science Applications International Corporation, San Diego, California, June.

Garg, S. K. and Pritchett, J. W. (2001), Development of New Geothermal Wellbore Holdup Correlations Using Flowing Well Data, Report No. SAIC-01/1061, Science Applications International Corporation, San Diego, California, October.

Garg, S. K., Pritchett, J. W., and Alexander, J. H. (2003), Development of a New Holdup Correlation for Geothermal Wells: A Preliminary Report, Transactions Geothermal Resources Council, Vol. 27, pp. 801–806.

Hadgu, T. (1989), Vertical Two-Phase Flow Studies and Modeling of Flow in Geothermal Wells, Ph.D. Thesis, University of Auckland, Auckland, New Zealand, July.

Hagedorn, A. R. and Brown, K. E. (1965), Experimental Study of Pressure Gradients Occurring During Continuous Two-Phase Flow in Small-Diameter Vertical Conduits, Journal of Petroleum Technology, pp. 475–484, April.

Hughmark, G. A. (1962), Holdup in gas-liquid flow, Chemical Engineering Progress, Vol. 53(4), pp. 62–65.

Hughmark, G. A., and Pressburg, B. S. (1961), Holdup and Pressure Drop with Gas-Liquid Flow in a Vertical Pipe, A.I.Ch.E. Journal, Vol. 7(4), pp. 677–682.

Orkiszewski, J. (1967), Predicting Two-Phase Pressure Drops in Vertical Pipe, Journal of Petroleum Technology, pp. 829-838, June.

Press, W. H., Flannery, B. P., Teukolsky, S. A., and Vetterling, W. T. (1986), Numerical Recipes, Cambridge University Press.

Pritchett, J. W. (1985), WELBOR: A Computer Program for Calculating Flow in a Producing Geothermal Well, Report No. SSS-R-85-7283, S-Cubed, La Jolla, California (now Science Applications International Corporation, San Diego, California).

Pritchett, J. W. (1993), Preliminary Study of Discharge Characteristics of Slim Holes Compared to Production Wells in Liquid-Dominated Geothermal Reservoirs, Proceedings 18th Workshop Geothermal Reservoir Engineering, Stanford University, Stanford, California, pp. 181–187.

APPENDIX A: DUKLER I CORRELATION FOR FRICTIONAL PRESSURE DROP

Frictional Pressure Gradient, F:

$$F = \frac{2 f_0 M^2}{d_w A^2 \rho_m} \tag{A.1}$$

where

M = total mass flow rate

d_w = Inside pipe diameter

A = Pipe cross-section area = $0.25\pi d_w^2$

ρ_m = Mixture density = $\rho_l Y_l + \rho_g (1 - Y_l)$

Y_l = Flowing liquid volume fraction = $S_l v_l \Big/ \left(S_l v_l + S_g v_g \right)$

$\rho_l (\rho_g)$ = Liquid (gas) density

$S_l (S_g)$ = *In-situ* liquid (gas) liquid volume fraction

Friction Factor, f_0:

$$f_0 = 0.0014 + \frac{0.125}{Rn^{0.32}} \tag{A.2}$$

where

Rn = Reynolds number = $d_w M / A \mu_m$

μ_m = Mixture viscosity = $\mu_l Y_l + \mu_g (1 - Y_l)$

$\mu_l (\mu_g)$ = Liquid (gas) viscosity

The above definitions for mixture density ρ_m and mixture viscosity μ_m are different from those employed by Hughmark (1962) (see Section 3).

The friction factor (A.2) is valid for smooth pipes, and was used by Dukler *et al.* (1964) to develop their correlation for the frictional pressure gradient. For rough pipes, a modification (based on Moody's friction factor) of equation (A.2) is employed in WELBOR (Pritchett, 1985). The Fortran subroutine (FAKFRK) for computing the friction factor is reproduced below.

```
      SUBROUTINE FAKFRK (RENLDS,ROUGH,DIAM, F)
C
C
C     PROGRAM TO CALCULATE STEADY TWO-PHASE FLUID UPFLOW IN A WELLBORE
C
C
      IMPLICIT DOUBLE PRECISION (A-H, O-Z)
C
C
      DATA POINT1 / 0.1D+00 /
      DATA RENSML / 1.D+01 /
      DATA RENBIG / 1.D+20 /
      DATA ZERO   / 0.D+00 /
C
      RENOLD = MAX(RENSML, MIN(RENBIG,RENLDS))
C
      IF (ROUGH .GT. ZERO) GO TO 20
C
C     Ordinary Dukler formulation for smooth pipes.
C
   10 F = 0.0014D+00 + 0.125D+00/(RENOLD**0.32D+00)
      RETURN
C
C     Cases of finite pipe roughness
C
   20 X = LOG (RENOLD)
      RELRUF = ROUGH / DIAM
      RELRUF = MIN (POINT1, RELRUF)
      Y = LOG (RELRUF)
      XA = -0.259375D+00 - 1.25D+00*Y
      XB =  5.740625D+00 - 1.25D+00*Y
      IF (X .LE. XA) GO TO 10
      IF (X .LT. XB) GO TO 30
C
C     Fully-developed rough-pipe turbulence (constant friction-factor region).
C
      H = 0.4D+00*Y - 0.877D+00
      GO TO 40
C
C     Transition from smooth- to rough-pipe region
C
   30 Z = (XB - X)
      H = 0.4D+00*Y - 0.877D+00 + 0.02666666666666667D+00 * Z*Z
   40 F = 0.0014D+00 + 0.125D+00*EXP(H)
      RETURN
```

APPENDIX B: PARAMETERS USED TO MATCH DOWNHOLE PRESSURE AND TEMPERATURE PROFILES

B.1 WELL A-1

Well Geometry:

Vertical Depth (meters)	Measured Depth (meters)	Angle with Vertical (Degrees)	Internal Diameter (mm)
253.0	253.0	0.000	384
793.1	809.8	14.068	315

Stable Temperature Profile:

Vertical Depth (meters)	Temperature (Degrees Celsius)
0	26.67
305	87.3
606	201.7
793.1	228.7

Other Model Input Parameters:

Discharge rate	= 107 kg/s
Pressure at 793.1 mTVD	= 18.34 bars
Flowing enthalpy at 793.1 mTVD	= 1105 kJ/kg
Fluid (liquid + steam) gas content at 793.1 mTVD	= 0.0018 kg/kg
Fluid (liquid + steam) salinity at 793.1 mTVD	= 0.0115 kg/kg
Hughmark parameter, η	= 0.11 for depths < 400 m = 0.11 + 0.0022 (depth – 400) for 400 m < depth < 450 m = 0.33 for depths > 450 m
Roughness factor, ε	= 0.00 mm for all depths
Effective thermal conductivity, κ	= 4.0 W/m-^{o}C

B.2 WELL A-2

Well Geometry:

Vertical Depth (meters)	Measured Depth (meters)	Angle with Vertical (Degrees)	Internal Diameter (mm)
261.5	261.5	0.000	384
812.3	828.8	13.853	315

Stable Temperature Profile:

Vertical Depth (meters)	Temperature (Degrees Celsius)
0	27
890	220

Other Model Input Parameters:

Discharge rate = 107 kg/s
Pressure at 812.3 mTVD = 18.83 bars
Flowing enthalpy at 812.3 mTVD = 1070 kJ/kg
Fluid (liquid + steam) gas content at 812.3 mTVD = 0.00107 kg/kg
Fluid (liquid + steam) salinity at 812.3 mTVD = 0.0134 kg/kg
Hughmark parameter, η = 0.12 for depths < 350 m
= 0.12 + 0.0046 (depth – 350) for 350 m < depth < 400 m
= 0.35 for depths > 400 m
Roughness factor, ε = 0.00 mm for all depths
Effective thermal conductivity, κ = 4.0 W/m-^{o}C

B.3 WELL A-4

Well Geometry:

Vertical Depth (meters)	Measured Depth (meters)	Angle with Vertical (Degrees)	Internal Diameter (mm)
277.4	277.4	0.000	384
888.5	901.6	11.759	315

Stable Temperature Profile:

Vertical Depth (meters)	Temperature (Degrees Celsius)
0	27
305	68
754	212
888.5	227

Other Model Input Parameters:

Discharge rate = 135 kg/s
Pressure at 888.5 mTVD = 23.49 bars
Flowing enthalpy at 888.5 mTVD = 1102 kJ/kg
Fluid (liquid + steam) gas content at 888.5 mTVD = 0.0011 kg/kg
Fluid (liquid + steam) salinity at 888.5 mTVD = 0.012 kg/kg
Hughmark parameter, η = 0.09 for depths < 350 m
= 0.09 + 0.0062 (depth – 350) for 350 m < depth < 400 m
= 0.40 for depths > 400 m
Roughness factor, ε = 0.00 mm for all depths
Effective thermal conductivity, κ = 4.0 W/m-^{o}C

B.4 WELL A-6

Well Geometry:

Vertical Depth (meters)	Measured Depth (meters)	Angle with Vertical (Degrees)	Internal Diameter (mm)
450.5	450.5	0.000	384
962.9	975.4	12.529	315
1216.2	1246.3	20.767	315

Stable Temperature Profile:

Vertical Depth (meters)	Temperature (Degrees Celsius)
0	27
610	121
906	238
1216	267

Other Model Input Parameters:

Discharge rate = 145 kg/s
Pressure at 1216.2 mTVD = 44.47 bars
Flowing enthalpy at 1216.2 mTVD = 1133 kJ/kg
Fluid (liquid + steam) gas content at 1216.2 mTVD = 0.00034 kg/kg
Fluid (liquid + steam) salinity at 1216.2 mTVD = 0.0162 kg/kg
Hughmark parameter, η = 0.20 for depths < 450 m
= 0.20 + 0.016 (depth – 450) for 450 m < depth < 500 m
= 1.00 for depths > 500 m
Roughness factor, ε = 0.00 mm for depth < 450.5 m
= 0.10 mm for depth > 450.5 m
Effective thermal conductivity, κ = 4.0 W/m-^{o}C

B.5 WELL A-7

Well Geometry:

Vertical Depth (meters)	Measured Depth (meters)	Angle with Vertical (Degrees)	Internal Diameter (mm)
494.1	494.1	0.000	384
762.0	769.6	13.489	315
1466.4	1517.3	19.595	315

Stable Temperature Profile:

Vertical Depth (meters)	Temperature (Degrees Celsius)
0	27
457	97
610	228
1466	274

Other Model Input Parameters:

Discharge rate = 202 kg/s
Pressure at 1466.4 mTVD = 59.08 bars
Flowing enthalpy at 1466.4 mTVD = 1100 kJ/kg
Fluid (liquid + steam) gas content at 1466.4 mTVD = 0.00072 kg/kg
Fluid (liquid + steam) salinity at 1466.4 mTVD = 0.0137 kg/kg
Hughmark parameter, η = 0.20 for all depths
Roughness factor, ε = 0.00 mm for all depths
Effective thermal conductivity, κ = 4.0 W/m-^{o}C

B.6 WELL A-8

Well Geometry:

Vertical Depth (meters)	Measured Depth (meters)	Angle with Vertical (Degrees)	Internal Diameter (mm)
563.9	563.9	0.000	384
1016.8	1024.7	10.625	315

Stable Temperature Profile:

Vertical Depth (meters)	Temperature (Degrees Celsius)
0	27
305	74
610	223
1020	242

Other Model Input Parameters:

Discharge rate = 101 kg/s
Pressure at 1016.8 mTVD = 22.17 bars
Flowing enthalpy at 1016.8 mTVD = 1072 kJ/kg
Fluid (liquid + steam) gas content at 1016.8 mTVD = 0.0011 kg/kg
Fluid (liquid + steam) salinity at 1016.8 mTVD = 0.0135 kg/kg
Hughmark parameter, η = 0.10 for depths < 550 m
= 0.10 + 0.009 (depth – 550) for 550 m < depth < 600 m
= 0.55 for depths > 600 m
Roughness factor, ε = 0.00 mm for all depths
Effective thermal conductivity, κ = 4.0 W/m-^{o}C

B.7 WELL A-9

Well Geometry:

Vertical Depth (meters)	Measured Depth (meters)	Angle with Vertical (Degrees)	Internal Diameter (mm)
559.0	559.0	0.000	384
1033.3	1048.2	14.177	315

Stable Temperature Profile:

Vertical Depth (meters)	Temperature (Degrees Celsius)
0	27
610	121
909	239
1034	251

Other Model Input Parameters:

Discharge rate = 139 kg/s
Pressure at 1033.3 mTVD = 31.10 bars
Flowing enthalpy at 1033.3 mTVD = 1131 kJ/kg
Fluid (liquid + steam) gas content at 1033.3 mTVD = 0.00086 kg/kg
Fluid (liquid + steam) salinity at 1033.3 mTVD = 0.0134 kg/kg
Hughmark parameter, η = 0.22 for depths < 550 m
= 0.22 + 0.0056 (depth – 550) for 550 m < depth < 600 m
= 0.50 for depths > 600 m
Roughness factor, ε = 0.00 mm for all depths
Effective thermal conductivity, κ = 4.0 W/m-^{o}C

B.8 WELL A-10

Well Geometry:

Vertical Depth (meters)	Measured Depth (meters)	Angle with Vertical (Degrees)	Internal Diameter (mm)
435.0	435.0	0.000	384
662.0	663.8	7.192	315
806.2	816.3	18.990	315
1240.0	1291.1	23.986	315

Stable Temperature Profile:

Vertical Depth (meters)	Temperature (Degrees Celsius)
0	27
610	121
897	226
1240	245

Other Model Input Parameters:

Discharge rate = 145 kg/s
Pressure at 1240.0 mTVD = 35.46 bars
Flowing enthalpy at 1240.0 mTVD = 1075 kJ/kg
Fluid (liquid + steam) gas content at 1240.0 mTVD = 0.0007 kg/kg
Fluid (liquid + steam) salinity at 1240.0 mTVD = 0.0129 kg/kg
Hughmark parameter, η = 0.09 for depths < 400 m
= 0.09 + 0.0066 (depth – 400) for 400 m < depth < 450 m
= 0.42 for depths > 450 m
Roughness factor, ε = 0.00 mm for all depths
Effective thermal conductivity, κ = 4.0 W/m-^{o}C

B.9 WELL A-11

Well Geometry:

Vertical Depth (meters)	Measured Depth (meters)	Angle with Vertical (Degrees)	Internal Diameter (mm)
444.1	444.1	0.000	384
1010.1	1052.2	21.445	315

Stable Temperature Profile:

Vertical Depth (meters)	Temperature (Degrees Celsius)
0	27
755	144
1010	250

Other Model Input Parameters:

Discharge rate = 126 kg/s
Pressure at 1010.1 mTVD = 27.20 bars
Flowing enthalpy at 1010.1 mTVD = 1098 kJ/kg
Fluid (liquid + steam) gas content at 1010.1 mTVD = 0.00053 kg/kg
Fluid (liquid + steam) salinity at 1010.1 mTVD = 0.0136 kg/kg
Hughmark parameter, η = 0.20 for depths < 450 m
= 0.20 + 0.010 (depth – 450) for
450 m < depth < 500 m
= 0.70 for depths > 500 m
Roughness factor, ε = 0.00 mm for all depths
Effective thermal conductivity, κ = 4.0 W/m-^{o}C

B.10 WELL A-12

Well Geometry:

Vertical Depth (meters)	Measured Depth (meters)	Angle with Vertical (Degrees)	Internal Diameter (mm)
377.6	337.6	0.000	384
876.0	889.4	13.140	315

Stable Temperature Profile:

Vertical Depth (meters)	Temperature (Degrees Celsius)
0	27
609	121
900	245

Other Model Input Parameters:

Discharge rate = 113 kg/s
Pressure at 876.0 mTVD = 21.65 bars
Flowing enthalpy at 876.0 mTVD = 1190 kJ/kg
Fluid (liquid + steam) gas content at 876.0 mTVD = 0.0052 kg/kg
Fluid (liquid + steam) salinity at 876.0 mTVD = 0.012 kg/kg
Hughmark parameter, η = 0.10 for depths < 450 m
= 0.10 + 0.001 (depth – 450) for 450 m < depth < 500 m
= 0.15 for depths > 500 m
Roughness factor, ε = 0.00 mm for all depths
Effective thermal conductivity, κ = 4.0 W/m-^{o}C

B.11 WELL A-13

Well Geometry:

Vertical Depth (meters)	Measured Depth (meters)	Angle with Vertical (Degrees)	Internal Diameter (mm)
392.3	392.3	0.000	384
983.9	1012.5	17.468	315

Stable Temperature Profile:

Vertical Depth (meters)	Temperature (Degrees Celsius)
0	27
606	121
893	250

Other Model Input Parameters:

Discharge rate = 88 kg/s
Pressure at 983.9 mTVD = 20.03 bars
Flowing enthalpy at 983.9 mTVD = 1296 kJ/kg
Fluid (liquid + steam) gas content at 983.9 mTVD = 0.0075 kg/kg
Fluid (liquid + steam) salinity at 983.9 mTVD = 0.0112 kg/kg
Hughmark parameter, η = 0.09 for all depths
Roughness factor, ε = 0.00 mm for all depths
Effective thermal conductivity, κ = 4.0 W/m-^{o}C

B.12 WELL A-14

Well Geometry:

Vertical Depth (meters)	Measured Depth (meters)	Angle with Vertical (Degrees)	Internal Diameter (mm)
295.0	295.0	0.000	384
932.4	932.7	1.758	315

Stable Temperature Profile:

Vertical Depth (meters)	Temperature (Degrees Celsius)
0	27
609	121
932	225

Other Model Input Parameters:

Discharge rate = 107 kg/s
Pressure at 932.4 mTVD = 23.67 bars
Flowing enthalpy at 932.4 mTVD = 1085 kJ/kg
Fluid (liquid + steam) gas content at 932.4 mTVD = 0.00032 kg/kg
Fluid (liquid + steam) salinity at 932.4 mTVD = 0.0139 kg/kg
Hughmark parameter, η = 0.14 for depths < 400 m
= 0.14 + 0.0052 (depth – 400) for 400 m < depth < 450 m
= 0.40 for depths > 450 m
Roughness factor, ε = 0.00 mm for all depths
Effective thermal conductivity, κ = 4.0 W/m-^{o}C

B.13 WELL A-16

Well Geometry:

Vertical Depth (meters)	Measured Depth (meters)	Angle with Vertical (Degrees)	Internal Diameter (mm)
375.8	375.8	0.000	384
877.8	923.8	23.644	315

Stable Temperature Profile:

Vertical Depth (meters)	Temperature (Degrees Celsius)
0	27
607	121
882	200

Other Model Input Parameters:

Discharge rate = 79 kg/s
Pressure at 877.8 mTVD = 21.70 bars
Flowing enthalpy at 877.8 mTVD = 1099 kJ/kg
Fluid (liquid + steam) gas content at 877.8 mTVD = 0.00027 kg/kg
Fluid (liquid + steam) salinity at 877.8 mTVD = 0.0126 kg/kg
Hughmark parameter, η = 0.20 for depths < 400 m
= 0.20 + 0.009 (depth – 400) for
400 m < depth < 450 m
= 0.65 for depths > 450 m
Roughness factor, ε = 0.00 mm for all depths
Effective thermal conductivity, κ = 4.0 W/m-^{o}C

B.14 WELL A-18

Well Geometry:

Vertical Depth (meters)	Measured Depth (meters)	Angle with Vertical (Degrees)	Internal Diameter (mm)
281.0	281.0	0.000	384
768.1	768.4	2.010	315

Stable Temperature Profile:

Vertical Depth (meters)	Temperature (Degrees Celsius)
0	27
305	71
730	215
800	220

Other Model Input Parameters:

Discharge rate = 40 kg/s
Pressure at 768.1 mTVD = 16.28 bars
Flowing enthalpy at 768.1 mTVD = 1269 kJ/kg
Fluid (liquid + steam) gas content at 768.1 mTVD = 0.0142 kg/kg
Fluid (liquid + steam) salinity at 768.1 mTVD = 0.0093 kg/kg
Hughmark parameter, η = 0.43 for depths < 350 m
= 0.43 + 0.0074 (depth – 350) for 350 m < depth < 400 m
= 0.80 for depths > 400 m
Roughness factor, ε = 0.00 mm for all depths
Effective thermal conductivity, κ = 4.0 W/m-^{o}C

B.15 WELL A-19

Well Geometry:

Vertical Depth (meters)	Measured Depth (meters)	Angle with Vertical (Degrees)	Internal Diameter (mm)
403.6	403.6	0.000	384
998.5	1021.7	15.748	315

Stable Temperature Profile:

Vertical Depth (meters)	Temperature (Degrees Celsius)
0	27
305	74
1040	233

Other Model Input Parameters:

Discharge rate = 123 kg/s
Pressure at 998.5 mTVD = 22.05 bars
Flowing enthalpy at 998.5 mTVD = 1108 kJ/kg
Fluid (liquid + steam) gas content at 998.5 mTVD = 0.0028 kg/kg
Fluid (liquid + steam) salinity at 998.5 mTVD = 0.0128 kg/kg
Hughmark parameter, η = 0.09 for depths < 450 m
= 0.09 + 0.0034 (depth – 450) for 450 m < depth < 500 m
= 0.26 for depths > 500 m
Roughness factor, ε = 0.00 mm for all depths
Effective thermal conductivity, κ = 4.0 W/m-^{o}C

B.16 WELL A-20

Well Geometry:

Vertical Depth (meters)	Measured Depth (meters)	Angle with Vertical (Degrees)	Internal Diameter (mm)
380.7	380.7	0.000	384
1023.8	1037.8	11.848	315

Stable Temperature Profile:

Vertical Depth (meters)	Temperature (Degrees Celsius)
0	27
305	74
607	153
1060	228

Other Model Input Parameters:

Discharge rate = 120 kg/s
Pressure at 1023.8 mTVD = 23.12 bars
Flowing enthalpy at 1023.8 mTVD = 1120 kJ/kg
Fluid (liquid + steam) gas content at 1023.8 mTVD = 0.0035 kg/kg
Fluid (liquid + steam) salinity at 1023.8 mTVD = 0.0101 kg/kg
Hughmark parameter, η = 0.10 for depths < 450 m
= 0.10 + 0.0042 (depth – 450) for 450 m < depth < 500 m
= 0.31 for depths >500 m
Roughness factor, ε = 0.00 mm for all depths
Effective thermal conductivity, κ = 4.0 W/m-^{o}C

B.17 WELL A-21

Well Geometry:

Vertical Depth (meters)	Measured Depth (meters)	Angle with Vertical (Degrees)	Internal Diameter (mm)
443.7	443.8	1.216	384
1010.1	1052.2	21.414	315

Stable Temperature Profile:

Vertical Depth (meters)	Temperature (Degrees Celsius)
0	20
1011	224

Other Model Input Parameters:

Discharge rate = 89.5 kg/s
Pressure at 1010.1 mTVD = 23.90 bars
Flowing enthalpy at 1010.1 mTVD = 1059 kJ/kg
Fluid (liquid + steam) gas content at 1010.1 mTVD = 0.0007 kg/kg
Fluid (liquid + steam) salinity at 1010.1 mTVD = 0.00715 kg/kg
Hughmark parameter, η = 0.13 for depths < 500 m
= 0.13 + 0.0054 (depth – 500) for 500 m < depth < 550 m
= 0.40 for depths > 550 m
Roughness factor, ε = 0.00 mm for all depths
Effective thermal conductivity, κ = 4.0 W/m-^{o}C

B.18 WELL B-3

Well Geometry:

Vertical Depth (meters)	Measured Depth (meters)	Angle with Vertical (Degrees)	Internal Diameter (mm)
433.7	433.7	0.000	315
847.1	851.6	8.416	315
1310.0	1329.8	14.533	221

Stable Temperature Profile:

Vertical Depth (meters)	Temperature (Degrees Celsius)
0	27
1310	228

Other Model Input Parameters:

Discharge rate = 36.5 kg/s
Pressure at 1310.0 mTVD = 26.85 bars
Flowing enthalpy at 1310.0 mTVD = 2278 kJ/kg
Fluid (liquid + steam) gas content at 1310.0 mTVD = 0.0023 kg/kg
Fluid (liquid + steam) salinity at 1310.0 mTVD = 0.00062 kg/kg
Hughmark parameter, η = 0.75 for depths < 800 m
= 0.75 – 0.0045 (depth – 800) for 800 m < depth < 900 m
= 0.30 for depths > 900 m
Roughness factor, ε = 0.00 mm for all depths
Effective thermal conductivity, κ = 4.0 W/m-^{o}C

B.19 WELL B-4

Well Geometry:

Vertical Depth (meters)	Measured Depth (meters)	Angle with Vertical (Degrees)	Internal Diameter (mm)
445.3	445.3	0.000	221
845.2	848.0	6.760	221

Stable Temperature Profile:

Vertical Depth (meters)	Temperature (Degrees Celsius)
0	27
845	226

Other Model Input Parameters:

Discharge rate = 17.8 kg/s
Pressure at 845.2 mTVD = 25.84 bars
Flowing enthalpy at 845.2 mTVD = 1572 kJ/kg
Fluid (liquid + steam) gas content at 845.2 mTVD = 0.0022 kg/kg
Fluid (liquid + steam) salinity at 845.2 mTVD = 0.0025 kg/kg
Hughmark parameter, η = 0.31 for all depths
Roughness factor, ε = 0.00 mm for all depths
Effective thermal conductivity, κ = 4.0 W/m-^{o}C

B.20 WELL B-5

Well Geometry:

Vertical Depth (meters)	Measured Depth (meters)	Angle with Vertical (Degrees)	Internal Diameter (mm)
415.1	415.1	0.000	221
843.7	851.3	10.711	221

Stable Temperature Profile:

Vertical Depth (meters)	Temperature (Degrees Celsius)
0	27
850	215

Other Model Input Parameters:

Discharge rate = 38.8 kg/s
Pressure at 843.7 mTVD = 20.72 bars
Flowing enthalpy at 843.7 mTVD = 1215 kJ/kg
Fluid (liquid + steam) gas content at 843.7 mTVD = 0.001 kg/kg
Fluid (liquid + steam) salinity at 843.7 mTVD = 0.0043 kg/kg
Hughmark parameter, η = 0.02 for depths < 450 m
= 0.02 + 0.0064 (depth – 450) for 450 m < depth < 500 m
= 0.34 for depths > 500 m
Roughness factor, ε = 0.00 mm for all depths
Effective thermal conductivity, κ = 4.0 W/m-^{o}C

B.21 WELL B-13

Well Geometry:

Vertical Depth (meters)	Measured Depth (meters)	Angle with Vertical (Degrees)	Internal Diameter (mm)
155.4	155.4	0.000	221
805.9	812.0	7.816	221

Stable Temperature Profile:

Vertical Depth (meters)	Temperature (Degrees Celsius)
0	27
806	200

Other Model Input Parameters:

Discharge rate = 11.0 kg/s
Pressure at 805.9 mTVD = 14.81 bars
Flowing enthalpy at 805.9 mTVD = 1566 kJ/kg
Fluid (liquid + steam) gas content at 805.9 mTVD = 0.0025 kg/kg
Fluid (liquid + steam) salinity at 805.9 mTVD = 0.00051 kg/kg
Hughmark parameter, η = 0.25 for depths < 350 m
= 0.25 – 0.001 (depth – 350) for 350 m < depth < 400 m
= 0.20 for depths > 400 m
Roughness factor, ε = 0.00 mm for all depths
Effective thermal conductivity, κ = 4.0 W/m-^{o}C

B.22 WELL C-1

Well Geometry:

Vertical Depth (meters)	Measured Depth (meters)	Angle with Vertical (Degrees)	Internal Diameter (mm)
244.4	244.4	0.000	221
818.0	818.1	1.070	221

Stable Temperature Profile:

Vertical Depth (meters)	Temperature (Degrees Celsius)
0	27
818	200

Other Model Input Parameters:

Discharge rate = 18.3 kg/s
Pressure at 818.0 mTVD = 15.58 bars
Flowing enthalpy at 818.0 mTVD = 1797 kJ/kg
Fluid (liquid + steam) gas content at 818.0 mTVD = 0.0003 kg/kg
Fluid (liquid + steam) salinity at 818.0 mTVD = 0.0025 kg/kg
Hughmark parameter, η = 0.44 for depths < 450 m
= 0.44 – 0.0004 (depth – 450) for 450 m < depth < 500 m
= 0.42 for depths > 500 m
Roughness factor, ε = 0.00 mm for all depths
Effective thermal conductivity, κ = 4.0 W/m-^{o}C

B.23 WELL C-2

Well Geometry:

Vertical Depth (meters)	Measured Depth (meters)	Angle with Vertical (Degrees)	Internal Diameter (mm)
587.3	587.3	0.000	221

Stable Temperature Profile:

Vertical Depth (meters)	Temperature (Degrees Celsius)
0	27
590	197

Other Model Input Parameters:

Discharge rate = 14.6 kg/s
Pressure at 587.3 mTVD = 14.58 bars
Flowing enthalpy at 587.3 mTVD = 2036 kJ/kg
Fluid (liquid + steam) gas content at 587.3 mTVD = 0.017 kg/kg
Fluid (liquid + steam) salinity at 587.3 mTVD = 0.0022 kg/kg
Hughmark parameter, η = 0.67 for depths < 250 m
= 0.67 – 0.0044 (depth – 250) for 250 m < depth < 300 m
= 0.45 for depths > 300 m
Roughness factor, ε = 0.00 mm for all depths
Effective thermal conductivity, κ = 4.0 W/m-^{o}C

B.24 WELL C-3

Well Geometry:

Vertical Depth (meters)	Measured Depth (meters)	Angle with Vertical (Degrees)	Internal Diameter (mm)
720.0	720.0	0.000	320

Stable Temperature Profile:

Vertical Depth (meters)	Temperature (Degrees Celsius)
0	27
892	196

Other Model Input Parameters:

Discharge rate = 19.7 kg/s
Pressure at 720.0 mTVD = 13.58 bars
Flowing enthalpy at 720.0 mTVD = 1893 kJ/kg
Fluid (liquid + steam) gas content at 720.0 mTVD = 0.0007 kg/kg
Fluid (liquid + steam) salinity at 720.0 mTVD = 0.0023 kg/kg
Hughmark parameter, η = 0.34 for depths < 350 m
= 0.34 + 0.0004 (depth – 350) for 350 m < depth < 400 m
= 0.36 for depths > 400 m
Roughness factor, ε = 0.00 mm for all depths
Effective thermal conductivity, κ = 4.0 W/m-^{o}C

B.25 WELL C-4

Well Geometry:

Vertical Depth (meters)	Measured Depth (meters)	Angle with Vertical (Degrees)	Internal Diameter (mm)
438.9	438.9	0.000	320
730.6	737.6	12.429	320

Stable Temperature Profile:

Vertical Depth (meters)	Temperature (Degrees Celsius)
0	27
740	197

Other Model Input Parameters:

Discharge rate = 22.0 kg/s
Pressure at 730.6 mTVD = 14.65 bars
Flowing enthalpy at 730.6 mTVD = 2105 kJ/kg
Fluid (liquid + steam) gas content at 730.6 mTVD = 0.0009 kg/kg
Fluid (liquid + steam) salinity at 730.6 mTVD = 0.00145 kg/kg
Hughmark parameter, η = 0.54 for depths < 350 m
= 0.54 + 0.0004 (depth – 350) for 350 m < depth < 400 m
= 0.56 for depths > 400 m
Roughness factor, ε = 0.00 mm for all depths
Effective thermal conductivity, κ = 4.0 W/m-^{o}C

B.26 WELL C-5

Well Geometry:

Vertical Depth (meters)	Measured Depth (meters)	Angle with Vertical (Degrees)	Internal Diameter (mm)
439.2	439.2	0.000	320
843.2	851.6	11.584	320

Stable Temperature Profile:

Vertical Depth (meters)	Temperature (Degrees Celsius)
0	27
850	212

Other Model Input Parameters:

Discharge rate = 39.4 kg/s
Pressure at 843.2 mTVD = 19.63 bars
Flowing enthalpy at 843.2 mTVD = 1825 kJ/kg
Fluid (liquid + steam) gas content at 843.2 mTVD = 0.0002 kg/kg
Fluid (liquid + steam) salinity at 843.2 mTVD = 0.0030 kg/kg
Hughmark parameter, η = 0.59 – 0.0002 (depth) for depths < 450 m
= 0.50 for depths > 450 m
Roughness factor, ε = 0.00 mm for all depths
Effective thermal conductivity, κ = 4.0 W/m-^{o}C

B.27 WELL C-6

Well Geometry:

Vertical Depth (meters)	Measured Depth (meters)	Angle with Vertical (Degrees)	Internal Diameter (mm)
484.6	484.6	0.000	217
1004.5	1025.0	15.832	217

Stable Temperature Profile:

Vertical Depth (meters)	Temperature (Degrees Celsius)
0	20
1005	240

Other Model Input Parameters:

Discharge rate = 64.9 kg/s
Pressure at 1004.5 mTVD = 30.98 bars
Flowing enthalpy at 1004.5 mTVD = 1110 kJ/kg
Fluid (liquid + steam) gas content at 1004.5 mTVD = 0.00059 kg/kg
Fluid (liquid + steam) salinity at 1004.5 mTVD = 0.002415 kg/kg
Hughmark parameter, η = 0.00 for depths < 400 m
= 0.00 + 0.016 (depth – 400) for 400 m < depth < 450 m
= 0.80 for depths > 450 m
Roughness factor, ε = 0.00 mm for all depths

B.28 WELL CS-1

Well Geometry:

Vertical Depth (meters)	Measured Depth (meters)	Angle with Vertical (Degrees)	Internal Diameter (mm)
237.7	237.7	0.000	315
679.8	680.6	3.444	315

Stable Temperature Profile:

Vertical Depth (meters)	Temperature (Degrees Celsius)
0	20
680	175

Other Model Input Parameters:

Discharge rate = 22.3 kg/s
Pressure at 679.8 mTVD = 8.92 bars
Flowing enthalpy at 679.8 mTVD = 1058 kJ/kg
Fluid (liquid + steam) gas content at 679.8 mTVD = 0.00356 kg/kg
Fluid (liquid + steam) salinity at 679.8 mTVD = 0.00897 kg/kg
Hughmark parameter, η = 0.33 for depths < 250 m
= 0.33 – 0.0004 (depth – 250) for 250 m < depth < 300 m
= 0.31 for depths > 300 m
Roughness factor, ε = 0.00 mm for all depths
Effective thermal conductivity, κ = 4.0 W/m-^{o}C

B.29 WELL KE1-4

Well Geometry:

Vertical Depth (meters)	Measured Depth (meters)	Angle with Vertical (Degrees)	Internal Diameter (mm)
1260.4	1260.4	0.000	102

Stable Temperature Profile:

Vertical Depth (meters)	Temperature (Degrees Celsius)
0	15
470	35
860	190
1000	220
1260	228

Other Model Input Parameters:

Discharge Test (November 12, 1983)

Discharge rate = 7.08 kg/s
Pressure at 1260.4 mTVD = 58.1 bars
Temperature at 1260.4 mTVD = 227.3 ^{o}C
Fluid (liquid + steam) gas content at 1260.4 mTVD = 0.0000 kg/kg
Fluid (liquid + steam) salinity at 1260.4 mTVD = 0.0000 kg/kg
Hughmark parameter, η = 0.10 for depths < 300 m
= 0.10 + 0.018 (depth – 300) for 300 m < depth < 350 m
= 1.00 for depths > 350 m
Roughness factor, ε = 0.00 mm for all depths
Effective thermal conductivity, κ = 1.3 W/m-^{o}C

Discharge Test (November 13, 1983)

Discharge rate = 8.44 kg/s
Pressure at 1260.4 mTVD = 57.75 bars
Temperature at 1260.4 mTVD = 227.45 ^{o}C
Fluid (liquid + steam) gas content at 1260.4 mTVD = 0.0000 kg/kg
Fluid (liquid + steam) salinity at 1260.4 mTVD = 0.0000 kg/kg
Hughmark parameter, η = 0.01 for depths < 450 m
= 0.01 + 0.0198 (depth – 450) for 450 m < depth < 500 m
= 1.00 for depths > 500 m
Roughness factor, ε = 0.00 mm for all depths
Effective thermal conductivity, κ = 0.8 W/m-^{o}C

B.30 WELL KE1-9

Well Geometry:

Vertical Depth (meters)	Measured Depth (meters)	Angle with Vertical (Degrees)	Internal Diameter (mm)
773.4	773.4	0.000	224

Stable Temperature Profile:

Vertical Depth (meters)	Temperature (Degrees Celsius)
0	20
320	100
600	190
1230	240

Other Model Input Parameters:

Discharge rate = 17.2 kg/s
Pressure at 773.4 mTVD = 18.18 bars
Flowing enthalpy at 773.4 mTVD = 1131 kJ/kg
Fluid (liquid + steam) gas content at 773.4 mTVD = 0.0000 kg/kg
Fluid (liquid + steam) salinity at 773.4 mTVD = 0.0000 kg/kg
Hughmark parameter, η = 0.21 for depths < 300 m
= 0.21 + 0.0148 (depth – 300) for 300 m < depth < 350 m
= 0.95 for depths > 350 m
Roughness factor, ε = 0.00 mm for all depths
Effective thermal conductivity, κ = 4 W/m-^{o}C

B.31 WELL KE1-11

Well Geometry:

Vertical Depth (meters)	Measured Depth (meters)	Angle with Vertical (Degrees)	Internal Diameter (mm)
980.9	980.9	0.000	224

Stable Temperature Profile:

Vertical Depth (meters)	Temperature (Degrees Celsius)
0	10
480	100
1000	255

Other Model Input Parameters:

Discharge rate = 18.5 kg/s
Pressure at 980.9 mTVD = 42.43 bars
Flowing enthalpy at 980.9 mTVD = 1150 kJ/kg
Fluid (liquid + steam) gas content at 980.9 mTVD = 0.0000 kg/kg
Fluid (liquid + steam) salinity at 980.9 mTVD = 0.0000 kg/kg
Hughmark parameter, η = 0.65 for depths < 550 m
= 0.65 – 0.006 (depth – 550) for 550 m < depth < 600 m
= 0.35 for depths > 600 m
Roughness factor, ε = 0.00 mm for all depths
Effective thermal conductivity, κ = 4 W/m-^{o}C

B.32 WELL KE1-17

Well Geometry:

Vertical Depth (meters)	Measured Depth (meters)	Angle with Vertical (Degrees)	Internal Diameter (mm)
200.0	200.0	0.000	224
848.1	858.7	10.293	224

Stable Temperature Profile:

Vertical Depth (meters)	Temperature (Degrees Celsius)
0	18
350	35
850	214

Other Model Input Parameters:

Discharge Test (March 30, 1986)

Discharge rate	= 41.8 kg/s
Pressure at 848.1 mTVD	= 25.93 bars
Flowing enthalpy at 848.1 mTVD	= 1000 kJ/kg
Fluid (liquid + steam) gas content at 848.1 mTVD	= 0.0000 kg/kg
Fluid (liquid + steam) salinity at 848.1 mTVD	= 0.0000 kg/kg
Hughmark parameter, η	= 0.40 for depths < 500 m = 0.40 + 0.012 (depth – 500) for 500 m < depth < 550 m = 1.00 for depths > 550 m
Roughness factor, ε	= 0.00 mm for depths < 550 m = 7.00 mm for depths > 550 m
Effective thermal conductivity, κ	= 4 W/m-^{o}C

Discharge Test (April 4, 1986)

Discharge rate	= 25.8 kg/s
Pressure at 848.1 mTVD	= 26.07 bars
Flowing enthalpy at 848.1 mTVD	= 1000 kJ/kg
Fluid (liquid + steam) gas content at 848.1 mTVD	= 0.0000 kg/kg
Fluid (liquid + steam) salinity at 848.1 mTVD	= 0.0000 kg/kg
Hughmark parameter, η	= 0.85 for depths < 450 m = 0.85 + 0.003 (depth – 450) for 450 m < depth < 500 m = 1.00 for depths > 500 m
Roughness factor, ε	= 0.00 mm for depths < 500 m = 10.00 mm for depths > 500 m
Effective thermal conductivity, κ	= 4 W/m-^{o}C

B.33 WELL KE1-19S

Well Geometry:

Vertical Depth (meters)	Measured Depth (meters)	Angle with Vertical (Degrees)	Internal Diameter (mm)
94.0	94.0	0.000	159
734.9	740.2	7.343	159

Stable Temperature Profile:

Vertical Depth (meters)	Temperature (Degrees Celsius)
0	20
405	100
740	180

Other Model Input Parameters:

Discharge Test (September 1, 1986)

Discharge rate	= 23.9 kg/s
Pressure at 734.9 mTVD	= 19.01 bars
Flowing enthalpy at 734.9 mTVD	= 1000 kJ/kg
Fluid (liquid + steam) gas content at 734.9 mTVD	= 0.0000 kg/kg
Fluid (liquid + steam) salinity at 734.9 mTVD	= 0.0000 kg/kg
Hughmark parameter, η	= 0.05 for depths < 350 m = 0.05 + 0.017 (depth – 350) for 350 m < depth < 400 m = 0.90 for depths > 400 m
Roughness factor, ε	= 0.00 mm for all depths
Effective thermal conductivity, κ	= 4 W/m-^{o}C

Discharge Test (September 16, 1986)

Discharge rate	= 14.5 kg/s
Pressure at 734.9 mTVD	= 19.42 bars
Flowing enthalpy at 734.9 mTVD	= 1000 kJ/kg
Fluid (liquid + steam) gas content at 734.9 mTVD	= 0.0000 kg/kg
Fluid (liquid + steam) salinity at 734.9 mTVD	= 0.0000 kg/kg
Hughmark parameter, η	= 0.35 for depths < 200 m = 0.35 + 0.013 (depth – 200) for 200 m < depth < 250 m = 1.00 for depths > 250 m
Roughness factor, ε	= 0.00 mm for all depths
Effective thermal conductivity, κ	= 4 W/m-^{o}C

B.34 WELL KE1-22:

Well Geometry:

Vertical Depth (meters)	Measured Depth (meters)	Angle with Vertical (Degrees)	Internal Diameter (mm)
873.9	875.0	2.873	224

Stable Temperature Profile:

Vertical Depth (meters)	Temperature (Degrees Celsius)
0	20
900	220

Other Model Input Parameters:

Discharge Test (February 10, 1987)

Discharge rate = 25.0 kg/s
Pressure at 873.9 mTVD = 30.42 bars
Flowing enthalpy at 873.9 mTVD = 995 kJ/kg
Fluid (liquid + steam) gas content at 873.9 mTVD = 0.0000 kg/kg
Fluid (liquid + steam) salinity at 873.9 mTVD = 0.0000 kg/kg
Hughmark parameter, η = 1.00 for all depths
Roughness factor, ε = 0.00 mm for all depths
Effective thermal conductivity, κ = 4 W/m-^{o}C

Discharge Test (February 25, 1987)

Discharge rate = 48.0 kg/s
Pressure at 734.9 mTVD = 29.71 bars
Flowing enthalpy at 734.9 mTVD = 995 kJ/kg
Fluid (liquid + steam) gas content at 734.9 mTVD = 0.0000 kg/kg
Fluid (liquid + steam) salinity at 734.9 mTVD = 0.0000 kg/kg
Hughmark parameter, η = 0.40 for depths < 250 m
= 0.40 + 0.012 (depth – 250) for 250 m < depth < 300 m
= 1.00 for depths > 300 m
Roughness factor, ε = 0.00 mm for all depths
Effective thermal conductivity, κ = 4 W/m-^{o}C

B.35 WELL GH-11

Well Geometry:

Vertical Depth (meters)	Measured Depth (meters)	Angle with Vertical (Degrees)	Internal Diameter (mm)
298.3	300.0	6.102	253
654.5	700.0	27.064	253

Stable Temperature Profile:

Vertical Depth (meters)	Temperature (Degrees Celsius)
0	10
400	195
800	210

Other Model Input Parameters:

Discharge Test (July 19, 1991)

Discharge rate	= 52.4 kg/s
Pressure at 654.5 mTVD	= 31.69 bars
Flowing enthalpy at 654.5 mTVD	= 1018 kJ/kg
Fluid (liquid + steam) gas content at 654.5 mTVD	= 0.0000 kg/kg
Fluid (liquid + steam) salinity at 654.5 mTVD	= 0.0000 kg/kg
Hughmark parameter, η	= 0.50 for depths < 250 m = 0.50 + 0.01 (depth – 250) for 250 m < depth < 300 m = 1.00 for depths > 300 m
Roughness factor, ε	= 0.40 mm for all depths
Effective thermal conductivity, κ	= 4 W/m-^{o}C

Discharge Test (July 20, 1991)

Discharge rate	= 62.8 kg/s
Pressure at 654.5 mTVD	= 28.06 bars
Flowing enthalpy at 654.5 mTVD	= 1018 kJ/kg
Fluid (liquid + steam) gas content at 654.5 mTVD	= 0.0000 kg/kg
Fluid (liquid + steam) salinity at 654.5 mTVD	= 0.0000 kg/kg
Hughmark parameter, η	= 0.15 for depths < 250 m = 0.15 + 0.017 (depth – 250) for 250 m < depth < 300 m = 1.00 for depths > 300 m
Roughness factor, ε	0.40 mm for all depths
Effective thermal conductivity, κ	= 4 W/m-^{o}C

B.36 WELL GH-20

Well Geometry:

Vertical Depth (meters)	Measured Depth (meters)	Angle with Vertical (Degrees)	Internal Diameter (mm)
298.7	300.0	5.336	224
785.8	850.0	27.670	224

Stable Temperature Profile:

Vertical Depth (meters)	Temperature (Degrees Celsius)
0	10
400	175
800	200

Other Model Input Parameters:

Discharge Test (April 24, 1991)

Discharge rate = 60.1 kg/s
Pressure at 785.8 mTVD = 47.43 bars
Flowing enthalpy at 785.8 mTVD = 1042 kJ/kg
Fluid (liquid + steam) gas content at 785.8 mTVD = 0.0000 kg/kg
Fluid (liquid + steam) salinity at 785.8 mTVD = 0.0000 kg/kg
Hughmark parameter, η = 1.00 for all depths
Roughness factor, ε = 0.016 mm for all depths
Effective thermal conductivity, κ = 4 W/m-^{o}C

Discharge Test (April 25, 1991)

Discharge rate = 69.9 kg/s
Pressure at 785.8 mTVD = 46.00 bars
Flowing enthalpy at 785.8 mTVD = 1042 kJ/kg
Fluid (liquid + steam) gas content at 785.8 mTVD = 0.0000 kg/kg
Fluid (liquid + steam) salinity at 785.8 mTVD = 0.0000 kg/kg
Hughmark parameter, η = 1.00 for all depths
Roughness factor, ε = 0.016 mm for all depths
Effective thermal conductivity, κ = 4 W/m-^{o}C

Discharge Test (April 26, 1991)

Discharge rate = 78.6 kg/s
Pressure at 785.8 mTVD = 44.95 bars
Flowing enthalpy at 785.8 mTVD = 1042 kJ/kg
Fluid (liquid + steam) gas content at 785.8 mTVD = 0.0000 kg/kg
Fluid (liquid + steam) salinity at 785.8 mTVD = 0.0000 kg/kg
Hughmark parameter, η = 1.00 for all depths
Roughness factor, ε = 0.016 mm for all depths
Effective thermal conductivity, κ = 4 W/m-^{o}C

B.37 WELL S-2(I):

Well Geometry:

Vertical Depth (meters)	Measured Depth (meters)	Angle with Vertical (Degrees)	Internal Diameter (mm)
703.3	703.3	0.000	102

Stable Temperature Profile:

Vertical Depth (meters)	Temperature (Degrees Celsius)
0	20
300	100
400	175
900	235

Other Model Input Parameters:

Discharge rate = 1.10 kg/s
Pressure at 703.3 mTVD = 6.73 bars
Flowing enthalpy at 703.3 mTVD = 2340 kJ/kg
Fluid (liquid + steam) gas content at 703.3 mTVD = 0.0000 kg/kg
Fluid (liquid + steam) salinity at 703.3 mTVD = 0.0000 kg/kg
Hughmark parameter, η = 0.30 for depths < 250 m
= 0.30 + 0.014 (depth – 250) for 250 m < depth < 300 m
= 1.00 for depths > 300 m
Roughness factor, ε = 0.103 mm for all depths
Effective thermal conductivity, κ = 4 W/m-^{o}C

APPENDIX C: NUMERICAL SIMULATIONS

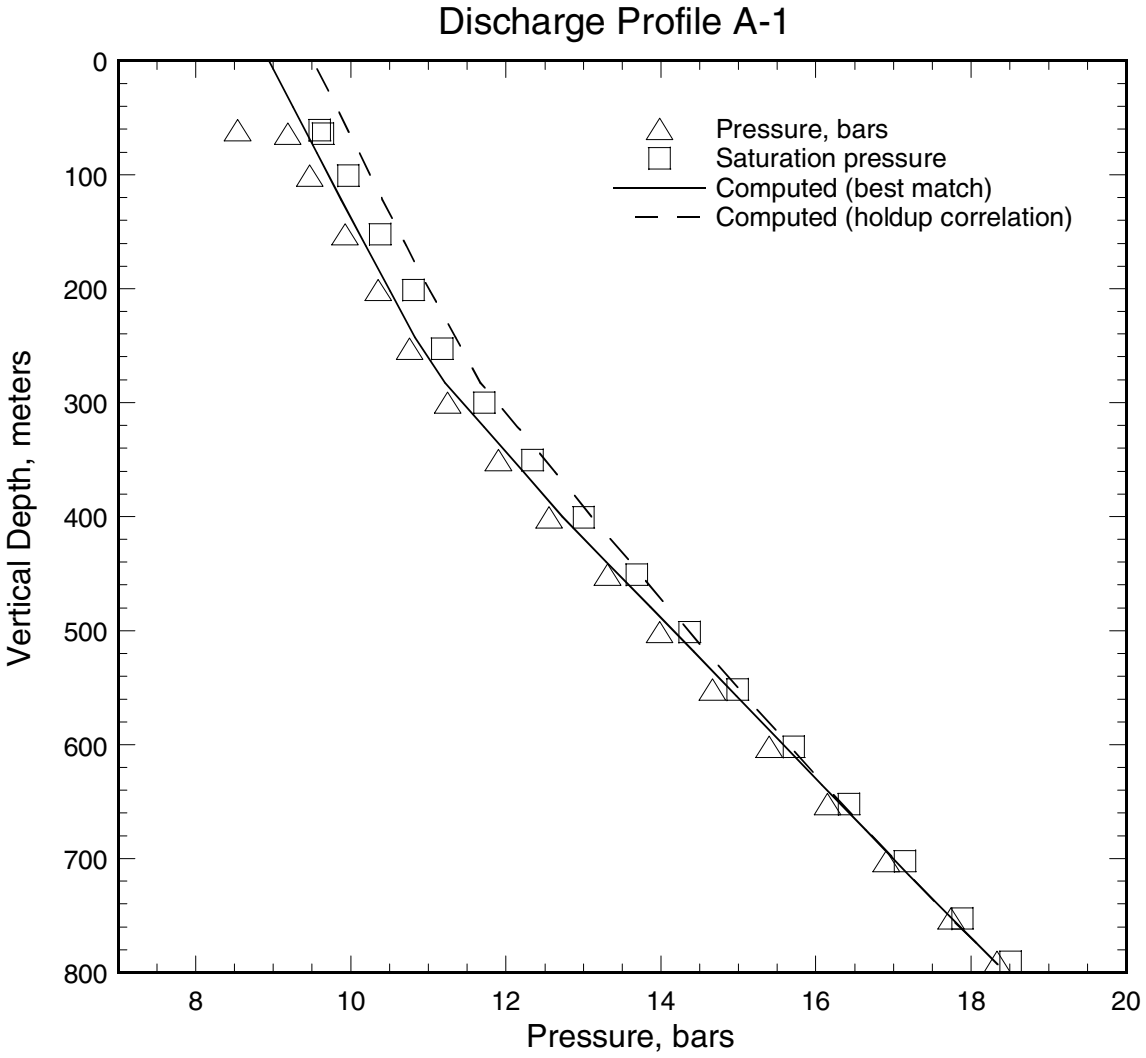

Figure C.1. Pressure profile (triangles) recorded in discharging well A-1. The squares indicate saturation pressure corresponding to the local measured temperature. The solid line is the computed pressure profile using an adjustable holdup correlation (see Section 2 for details). The computed pressure profile using the correlation(s) for *K(Z)* developed in Section 3 is shown as a dashed line.

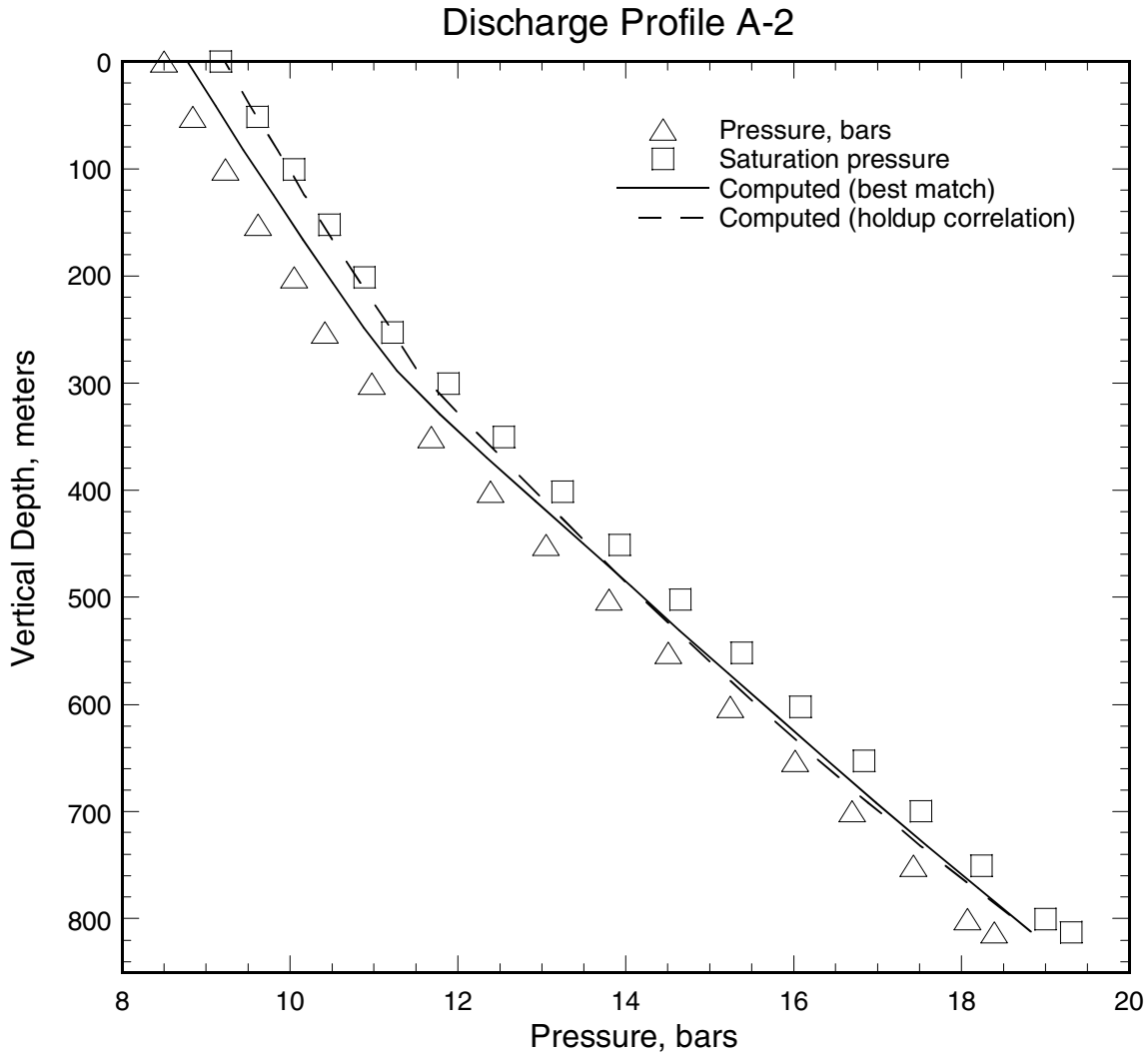

Figure C.2. Pressure profile (triangles) recorded in discharging well A-2. The squares indicate saturation pressure corresponding to the local measured temperature. The solid line is the computed pressure profile using an adjustable holdup correlation (see Section 2 for details). The computed pressure profile using the correlation(s) for *K(Z)* developed in Section 3 is shown as a dashed line.

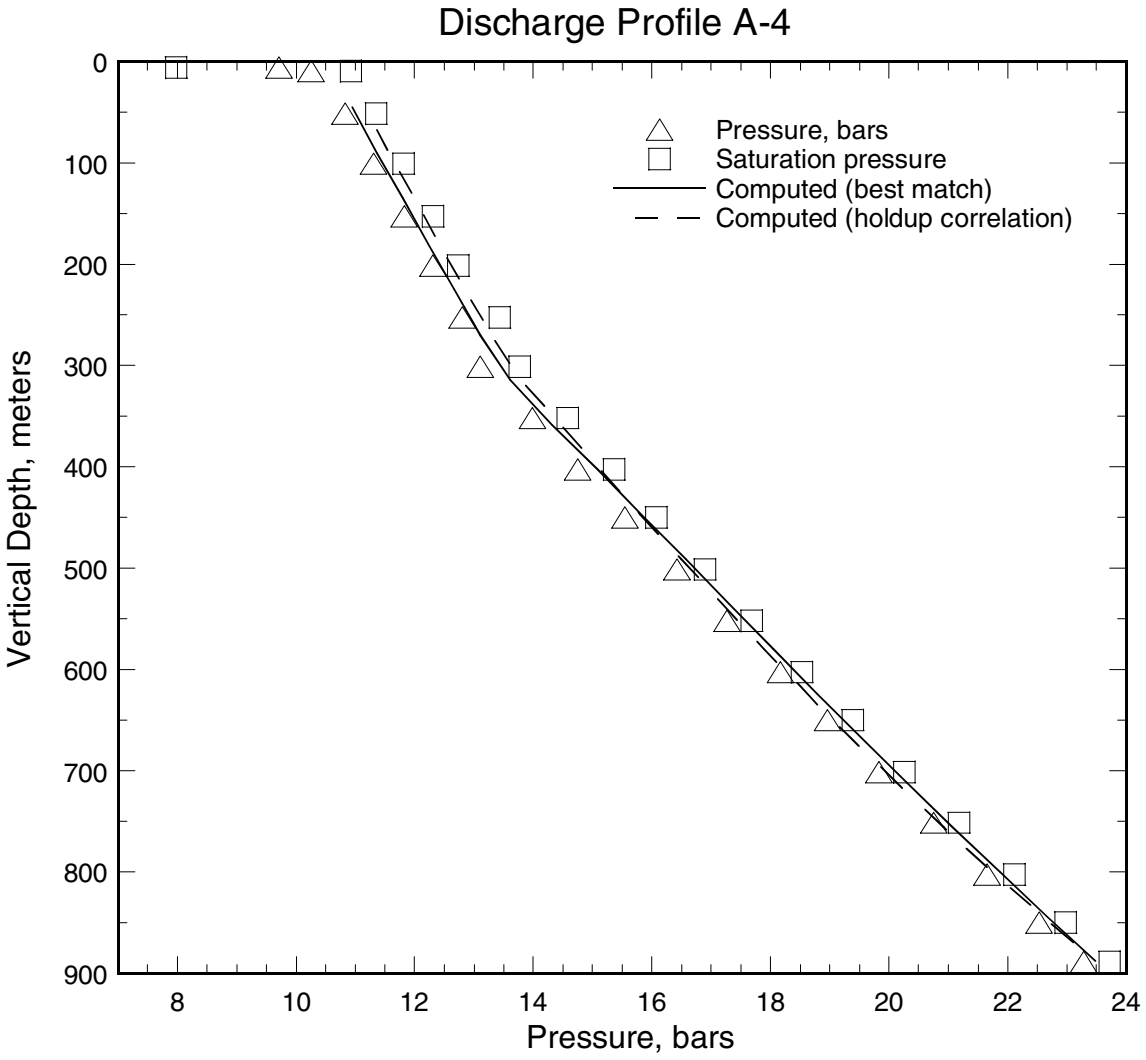

Figure C.3. Pressure profile (triangles) recorded in discharging well A-4. The squares indicate saturation pressure corresponding to the local measured temperature. The solid line is the computed pressure profile using an adjustable holdup correlation (see Section 2 for details). The computed pressure profile using the correlation(s) for *K(Z)* developed in Section 3 is shown as a dashed line.

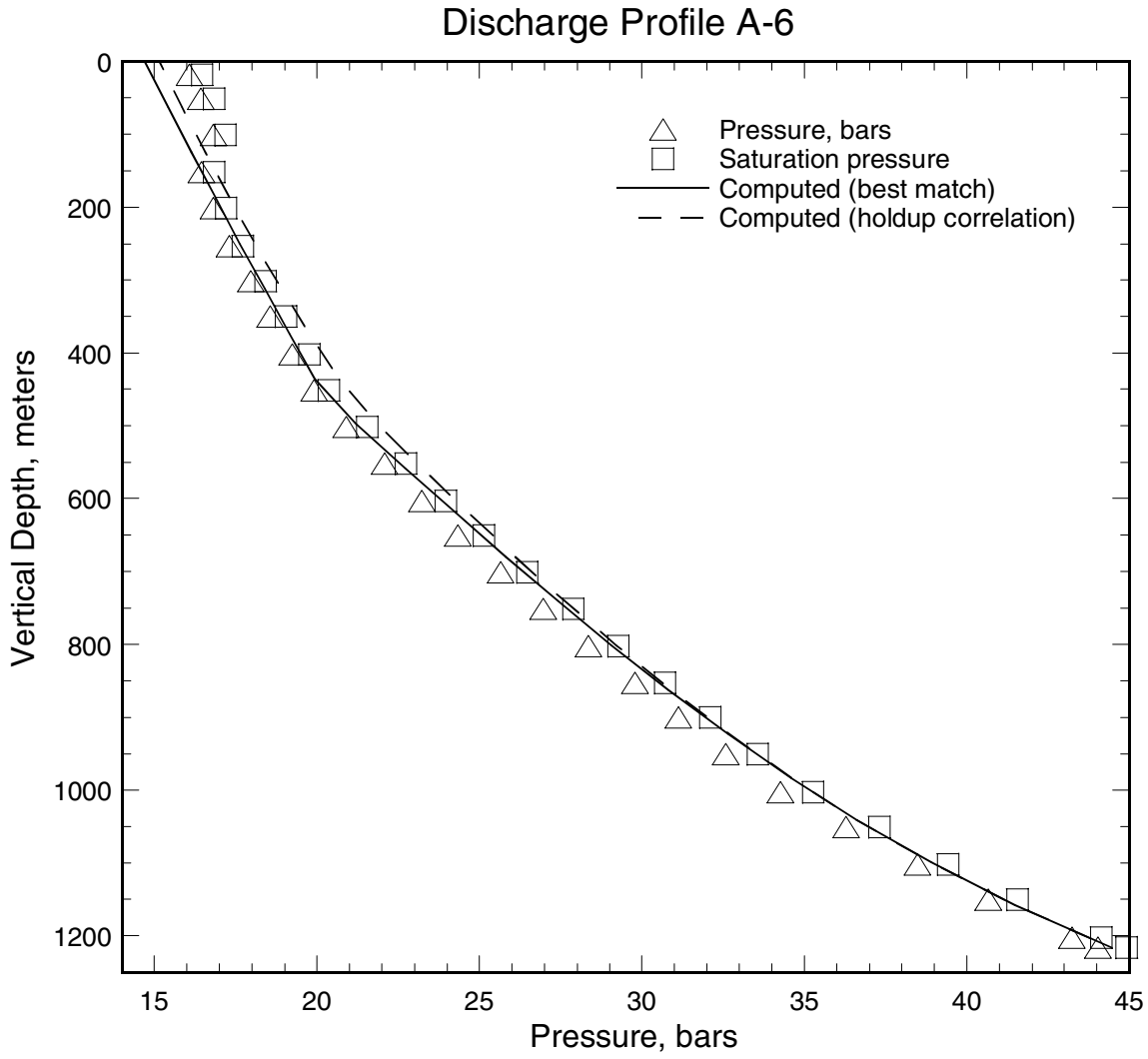

Figure C.4. Pressure profile (triangles) recorded in discharging well A-6. The squares indicate saturation pressure corresponding to the local measured temperature. The solid line is the computed pressure profile using an adjustable holdup correlation (see Section 2 for details). The computed pressure profile using the correlation(s) for *K(Z)* developed in Section 3 is shown as a dashed line.

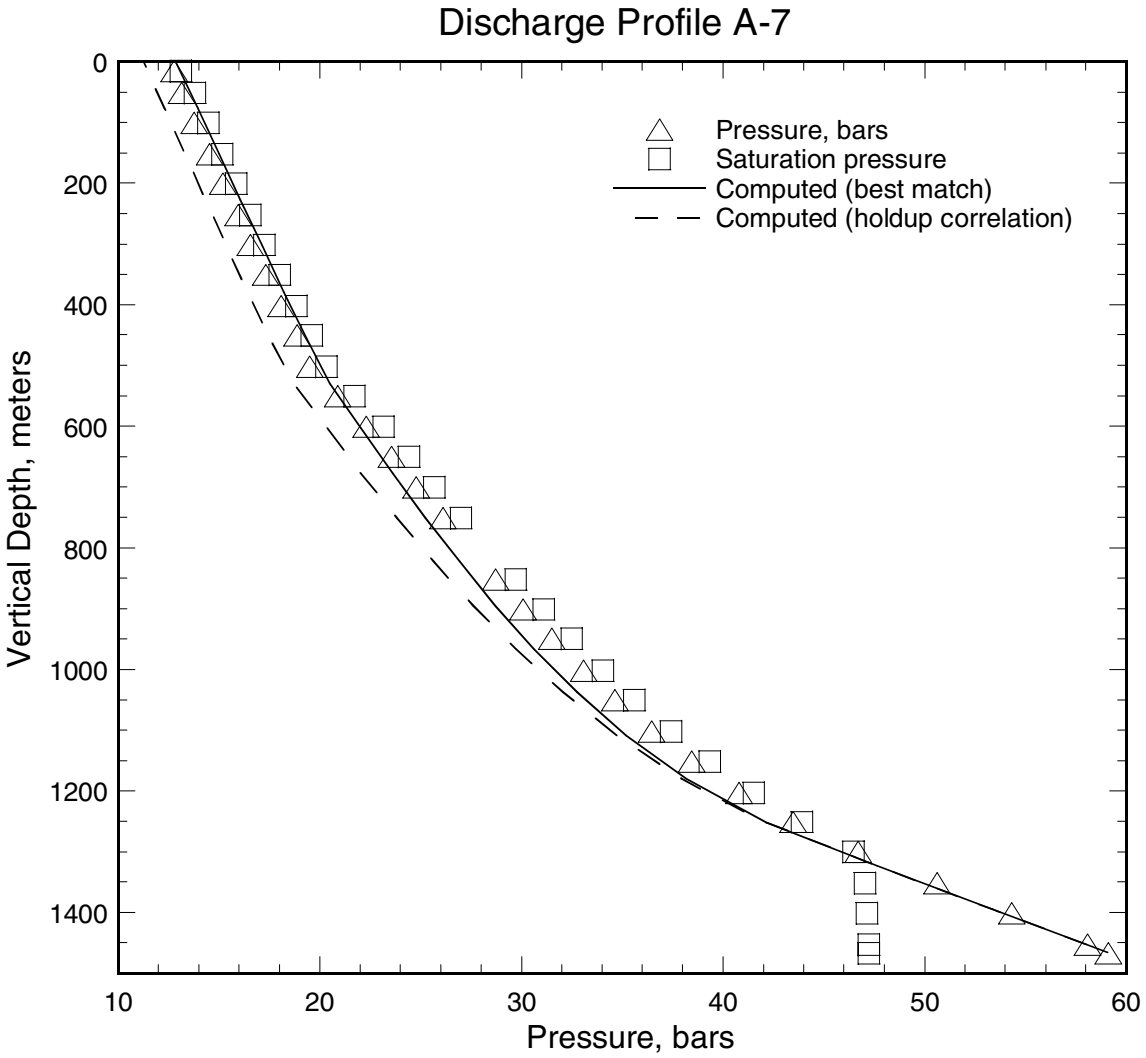

Figure C.5. Pressure profile (triangles) recorded in discharging well A-7. The squares indicate saturation pressure corresponding to the local measured temperature. The solid line is the computed pressure profile using an adjustable holdup correlation (see Section 2 for details). The computed pressure profile using the correlation(s) for *K(Z)* developed in Section 3 is shown as a dashed line.

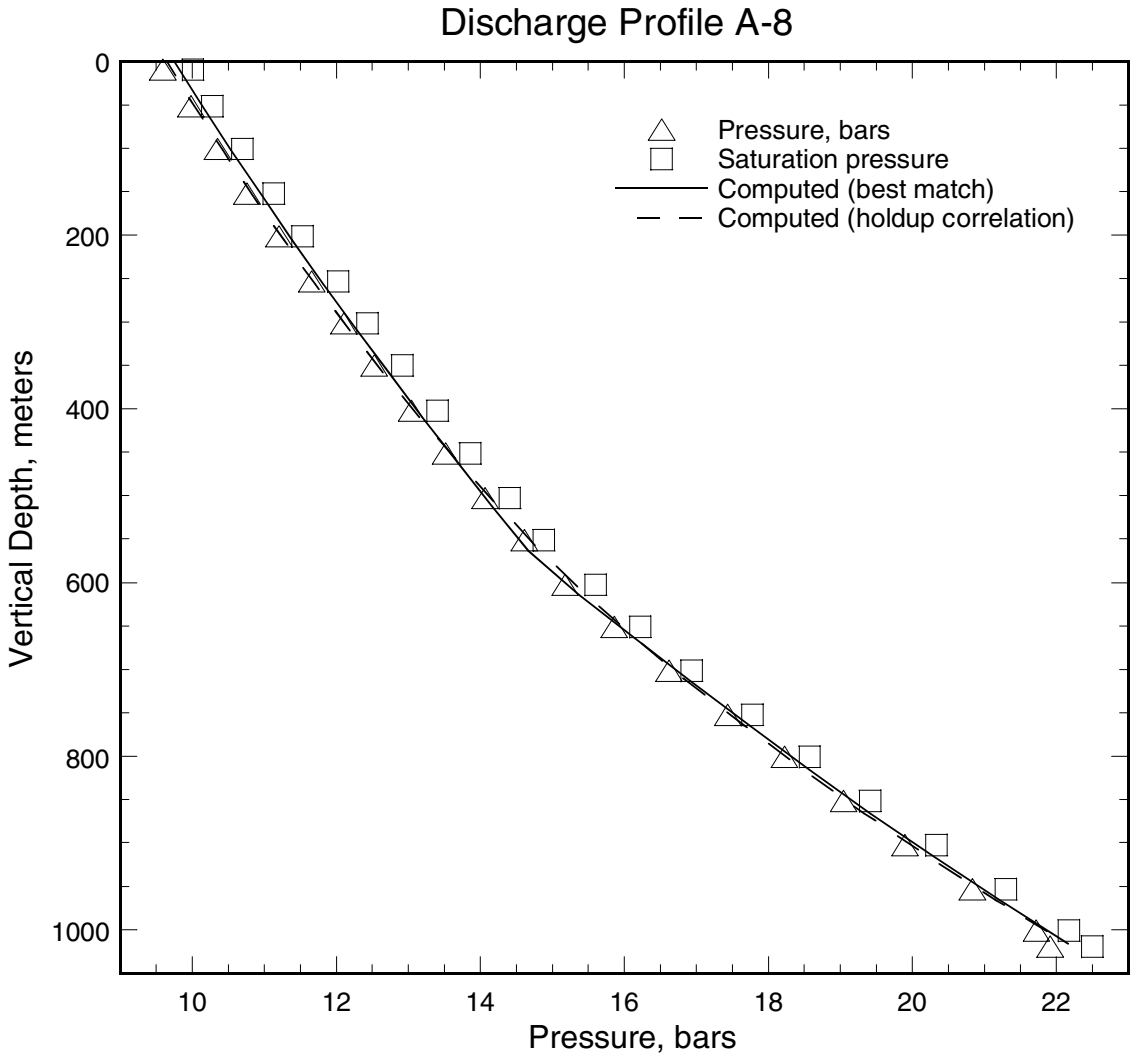

Figure C.6. Pressure profile (triangles) recorded in discharging well A-8. The squares indicate saturation pressure corresponding to the local measured temperature. The solid line is the computed pressure profile using an adjustable holdup correlation (see Section 2 for details). The computed pressure profile using the correlation(s) for *K(Z)* developed in Section 3 is shown as a dashed line.

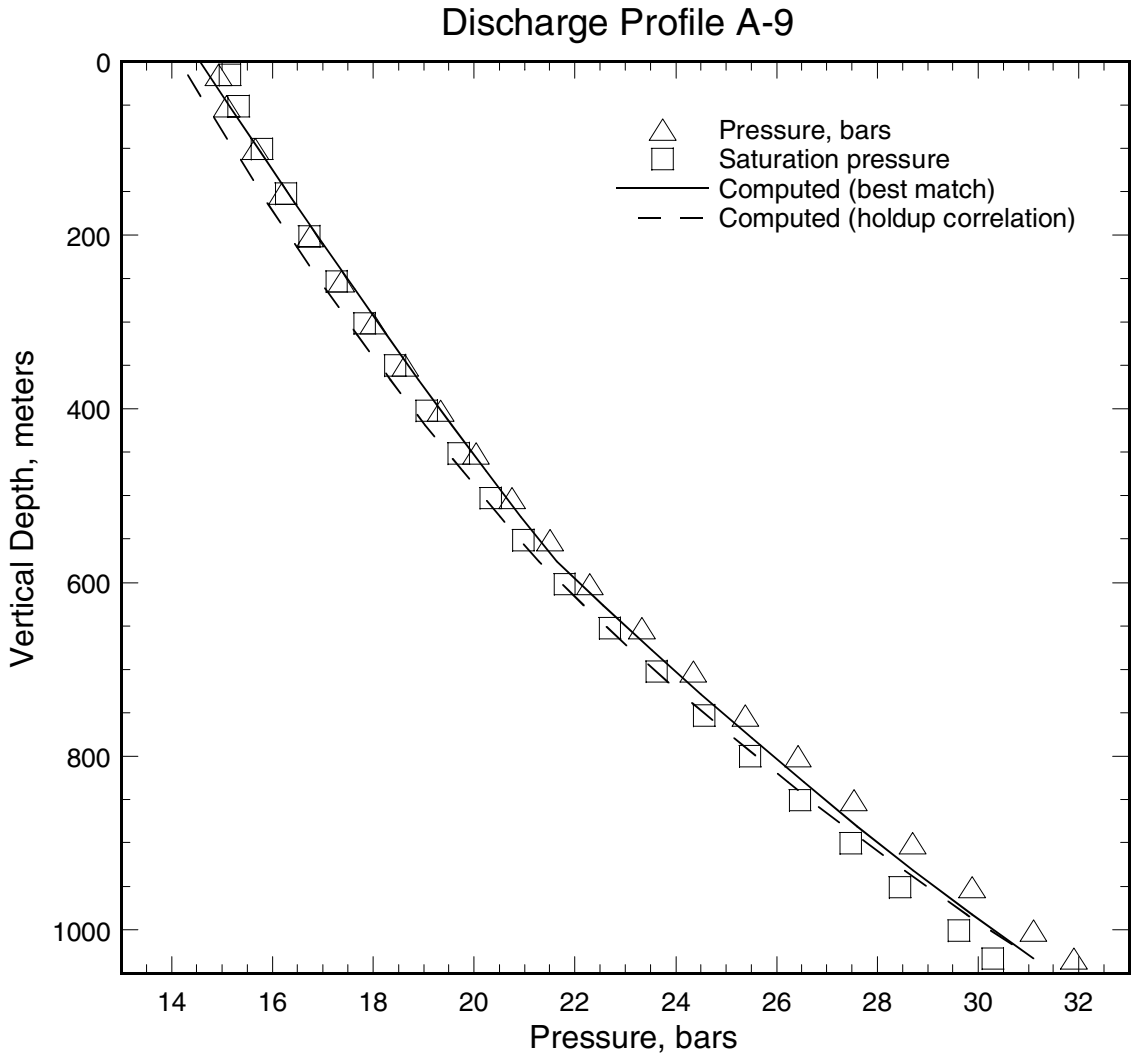

Figure C.7. Pressure profile (triangles) recorded in discharging well A-9. The squares indicate saturation pressure corresponding to the local measured temperature. The solid line is the computed pressure profile using an adjustable holdup correlation (see Section 2 for details). The computed pressure profile using the correlation(s) for *K(Z)* developed in Section 3 is shown as a dashed line.

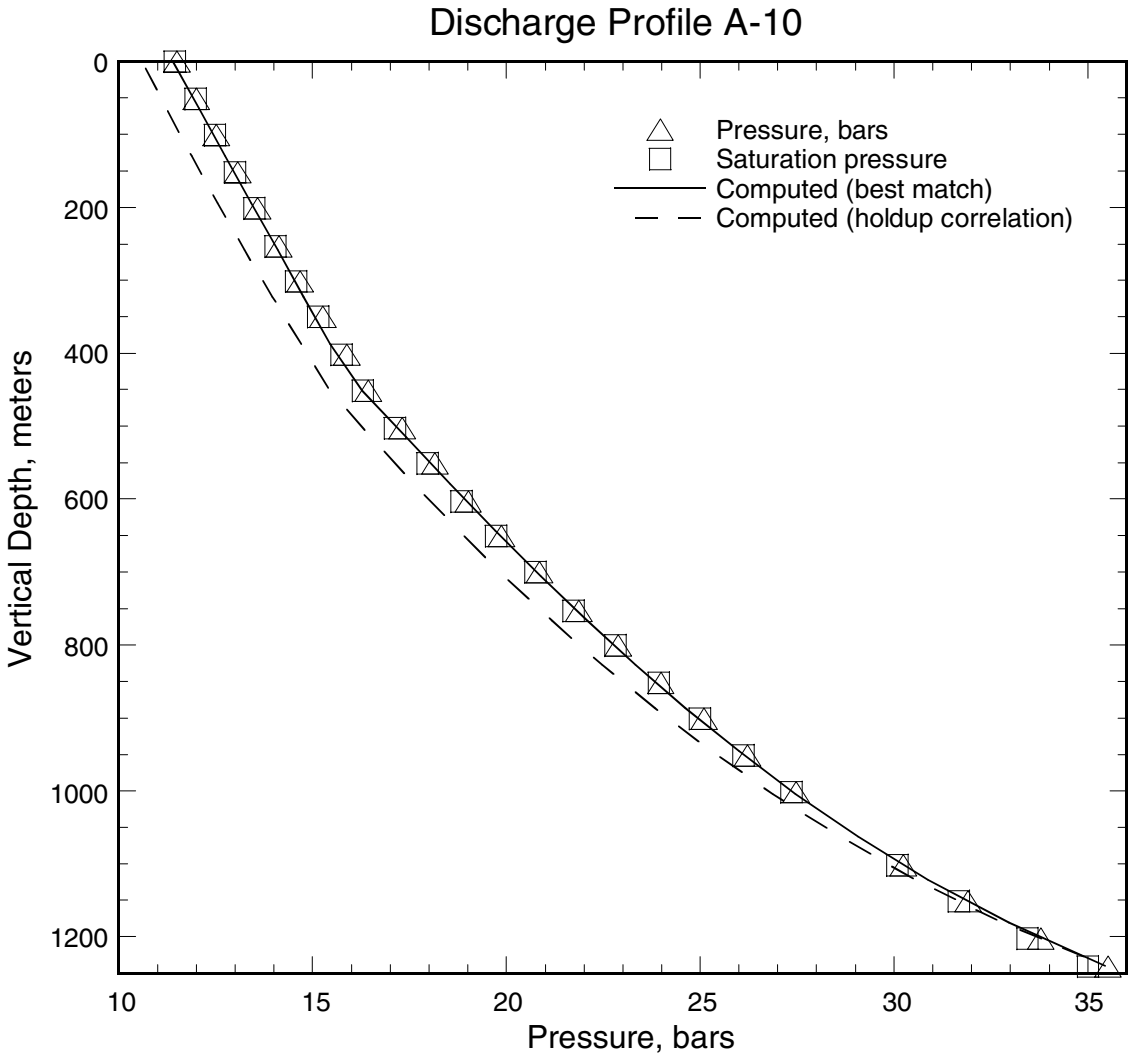

Figure C.8. Pressure profile (triangles) recorded in discharging well A-10. The squares indicate saturation pressure corresponding to the local measured temperature. The solid line is the computed pressure profile using an adjustable holdup correlation (see Section 2 for details). The computed pressure profile using the correlation(s) for *K(Z)* developed in Section 3 is shown as a dashed line.

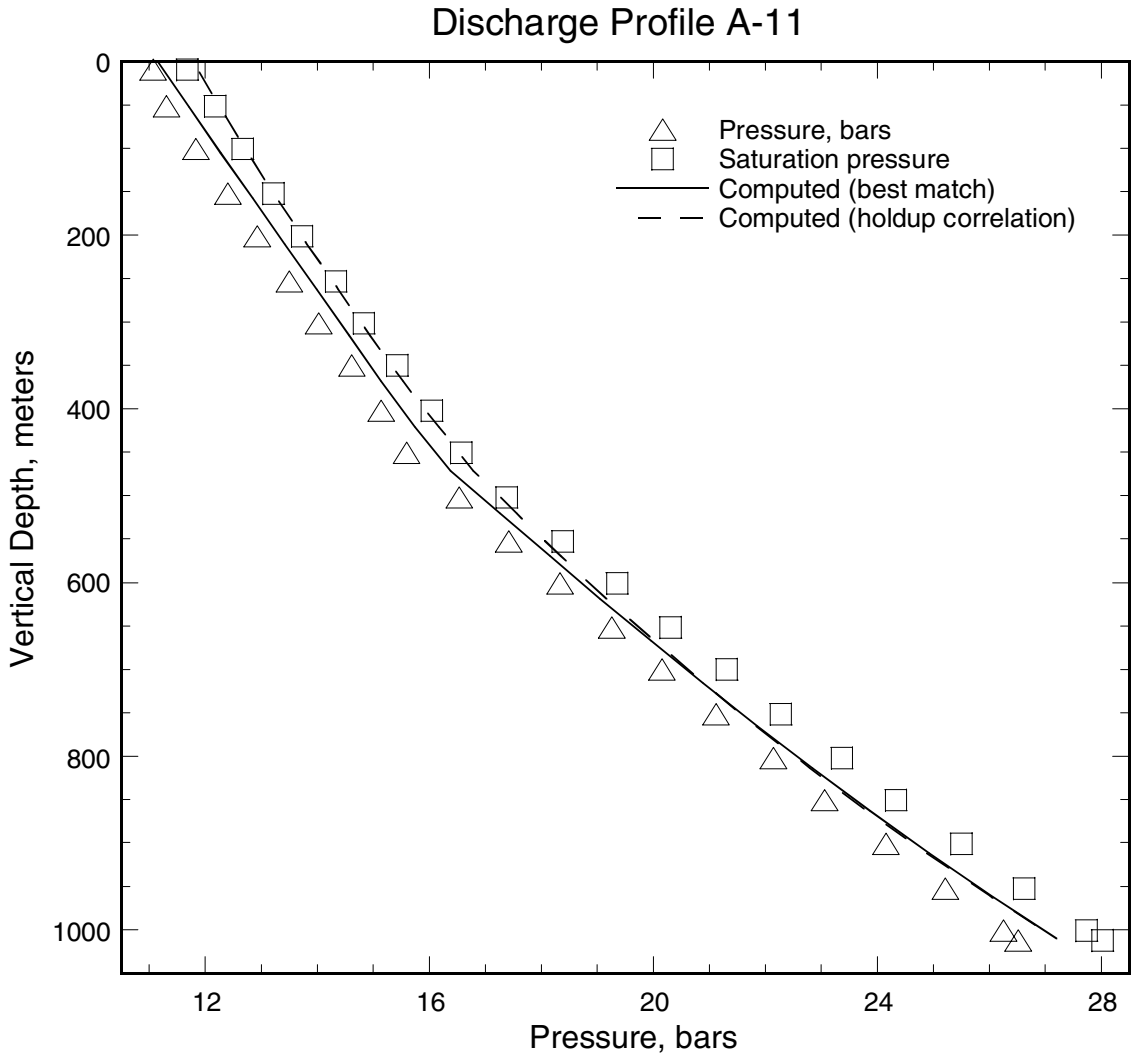

Figure C.9. Pressure profile (triangles) recorded in discharging well A-11. The squares indicate saturation pressure corresponding to the local measured temperature. The solid line is the computed pressure profile using an adjustable holdup correlation (see Section 2 for details). The computed pressure profile using the correlation(s) for *K(Z)* developed in Section 3 is shown as a dashed line.

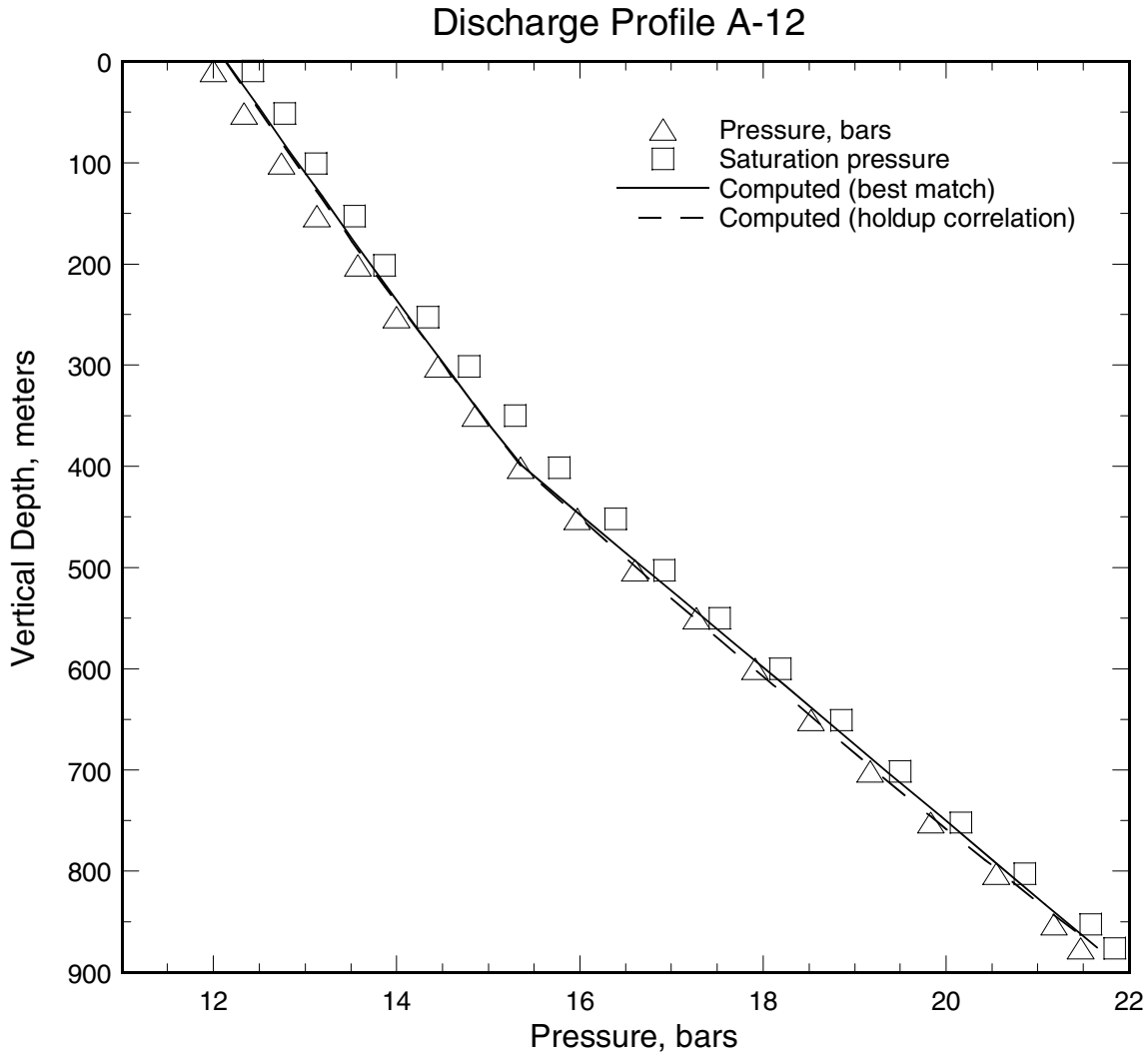

Figure C.10. Pressure profile (triangles) recorded in discharging well A-12. The squares indicate saturation pressure corresponding to the local measured temperature. The solid line is the computed pressure profile using an adjustable holdup correlation (see Section 2 for details). The computed pressure profile using the correlation(s) for *K(Z)* developed in Section 3 is shown as a dashed line.

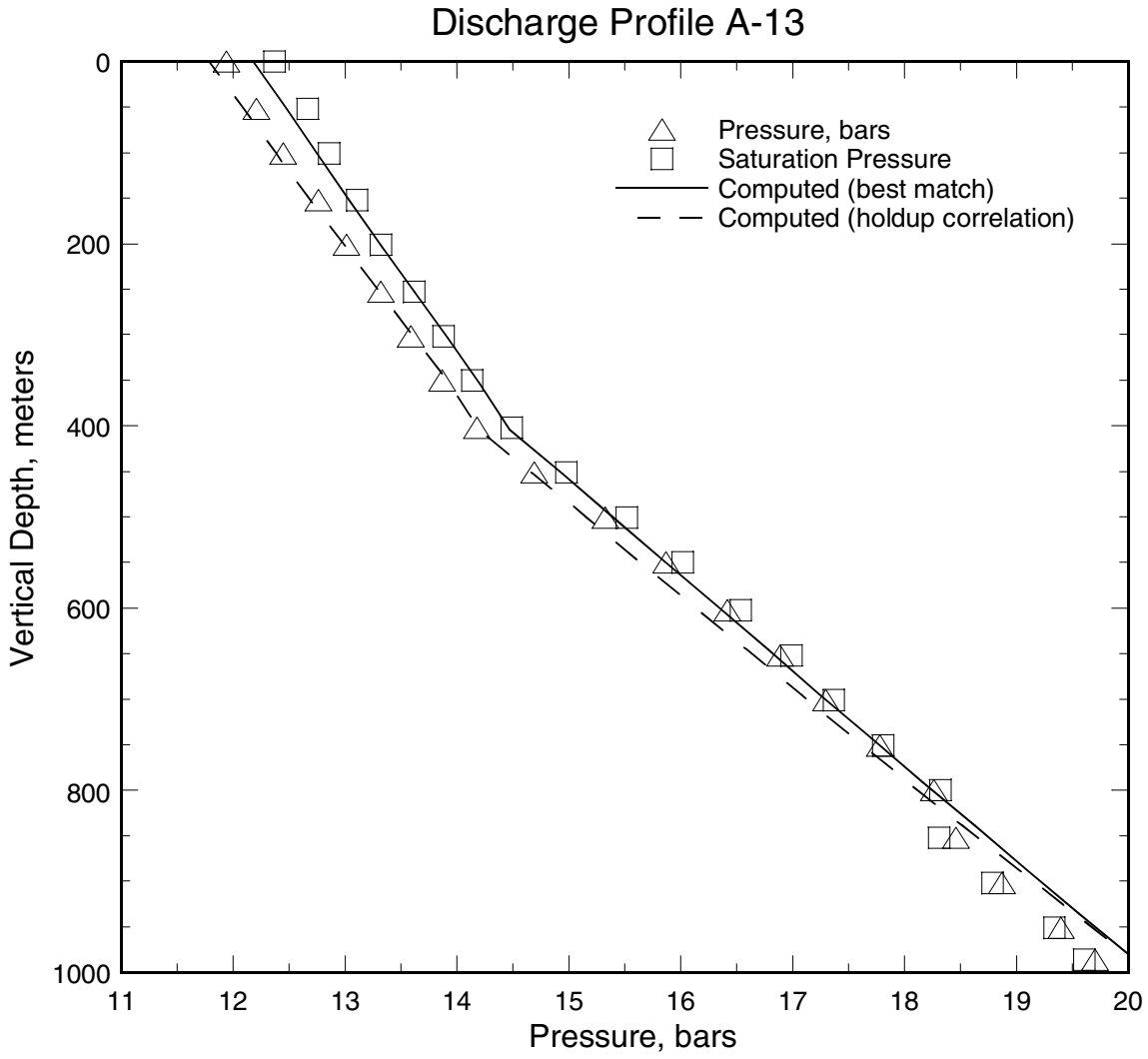

Figure C.11. Pressure profile (triangles) recorded in discharging well A-13. The squares indicate saturation pressure corresponding to the local measured temperature. The solid line is the computed pressure profile using an adjustable holdup correlation (see Section 2 for details). The computed pressure profile using the correlation(s) for *K(Z)* developed in Section 3 is shown as a dashed line.

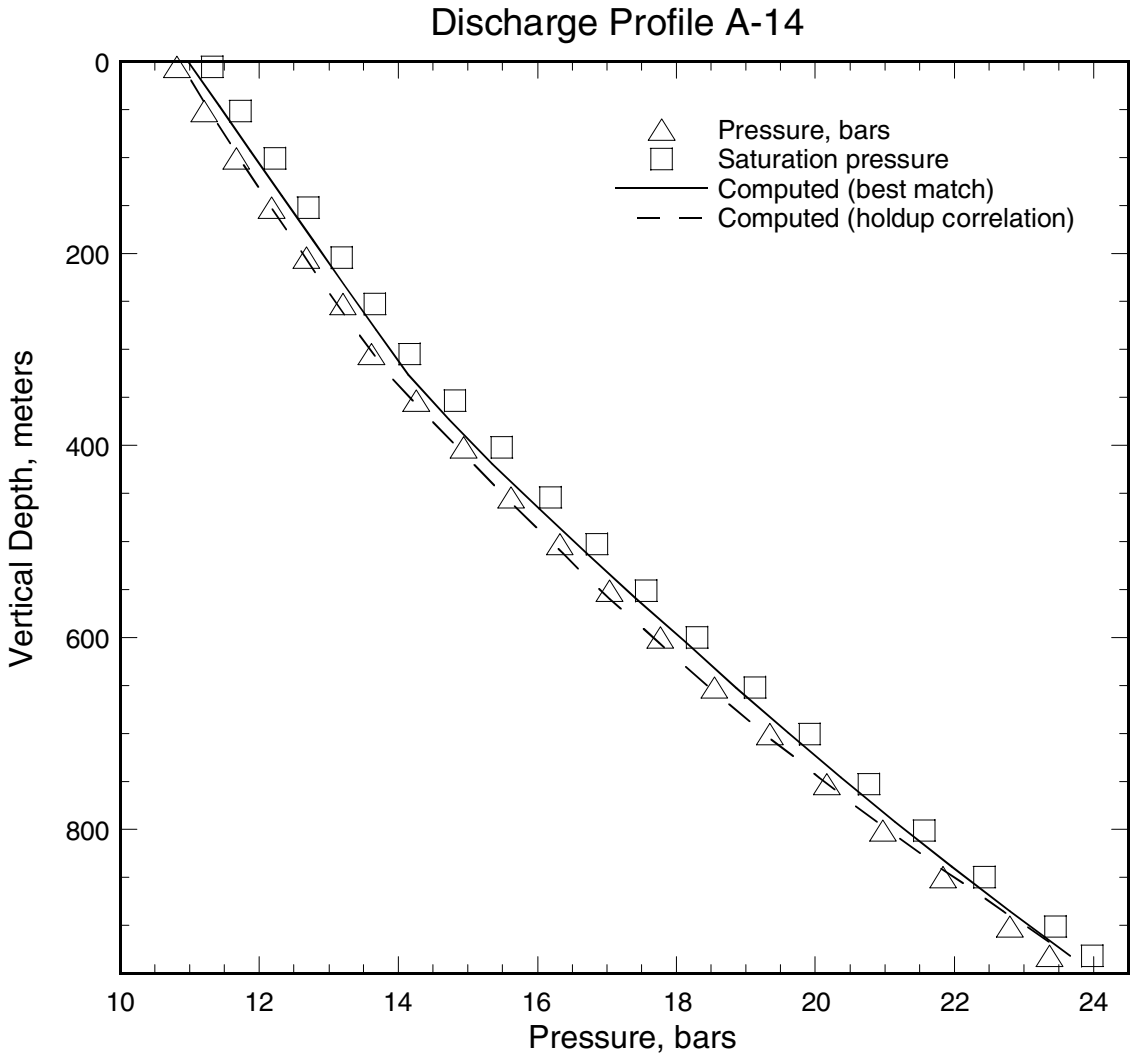

Figure C.12. Pressure profile (triangles) recorded in discharging well A-14. The squares indicate saturation pressure corresponding to the local measured temperature. The solid line is the computed pressure profile using an adjustable holdup correlation (see Section 2 for details). The computed pressure profile using the correlation(s) for *K(Z)* developed in Section 3 is shown as a dashed line.

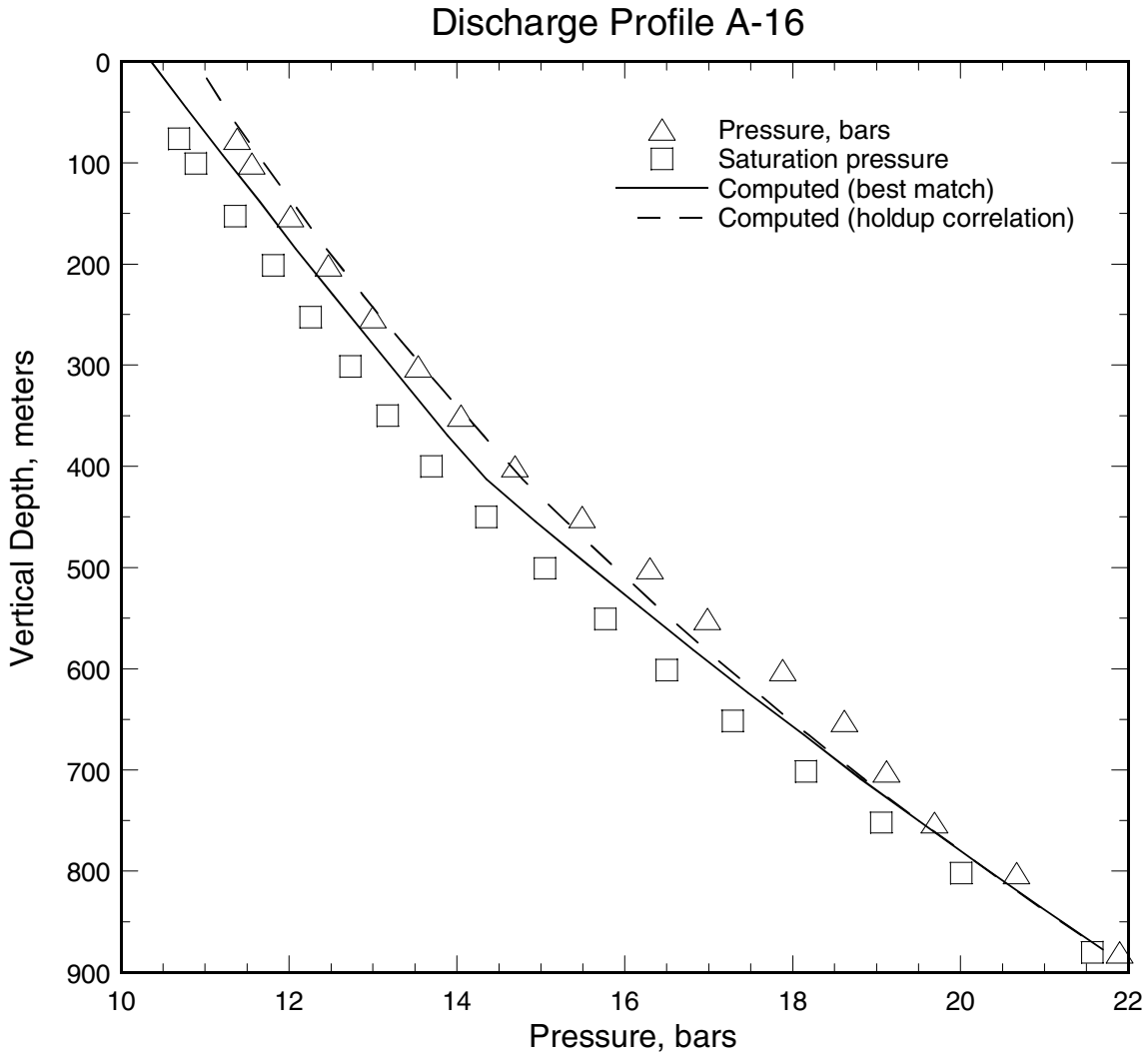

Figure C.13. Pressure profile (triangles) recorded in discharging well A-16. The squares indicate saturation pressure corresponding to the local measured temperature. The solid line is the computed pressure profile using an adjustable holdup correlation (see Section 2 for details). The computed pressure profile using the correlation(s) for *K(Z)* developed in Section 3 is shown as a dashed line.

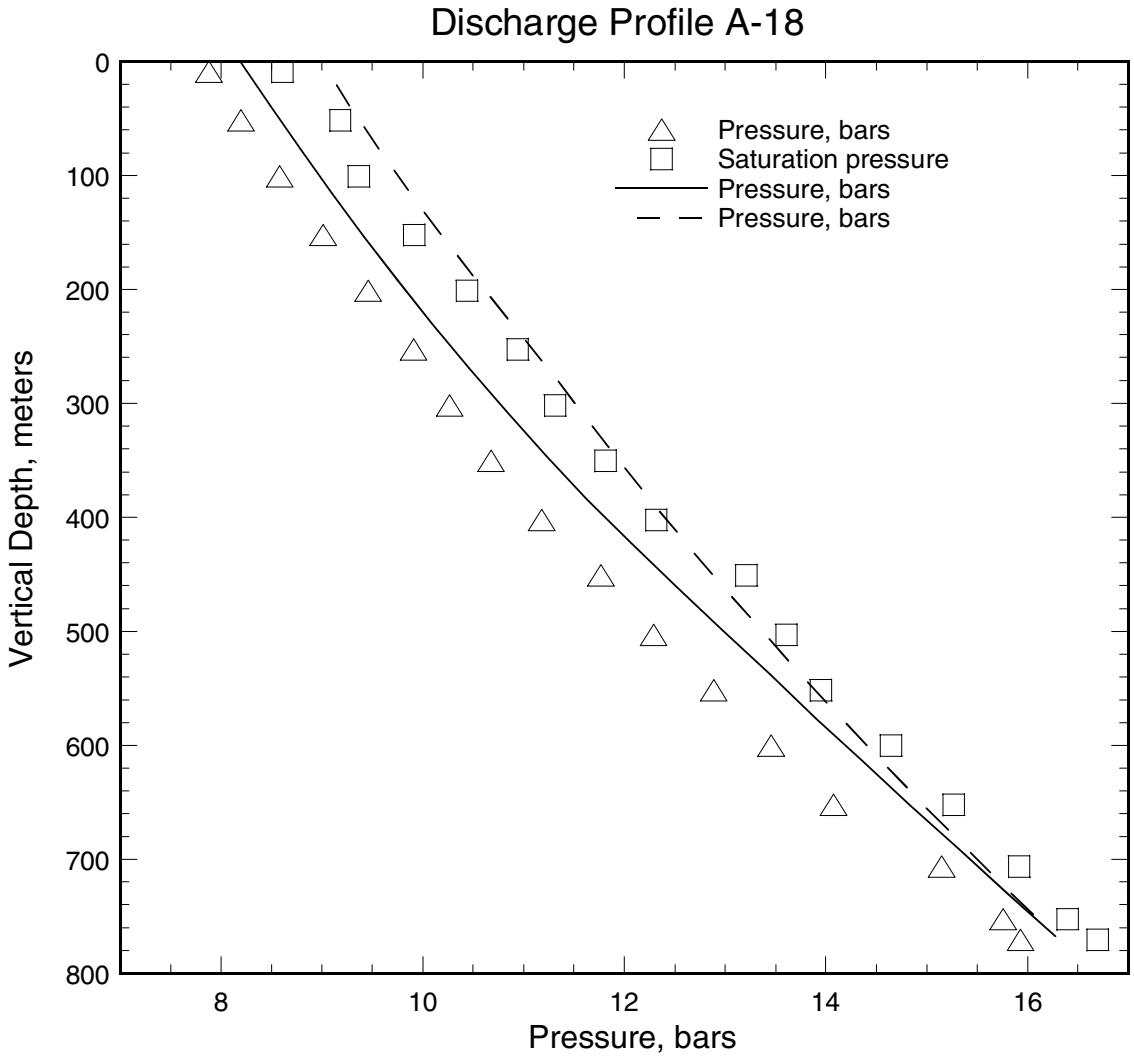

Figure C.14. Pressure profile (triangles) recorded in discharging well A-18. The squares indicate saturation pressure corresponding to the local measured temperature. The solid line is the computed pressure profile using an adjustable holdup correlation (see Section 2 for details). The computed pressure profile using the correlation(s) for *K(Z)* developed in Section 3 is shown as a dashed line.

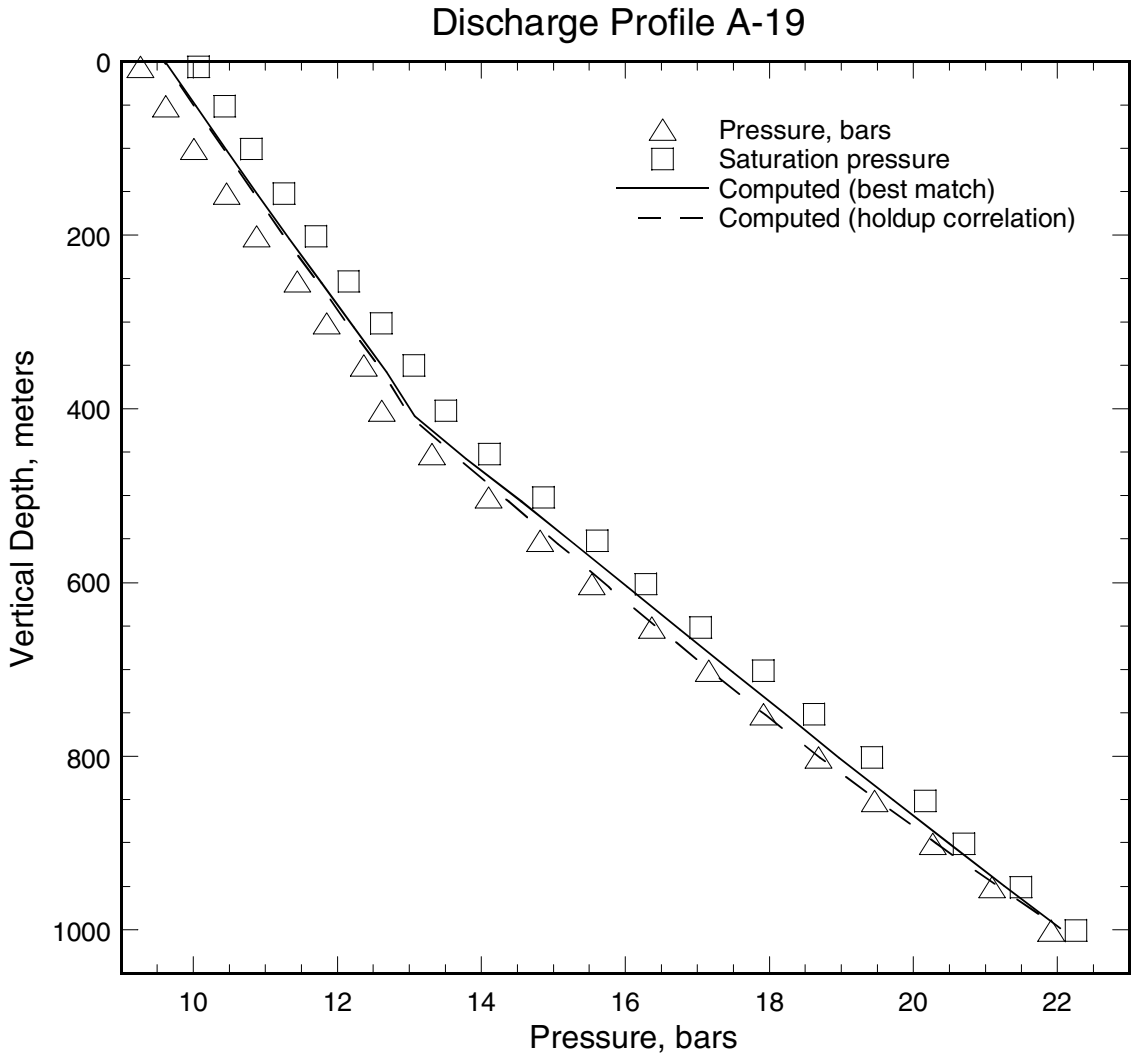

Figure C.15. Pressure profile (triangles) recorded in discharging well A-19. The squares indicate saturation pressure corresponding to the local measured temperature. The solid line is the computed pressure profile using an adjustable holdup correlation (see Section 2 for details). The computed pressure profile using the correlation(s) for *K(Z)* developed in Section 3 is shown as a dashed line.

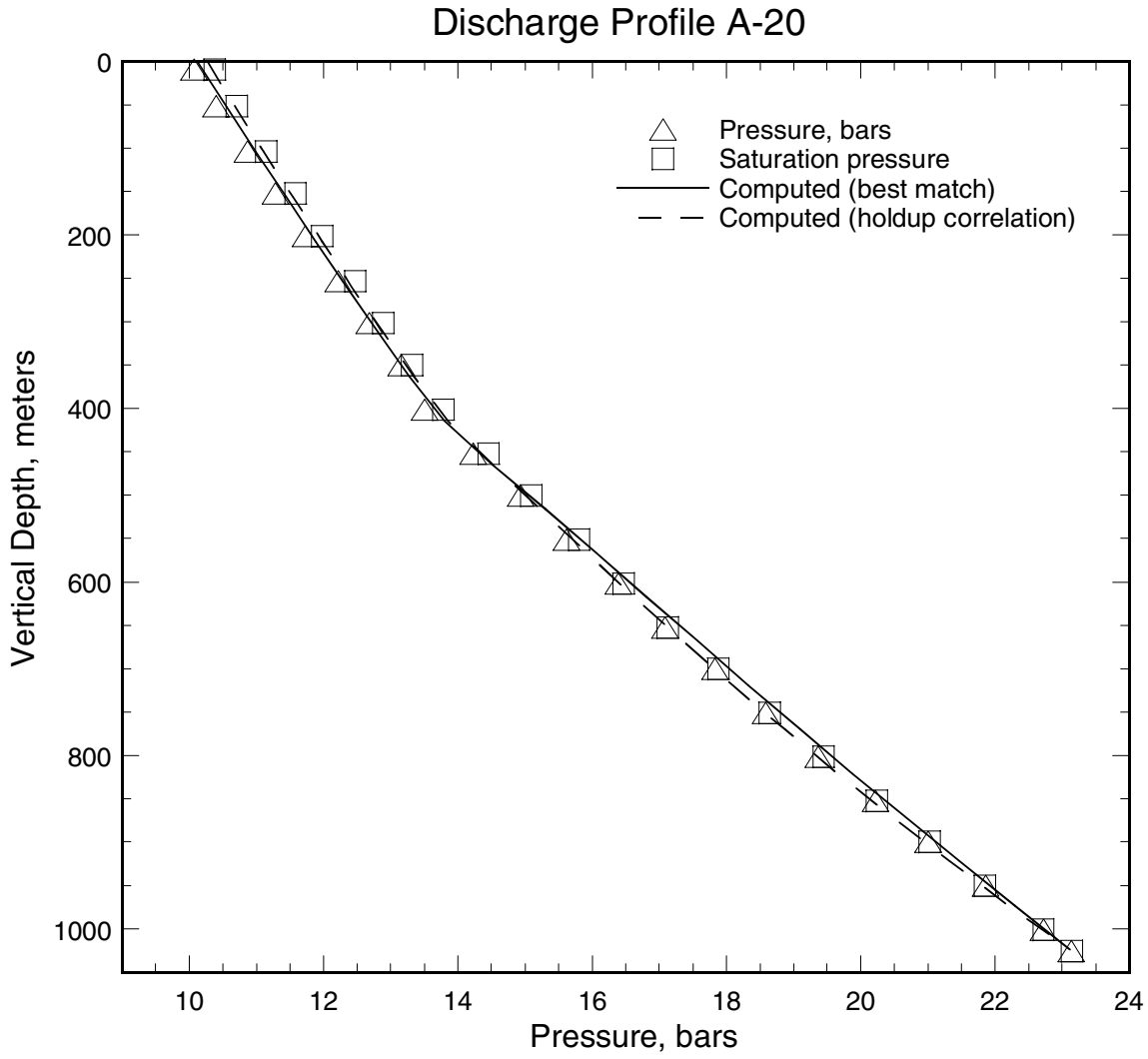

Figure C.16. Pressure profile (triangles) recorded in discharging well A-20. The squares indicate saturation pressure corresponding to the local measured temperature. The solid line is the computed pressure profile using an adjustable holdup correlation (see Section 2 for details). The computed pressure profile using the correlation(s) for *K(Z)* developed in Section 3 is shown as a dashed line.

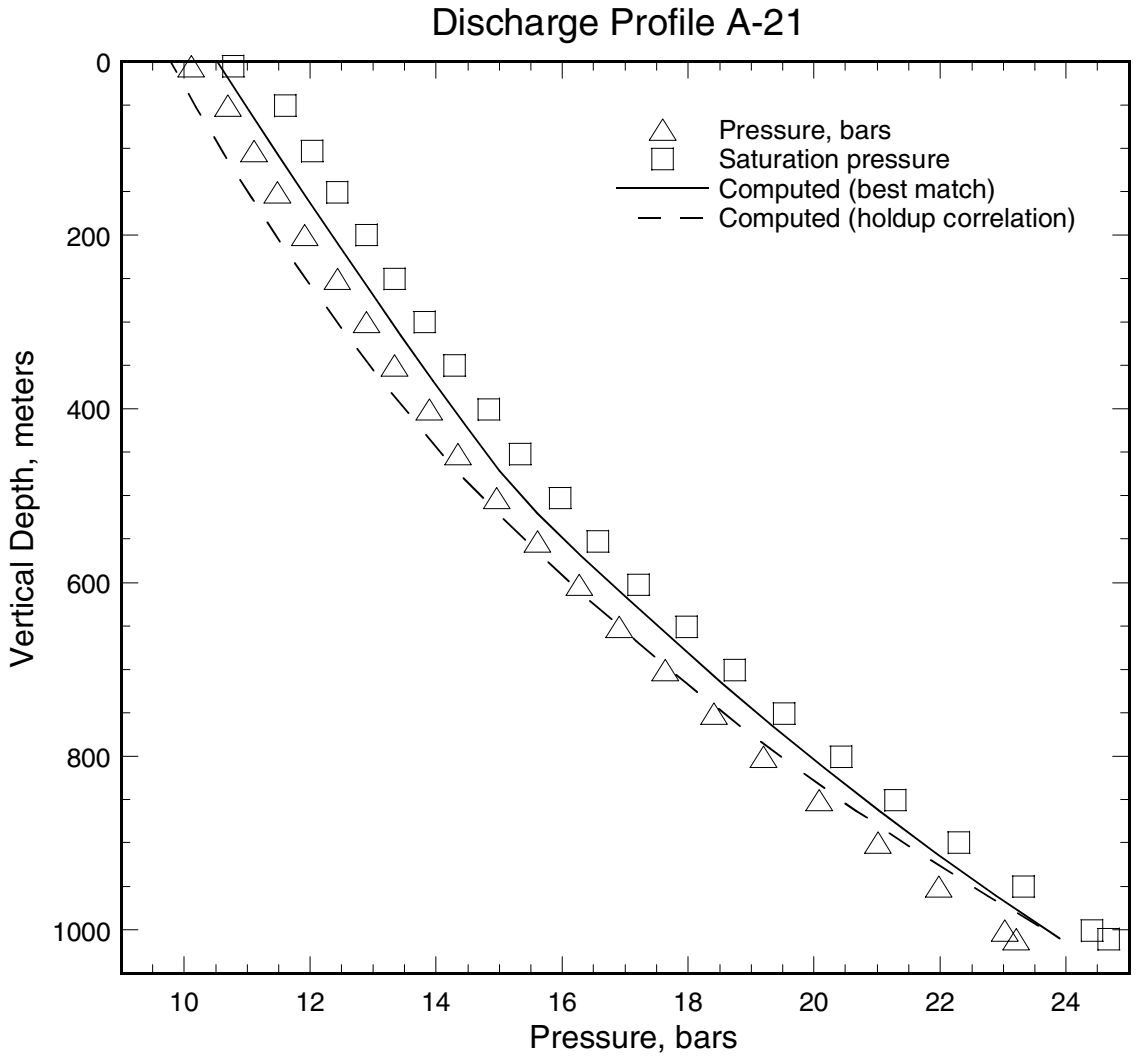

Figure C.17. Pressure profile (triangles) recorded in discharging well A-21. The squares indicate saturation pressure corresponding to the local measured temperature. The solid line is the computed pressure profile using an adjustable holdup correlation (see Section 2 for details). The computed pressure profile using the correlation(s) for *K(Z)* developed in Section 3 is shown as a dashed line.

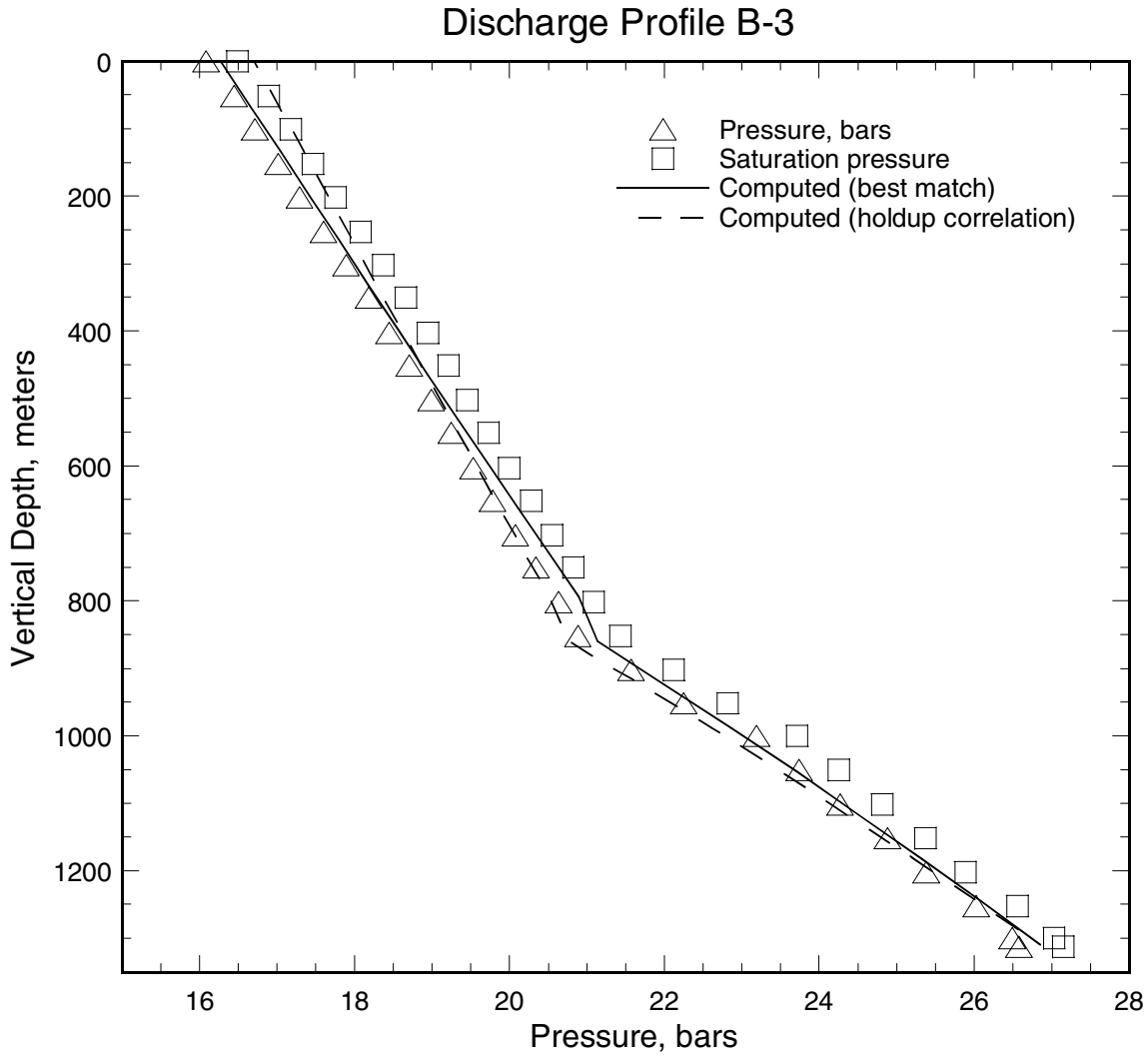

Figure C.18. Pressure profile (triangles) recorded in discharging well B-3. The squares indicate saturation pressure corresponding to the local measured temperature. The solid line is the computed pressure profile using an adjustable holdup correlation (see Section 2 for details). The computed pressure profile using the correlation(s) for *K(Z)* developed in Section 3 is shown as a dashed line.

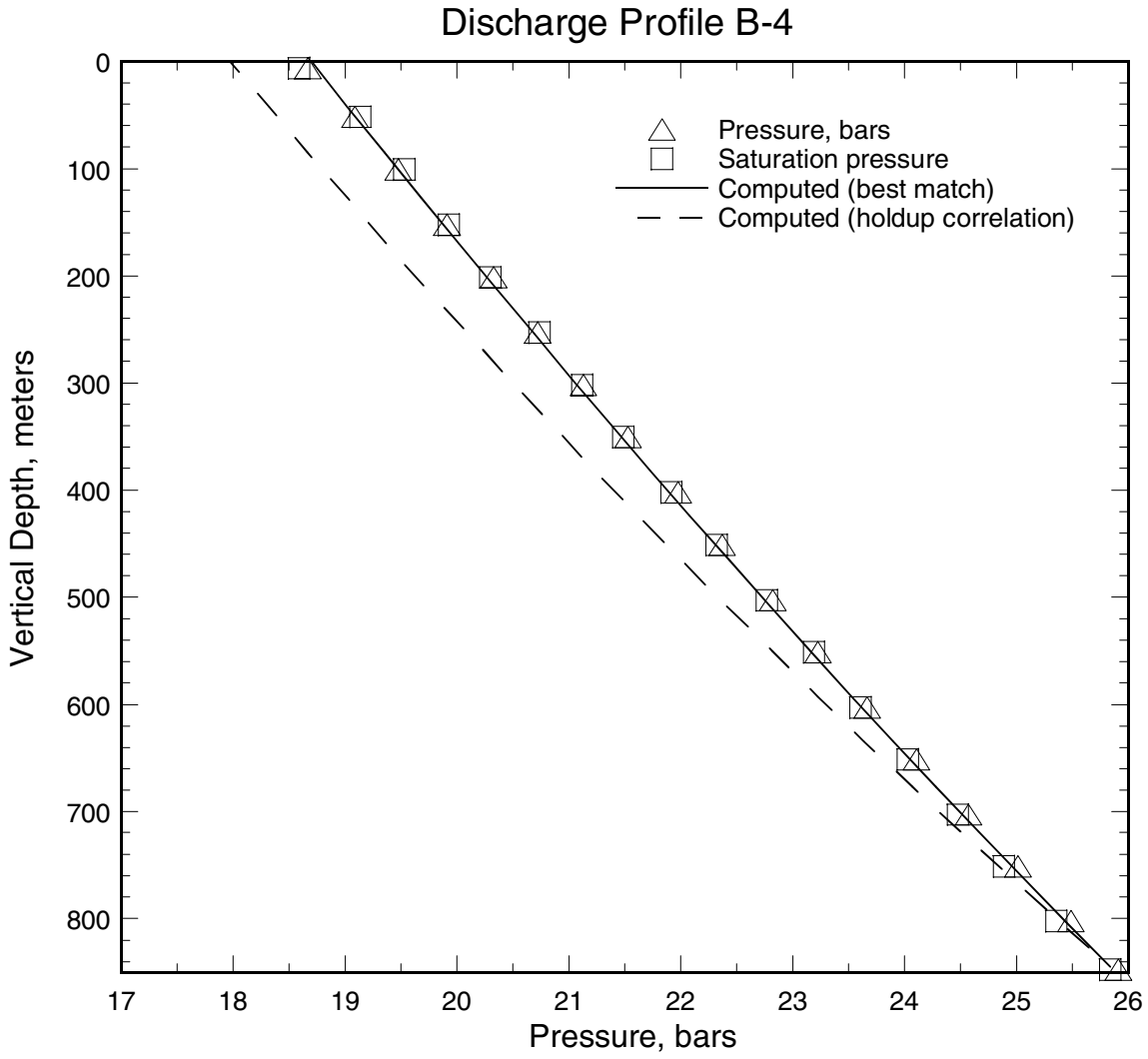

Figure C.19. Pressure profile (triangles) recorded in discharging well B-4. The squares indicate saturation pressure corresponding to the local measured temperature. The solid line is the computed pressure profile using an adjustable holdup correlation (see Section 2 for details). The computed pressure profile using the correlation(s) for *K(Z)* developed in Section 3 is shown as a dashed line.

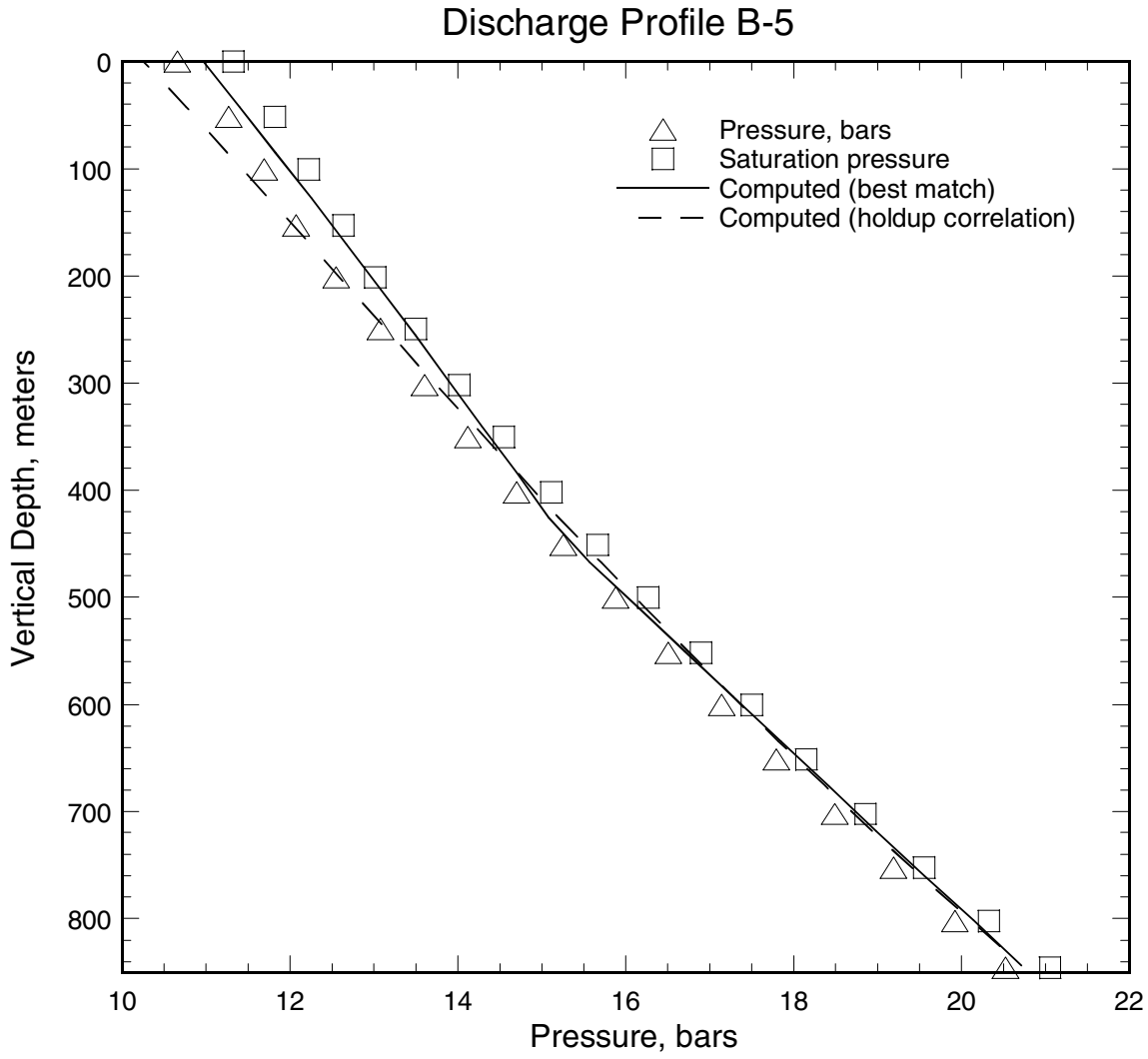

Figure C.20. Pressure profile (triangles) recorded in discharging well B-5. The squares indicate saturation pressure corresponding to the local measured temperature. The solid line is the computed pressure profile using an adjustable holdup correlation (see Section 2 for details). The computed pressure profile using the correlation(s) for *K(Z)* developed in Section 3 is shown as a dashed line.

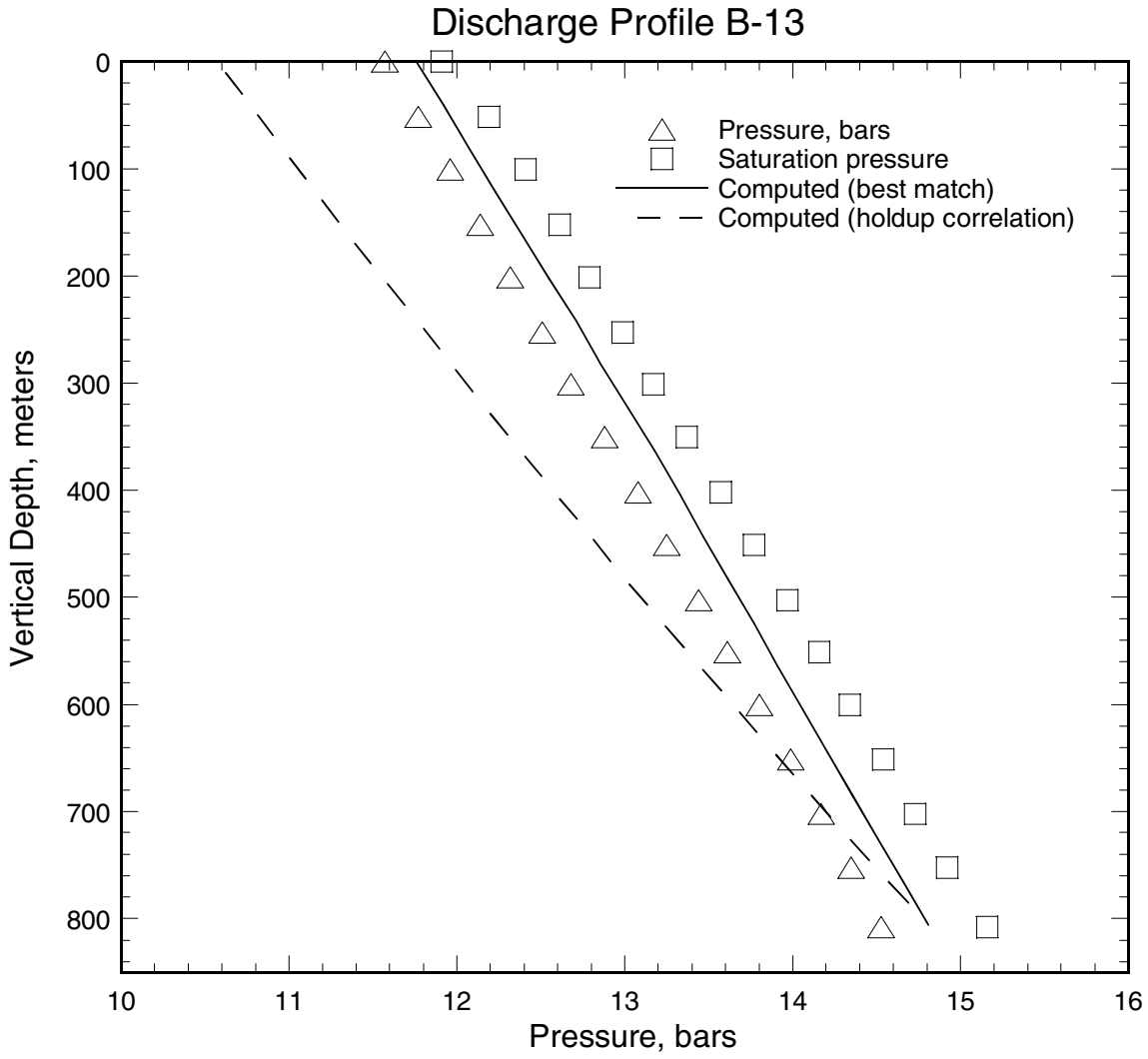

Figure C.21. Pressure profile (triangles) recorded in discharging well B-13. The squares indicate saturation pressure corresponding to the local measured temperature. The solid line is the computed pressure profile using an adjustable holdup correlation (see Section 2 for details). The computed pressure profile using the correlation(s) for *K(Z)* developed in Section 3 is shown as a dashed line.

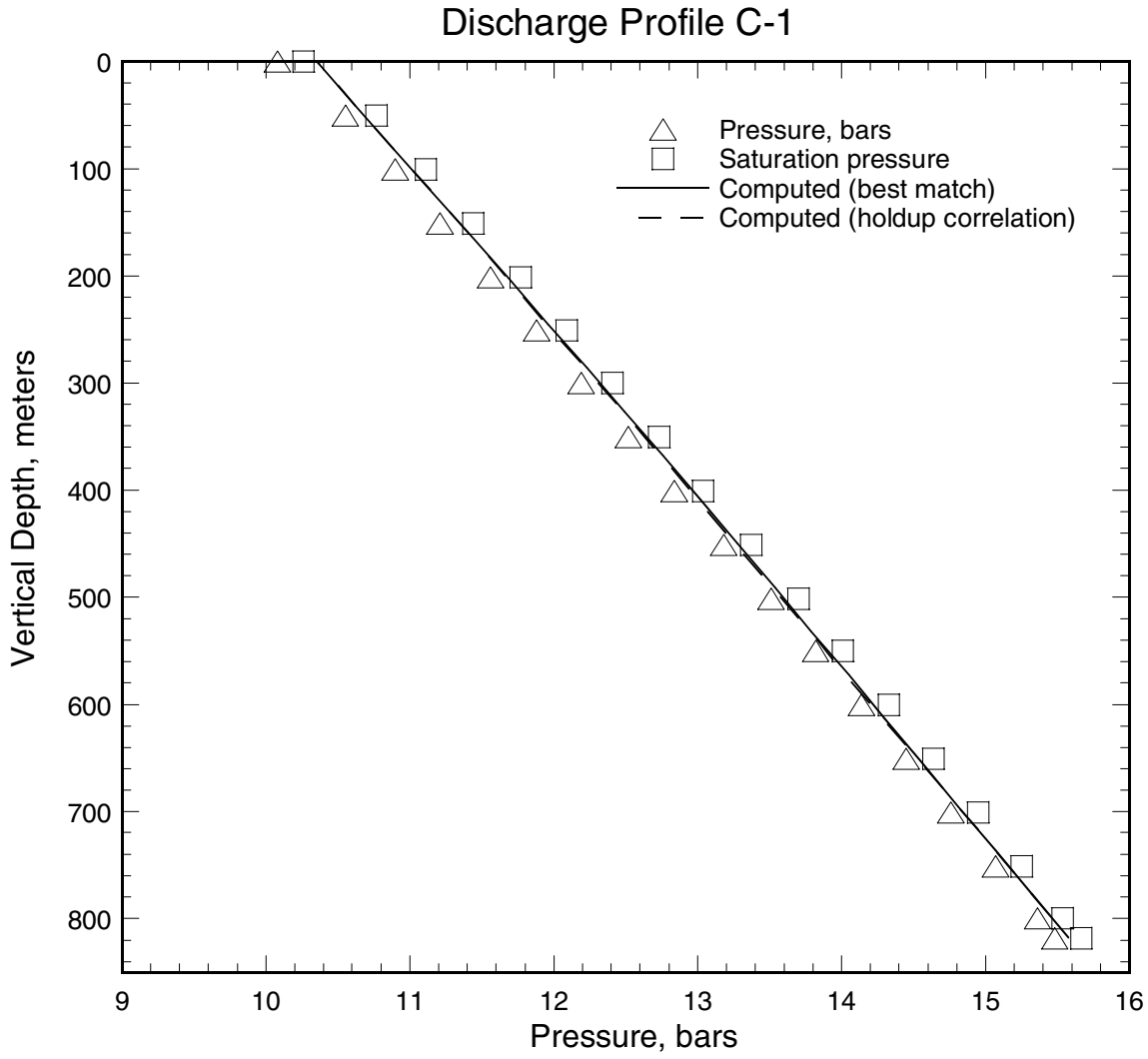

Figure C.22. Pressure profile (triangles) recorded in discharging well C-1. The squares indicate saturation pressure corresponding to the local measured temperature. The solid line is the computed pressure profile using an adjustable holdup correlation (see Section 2 for details). The computed pressure profile using the correlation(s) for *K(Z)* developed in Section 3 is shown as a dashed line.

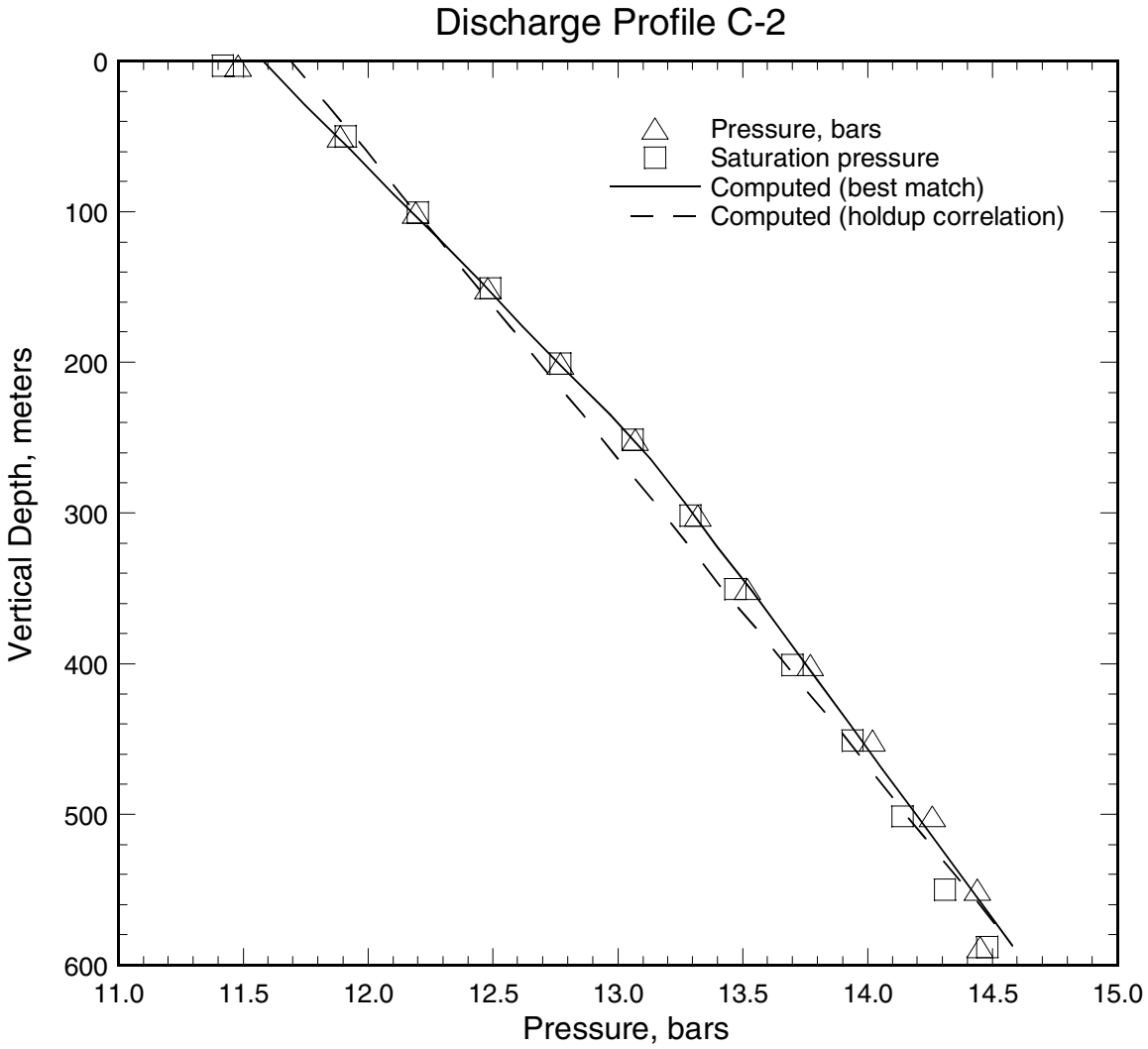

Figure C.23. Pressure profile (triangles) recorded in discharging well C-2. The squares indicate saturation pressure corresponding to the local measured temperature. The solid line is the computed pressure profile using an adjustable holdup correlation (see Section 2 for details). The computed pressure profile using the correlation(s) for *K(Z)* developed in Section 3 is shown as a dashed line.

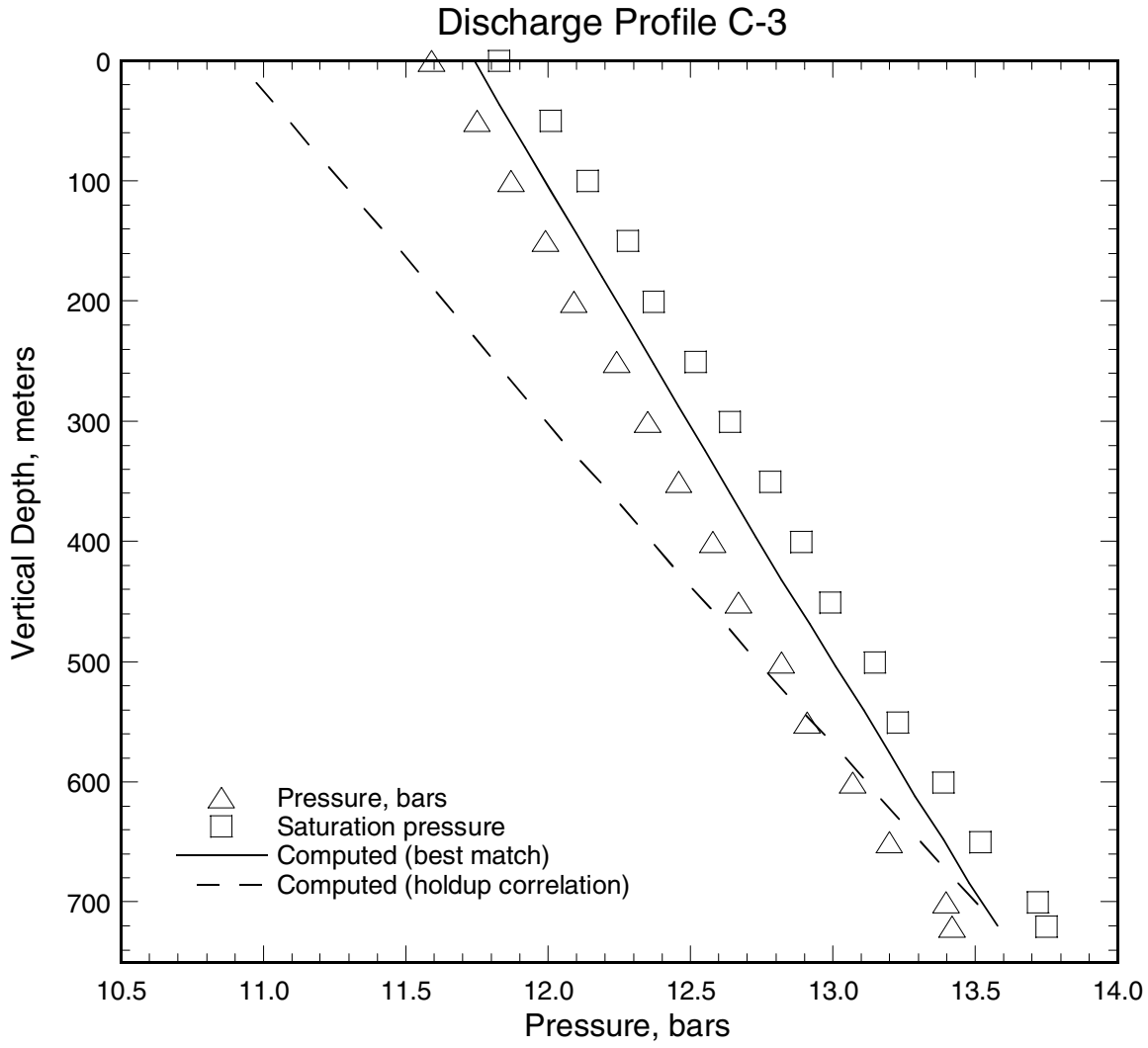

Figure C.24. Pressure profile (triangles) recorded in discharging well C-3. The squares indicate saturation pressure corresponding to the local measured temperature. The solid line is the computed pressure profile using an adjustable holdup correlation (see Section 2 for details). The computed pressure profile using the correlation(s) for *K(Z)* developed in Section 3 is shown as a dashed line.

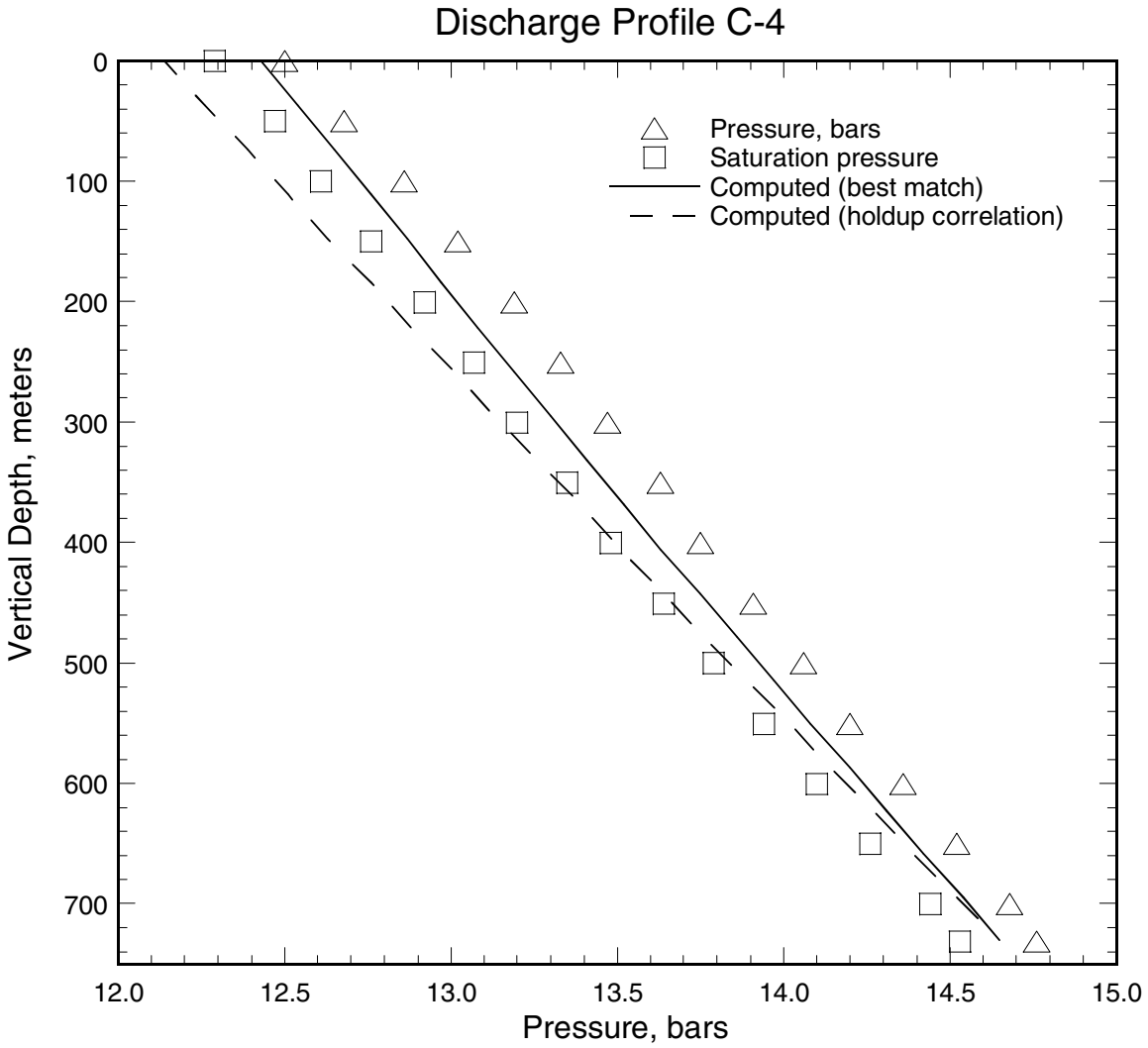

Figure C.25. Pressure profile (triangles) recorded in discharging well C-4. The squares indicate saturation pressure corresponding to the local measured temperature. The solid line is the computed pressure profile using an adjustable holdup correlation (see Section 2 for details). The computed pressure profile using the correlation(s) for *K(Z)* developed in Section 3 is shown as a dashed line.

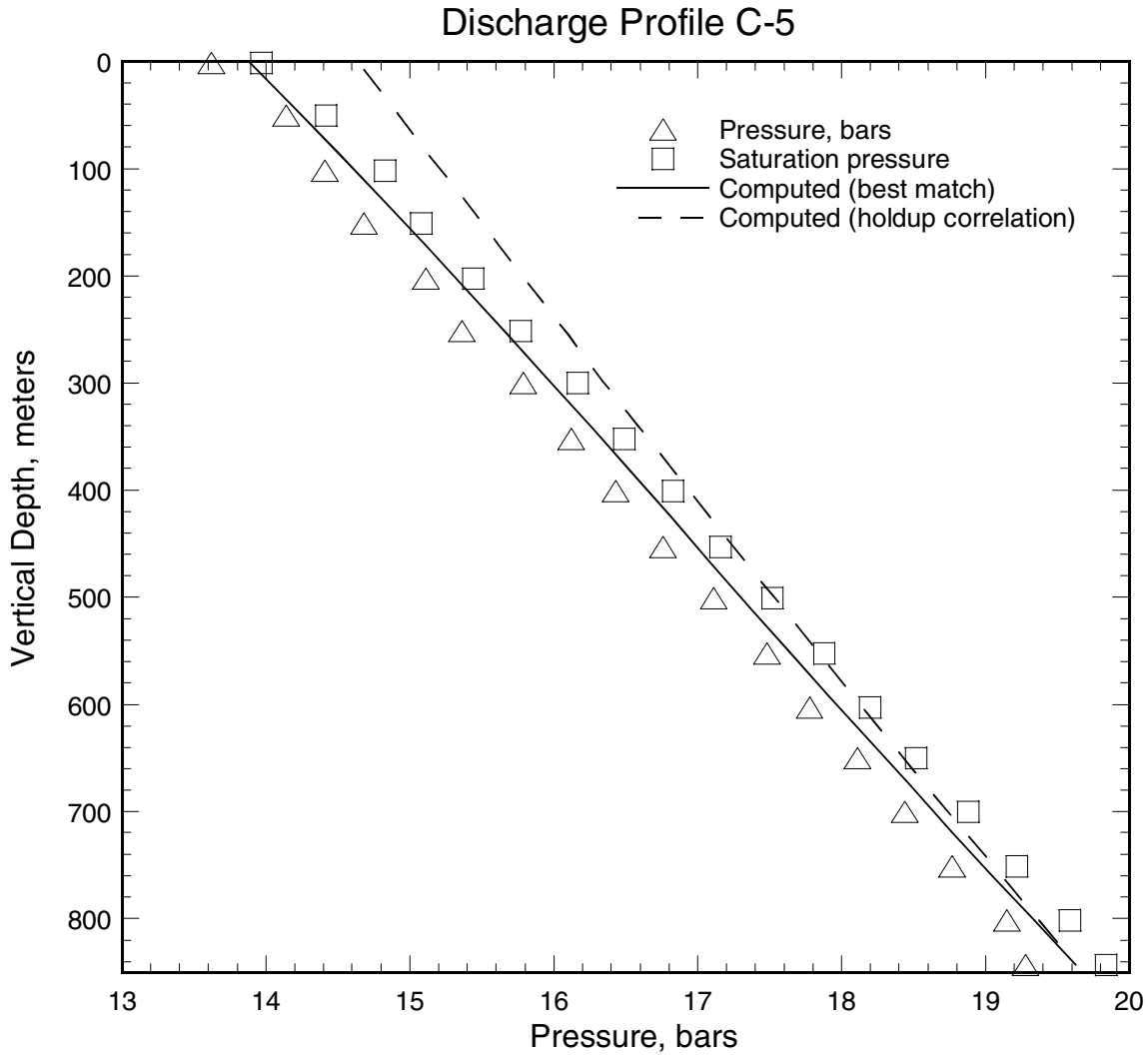

Figure C.26. Pressure profile (triangles) recorded in discharging well C-5. The squares indicate saturation pressure corresponding to the local measured temperature. The solid line is the computed pressure profile using an adjustable holdup correlation (see Section 2 for details). The computed pressure profile using the correlation(s) for *K(Z)* developed in Section 3 is shown as a dashed line.

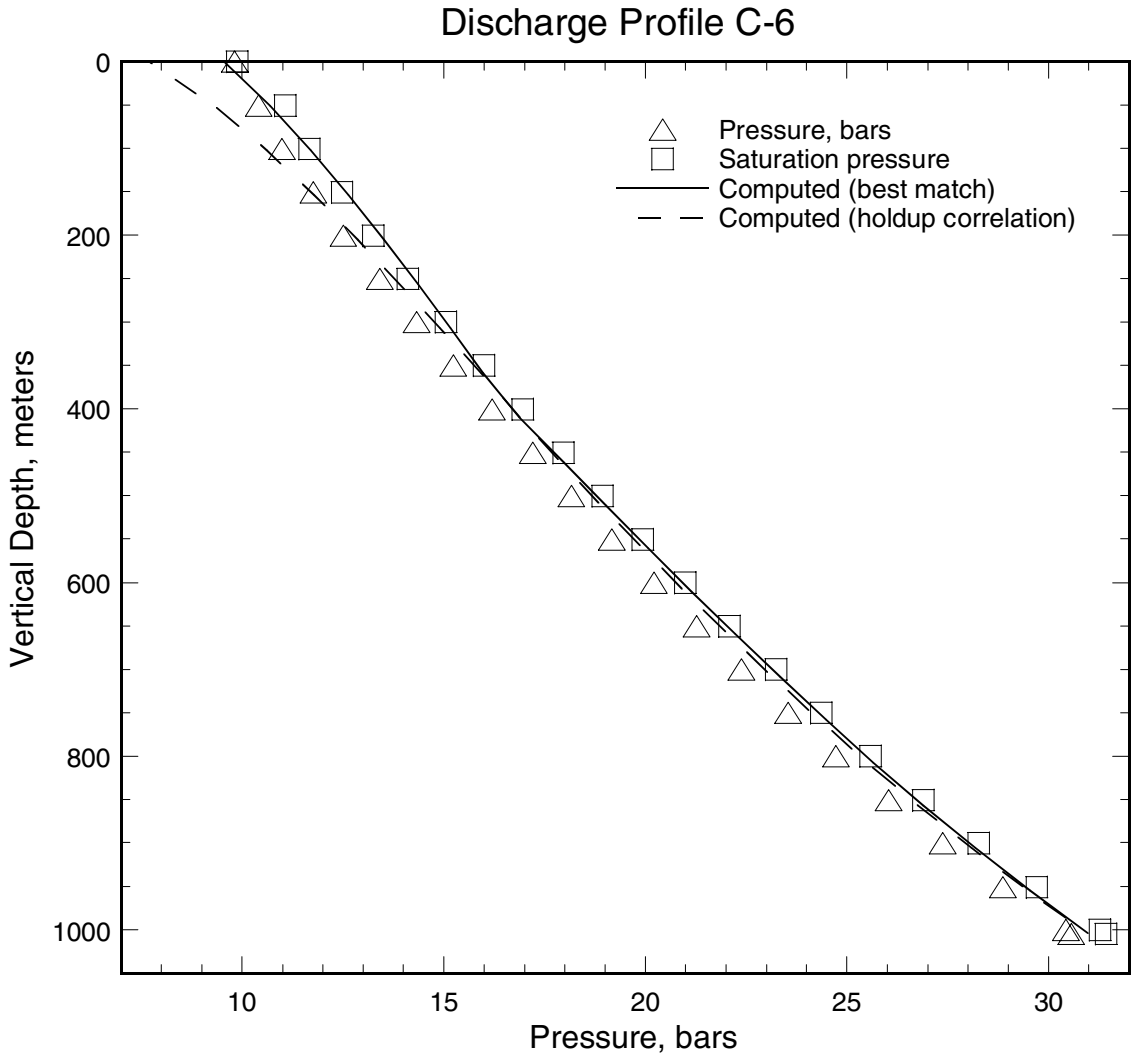

Figure C.27. Pressure profile (triangles) recorded in discharging well C-6. The squares indicate saturation pressure corresponding to the local measured temperature. The solid line is the computed pressure profile using an adjustable holdup correlation (see Section 2 for details). The computed pressure profile using the correlation(s) for *K(Z)* developed in Section 3 is shown as a dashed line.

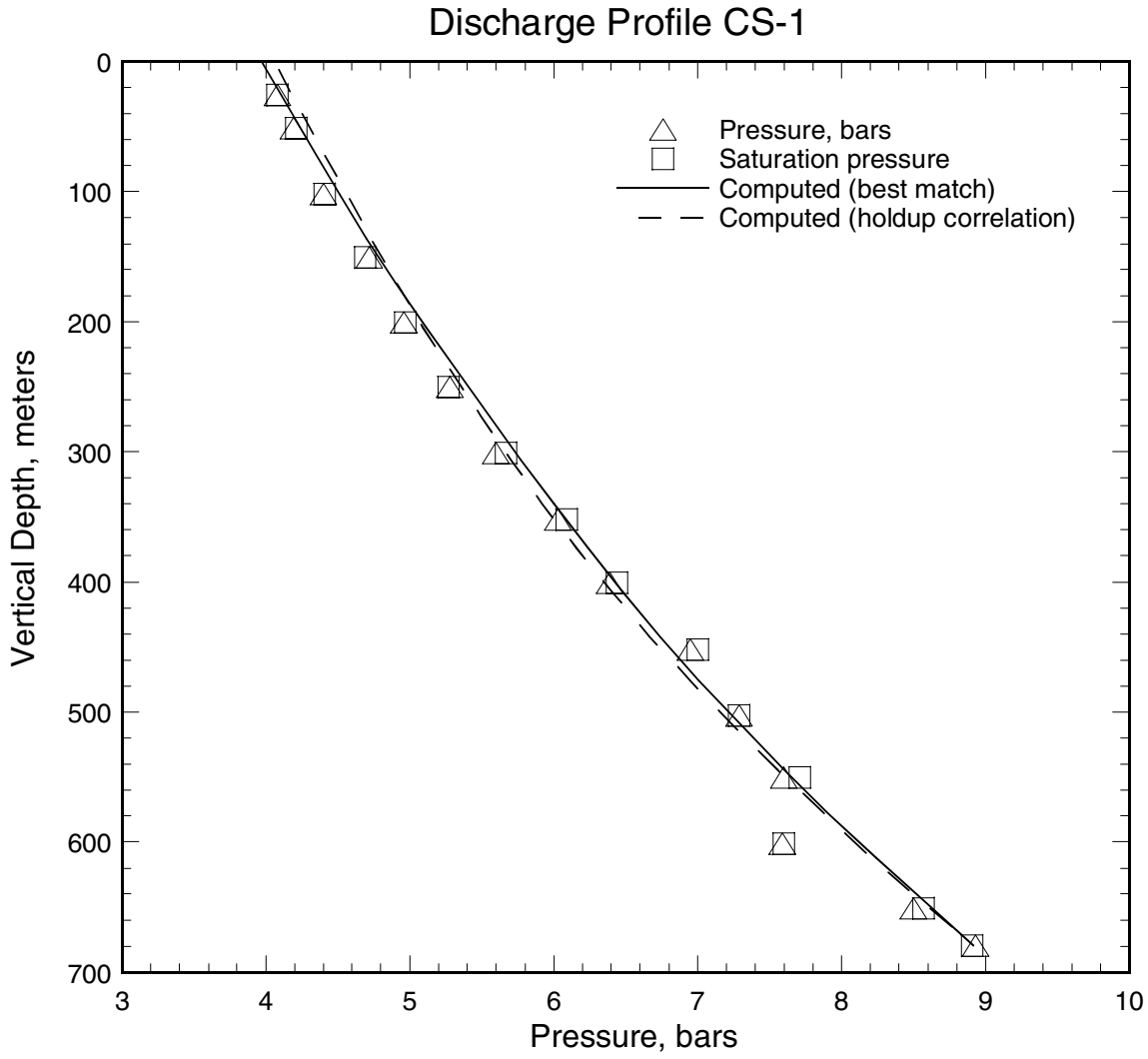

Figure C.28. Pressure profile (triangles) recorded in discharging well CS-1. The squares indicate saturation pressure corresponding to the local measured temperature. The solid line is the computed pressure profile using an adjustable holdup correlation (see Section 2 for details). The computed pressure profile using the correlation(s) for *K(Z)* developed in Section 3 is shown as a dashed line.

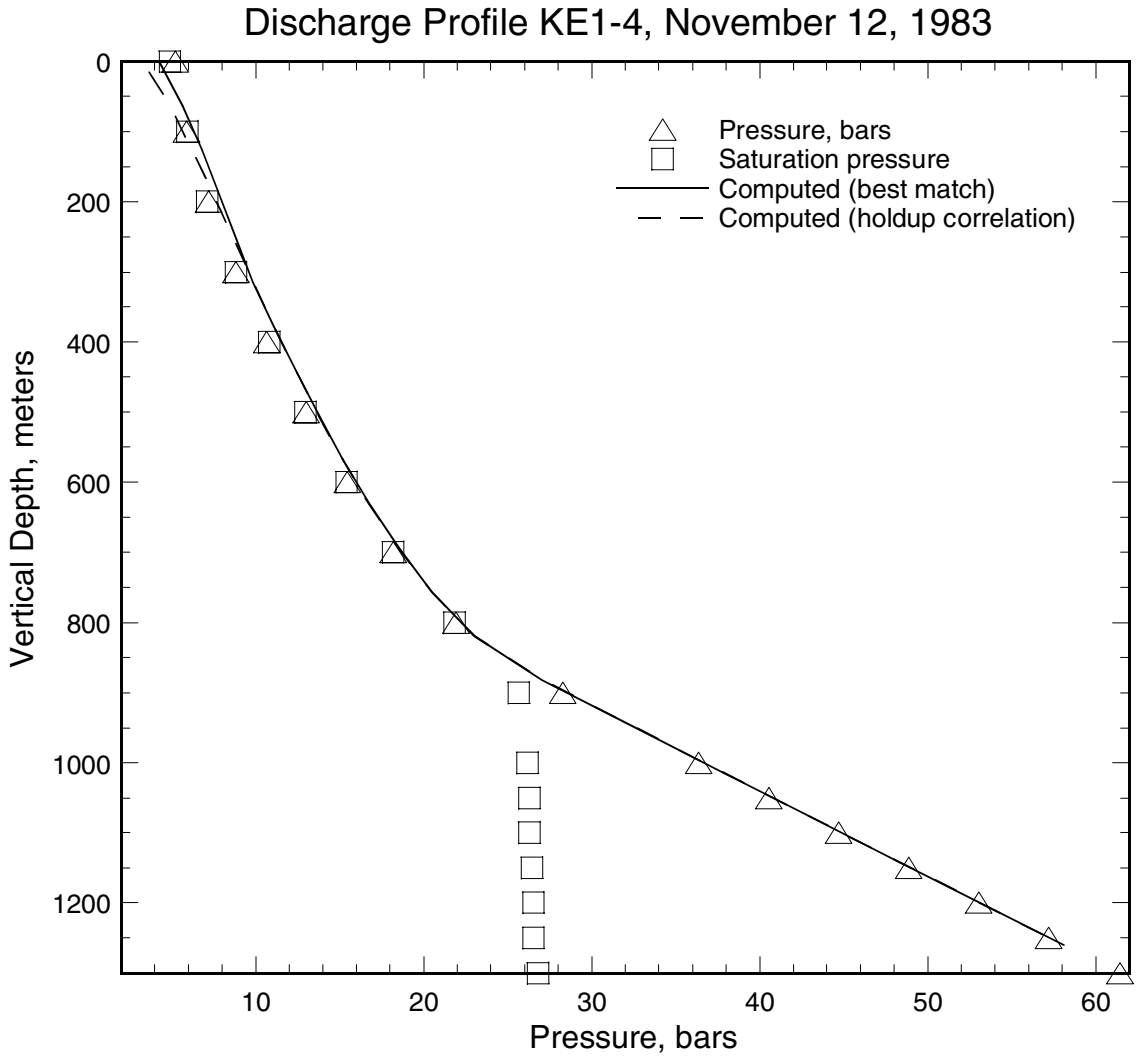

Figure C.29. Pressure profile (triangles) recorded in slim hole KE1-4 on November 12, 1983. The squares indicate saturation pressure corresponding to the local measured temperature. The solid line is the computed pressure profile using an adjustable holdup correlation (see Section 2 for details). The computed pressure profile using the correlation(s) for *K(Z)* developed in Section 3, shown as a dashed line, was obtained using a reduced discharge rate (6.5 kg/s instead of 7.08 kg/s).

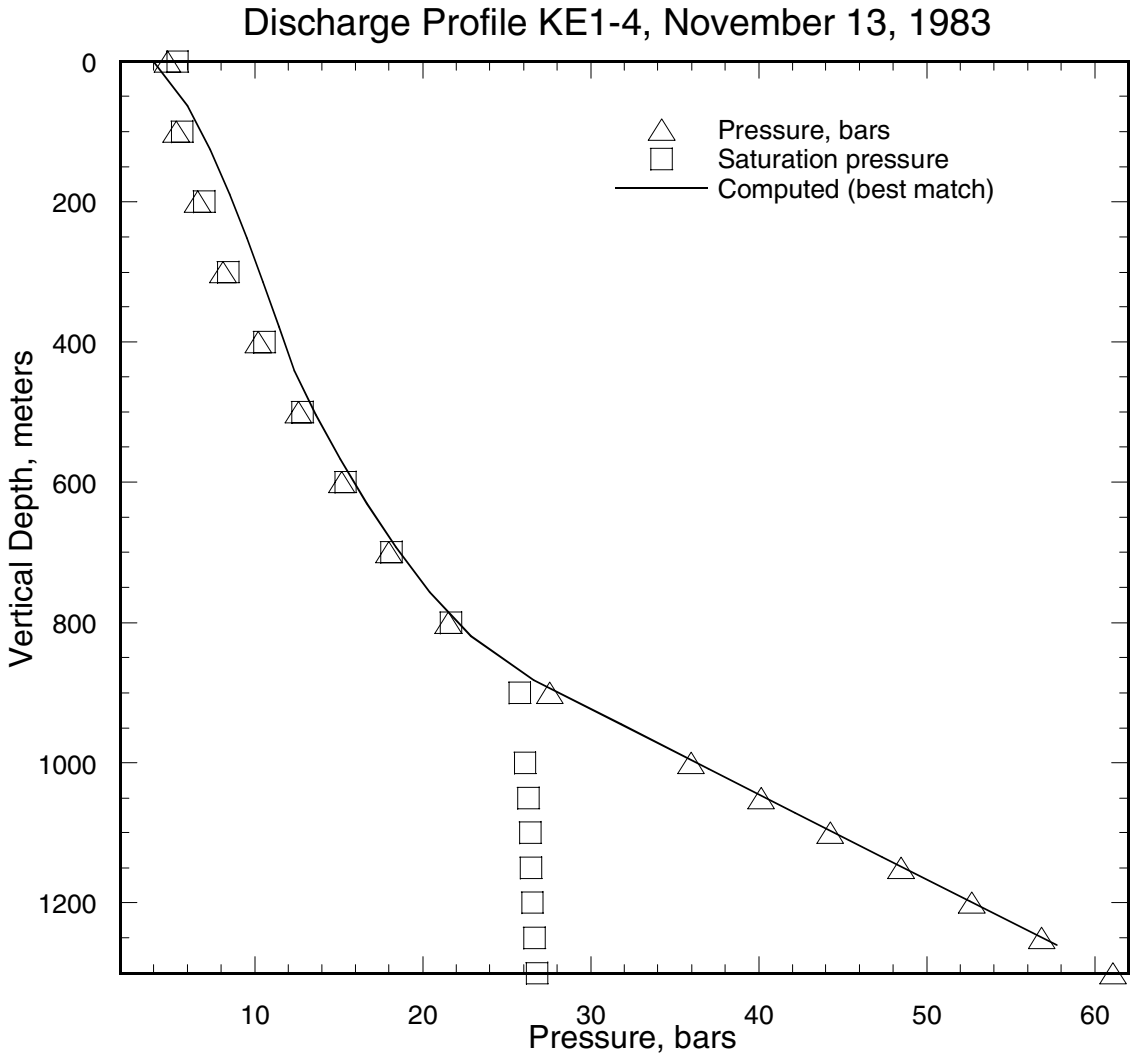

Figure C.30. Pressure profile (triangles) recorded in slim hole KE1-4 on November 13, 1983. The squares indicate saturation pressure corresponding to the local measured temperature. The solid line is the computed pressure profile using an adjustable holdup correlation (see Section 2 for details). The correlation for *K(Z)* developed in Section 3 results in choking (see Section 3 for details) for discharge rates greater than 6.5 kg/s; for the computed profile corresponding to the latter discharge rate, see Figure C.29.

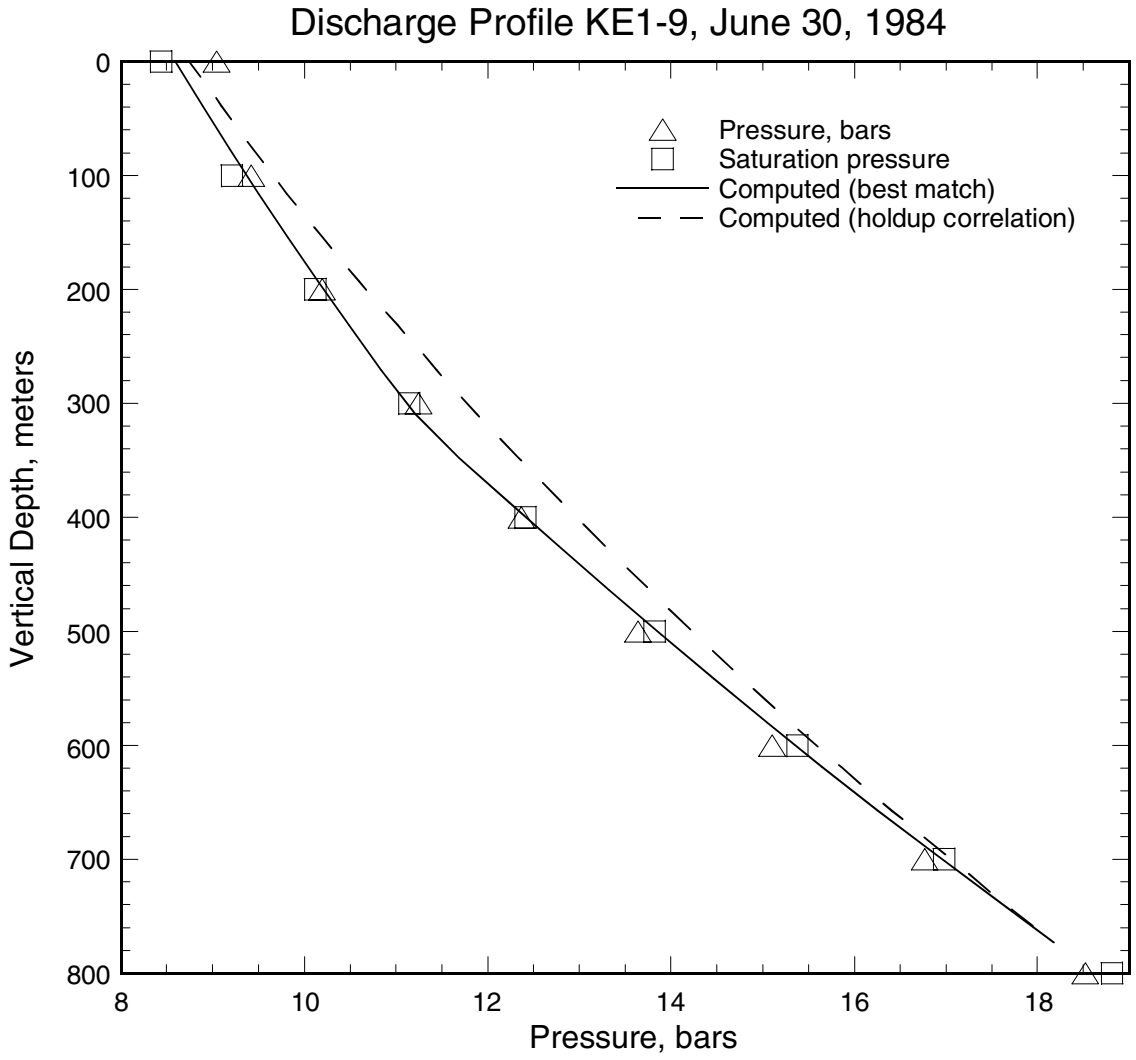

Figure C.31. Pressure profile (triangles) recorded in discharging well KE1-9. The squares indicate saturation pressure corresponding to the local measured temperature. The solid line is the computed pressure profile using an adjustable holdup correlation (see Section 2 for details). The computed pressure profile using the correlation(s) for *K(Z)* developed in Section 3 is shown as a dashed line.

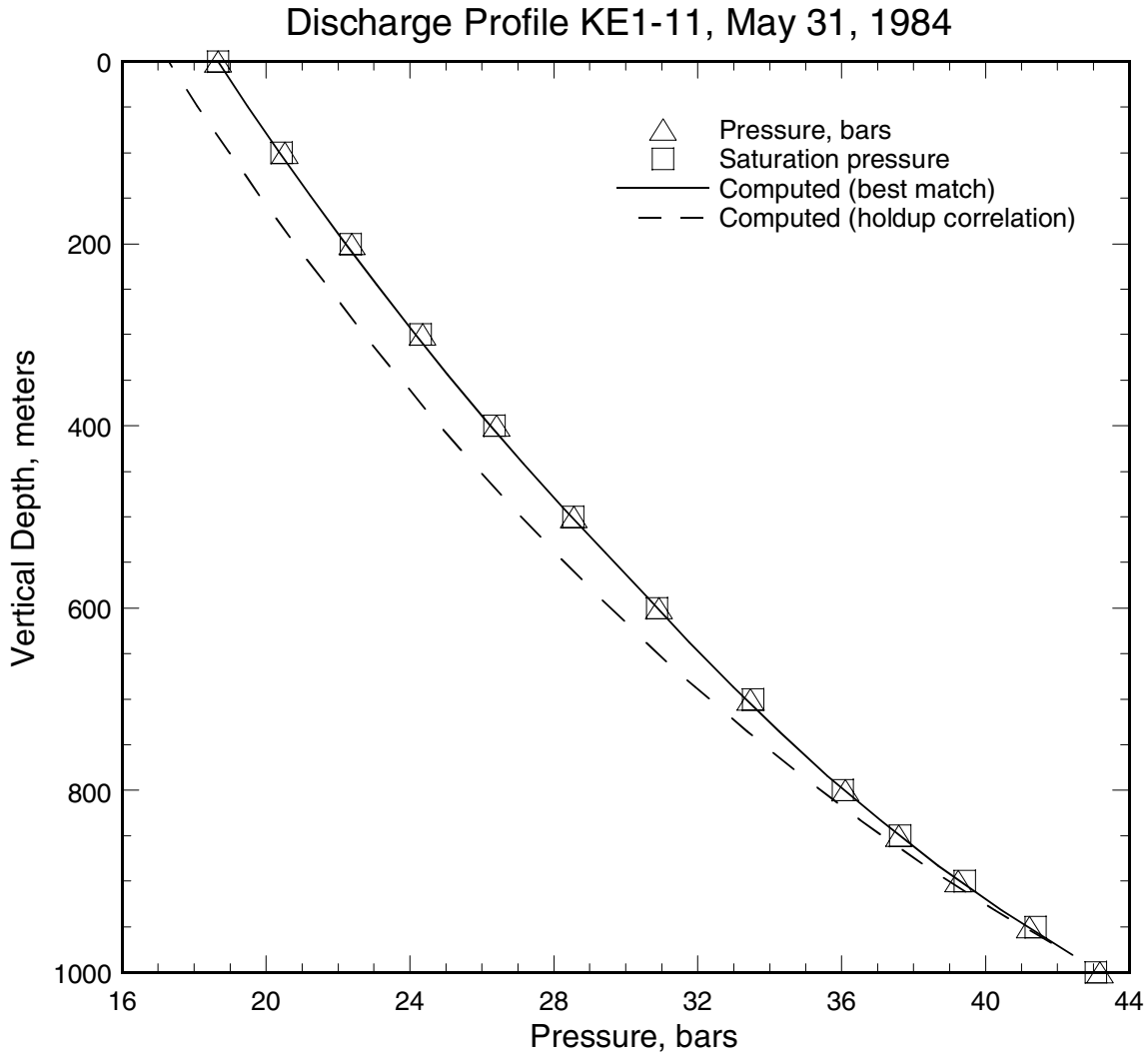

Figure C.32. Pressure profile (triangles) recorded in discharging well KE1-11. The squares indicate saturation pressure corresponding to the local measured temperature. The solid line is the computed pressure profile using an adjustable holdup correlation (see Section 2 for details). The computed pressure profile using the correlation(s) for *K(Z)* developed in Section 3 is shown as a dashed line.

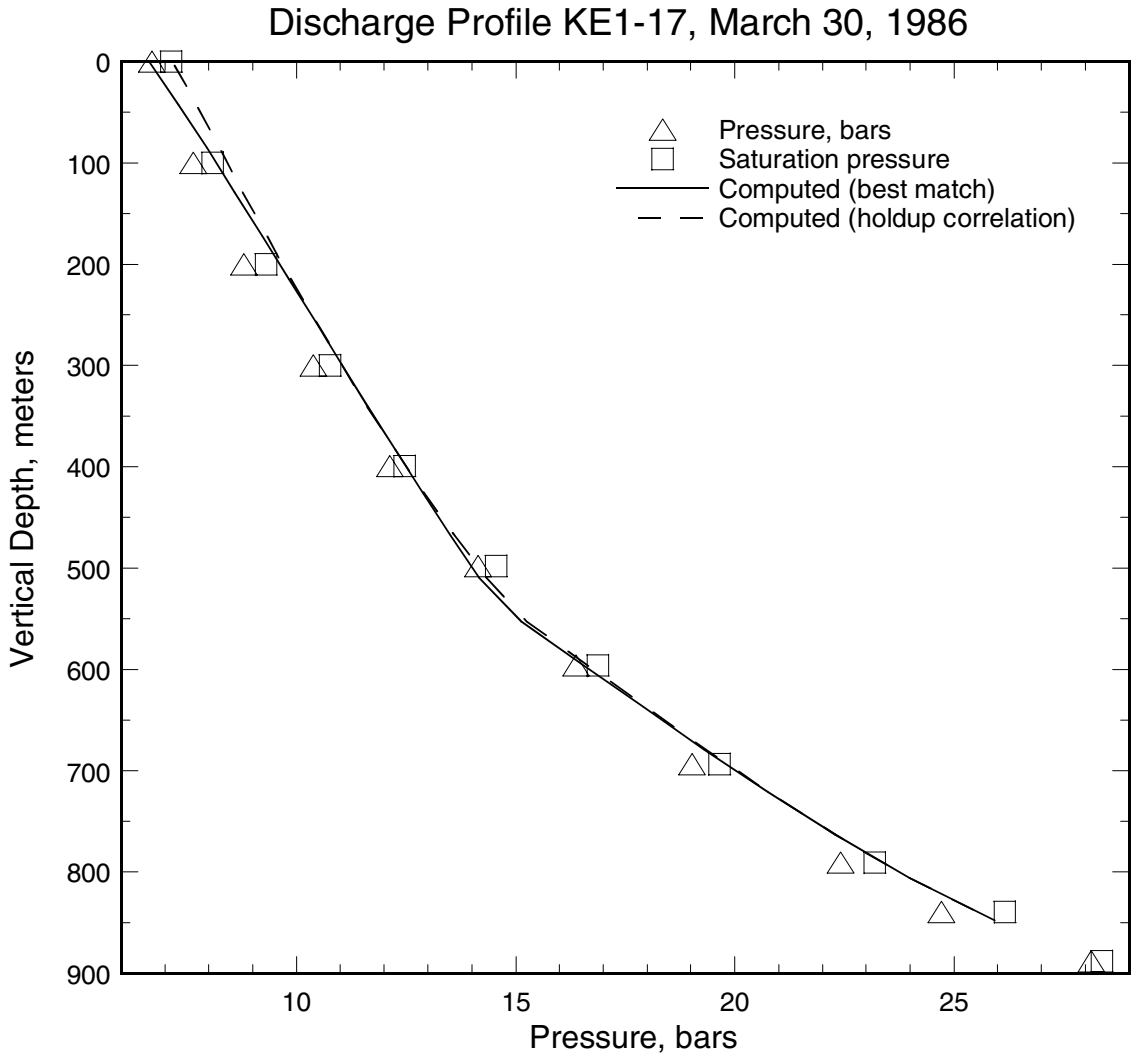

Figure C.33. Pressure profile (triangles) recorded in well KE1-17 on March 30, 1986. The squares indicate saturation pressure corresponding to the local measured temperature. The solid line is the computed pressure profile using an adjustable holdup correlation (see Section 2 for details). The computed pressure profile using the correlation(s) for *K(Z)* developed in Section 3 is shown as a dashed line.

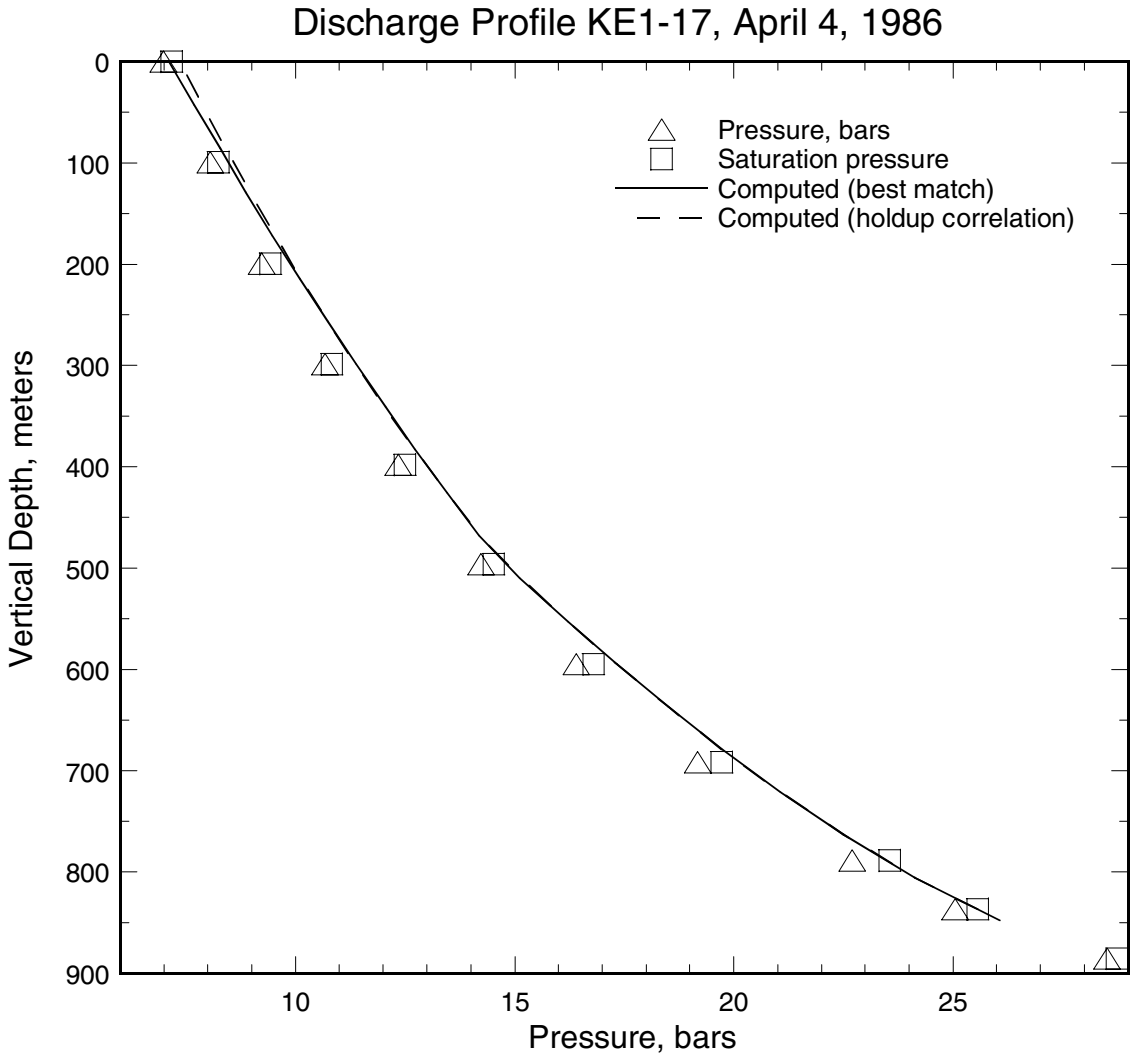

Figure C.34. Pressure profile (triangles) recorded in well KE1-17 on April 4, 1986. The squares indicate saturation pressure corresponding to the local measured temperature. The solid line is the computed pressure profile using an adjustable holdup correlation (see Section 2 for details). The computed pressure profile using the correlation(s) for *K(Z)* developed in Section 3 is shown as a dashed line.

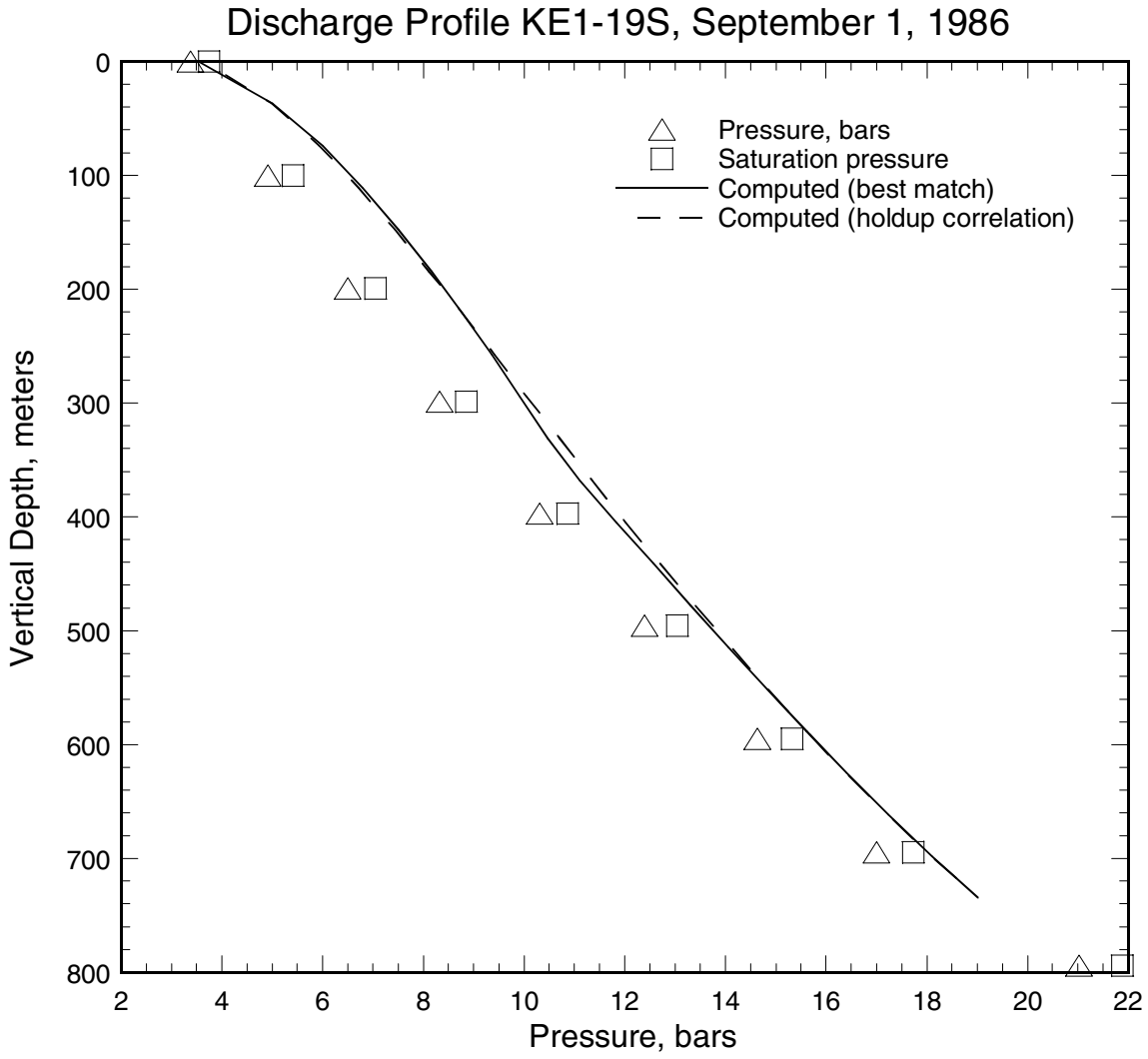

Figure C.35. Pressure profile (triangles) recorded in well KE1-19S on September 1, 1986. The squares indicate saturation pressure corresponding to the local measured temperature. The solid line is the computed pressure profile using an adjustable holdup correlation (see Section 2 for details). The computed pressure profile using the correlation(s) for *K(Z)* developed in Section 3, shown as a dashed line, was obtained using a reduced discharge rate (23.0 kg/s instead of 23.9 kg/s).

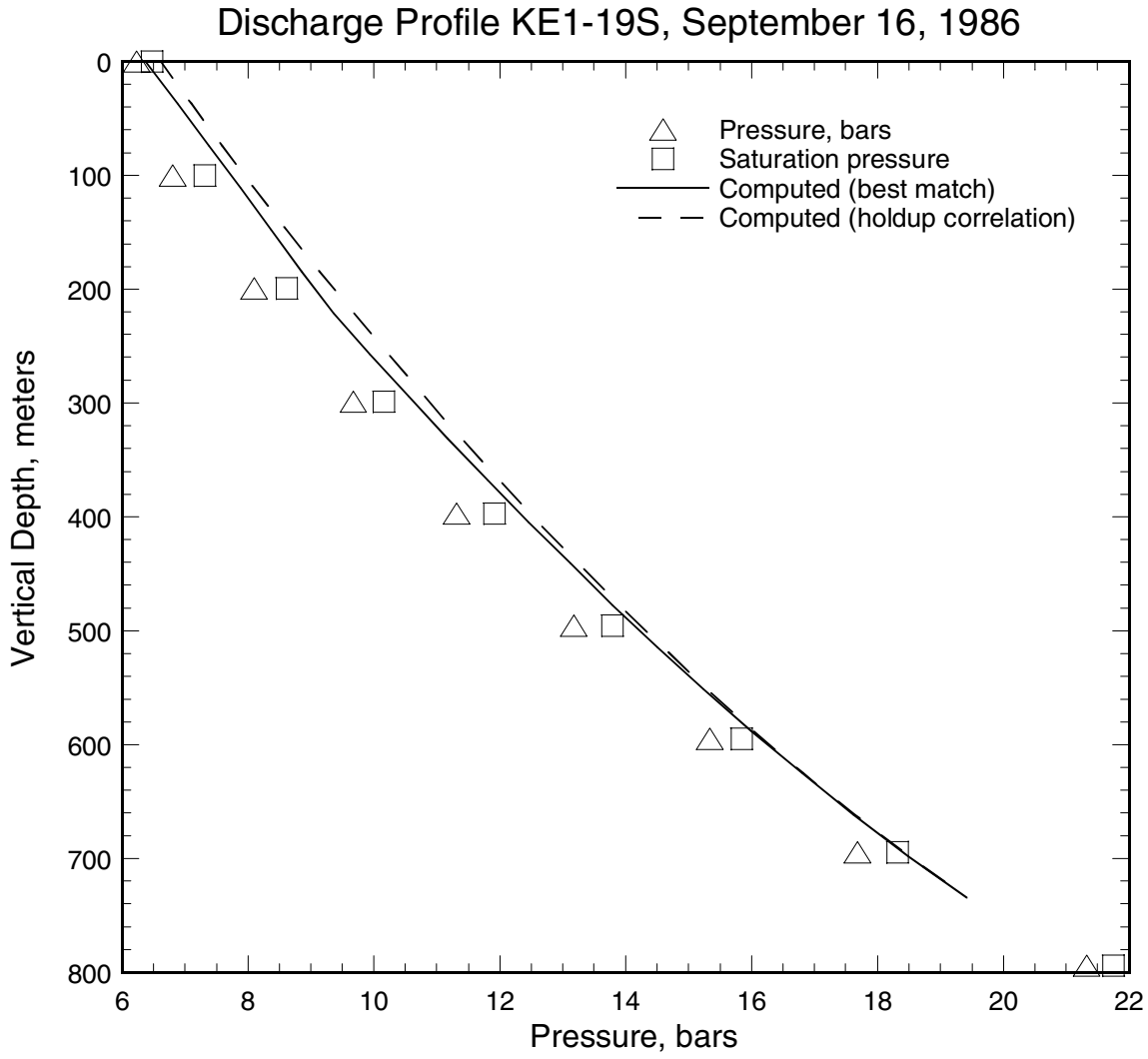

Figure C.36. Pressure profile (triangles) recorded in well KE1-19S on September 16, 1986. The squares indicate saturation pressure corresponding to the local measured temperature. The solid line is the computed pressure profile using an adjustable holdup correlation (see Section 2 for details). The computed pressure profile using the correlation(s) for *K(Z)* developed in Section 3 is shown as a dashed line.

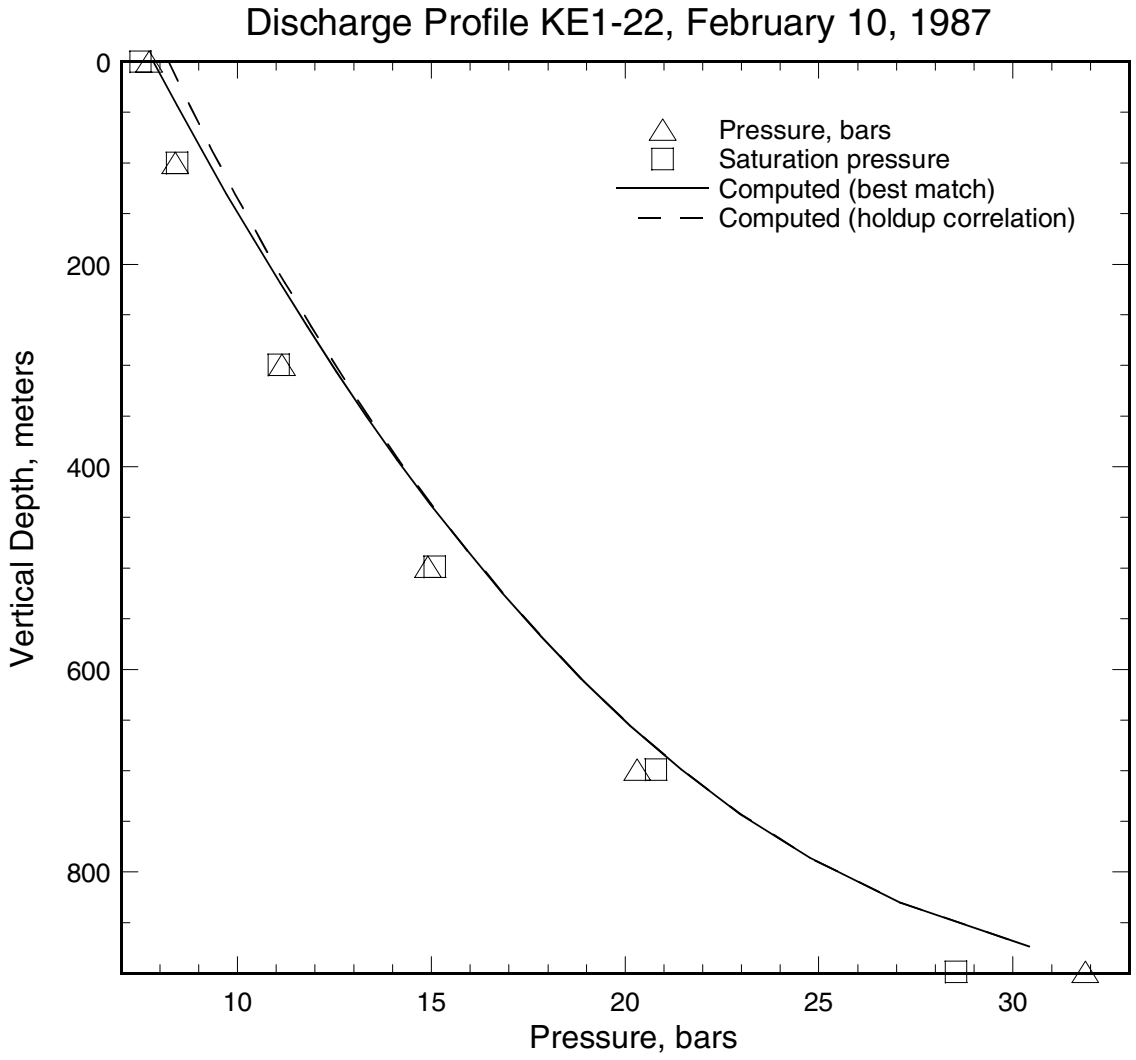

Figure C.37. Pressure profile (triangles) recorded in well KE1-22 on February 10, 1987. The squares indicate saturation pressure corresponding to the local measured temperature. The solid line is the computed pressure profile using an adjustable holdup correlation (see Section 2 for details). The computed pressure profile using the correlation(s) for *K(Z)* developed in Section 3 is shown as a dashed line.

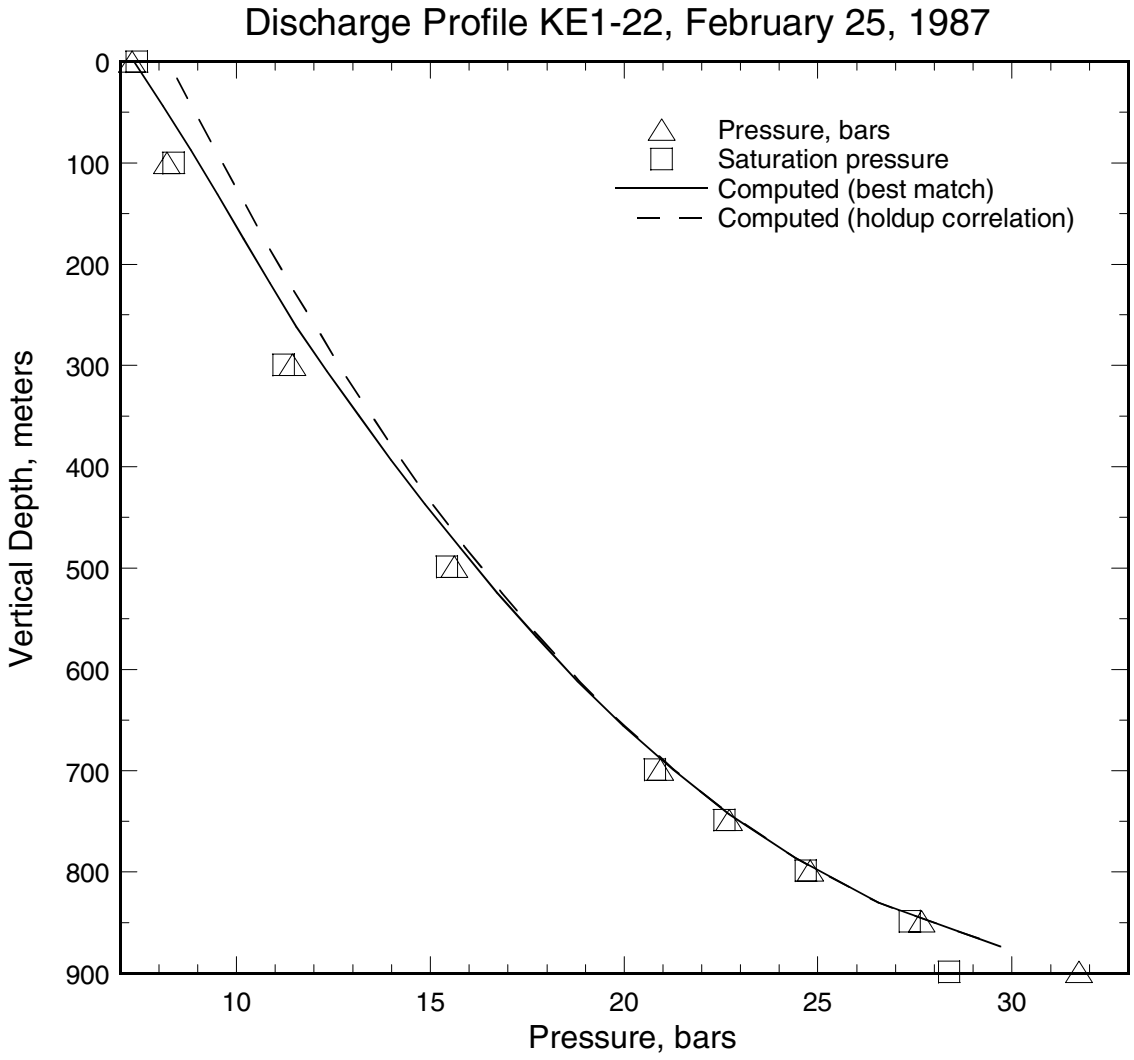

Figure C.38. Pressure profile (triangles) recorded in well KE1-22 on February 25, 1987. The squares indicate saturation pressure corresponding to the local measured temperature. The solid line is the computed pressure profile using an adjustable holdup correlation (see Section 2 for details). The computed pressure profile using the correlation(s) for *K(Z)* developed in Section 3 is shown as a dashed line.

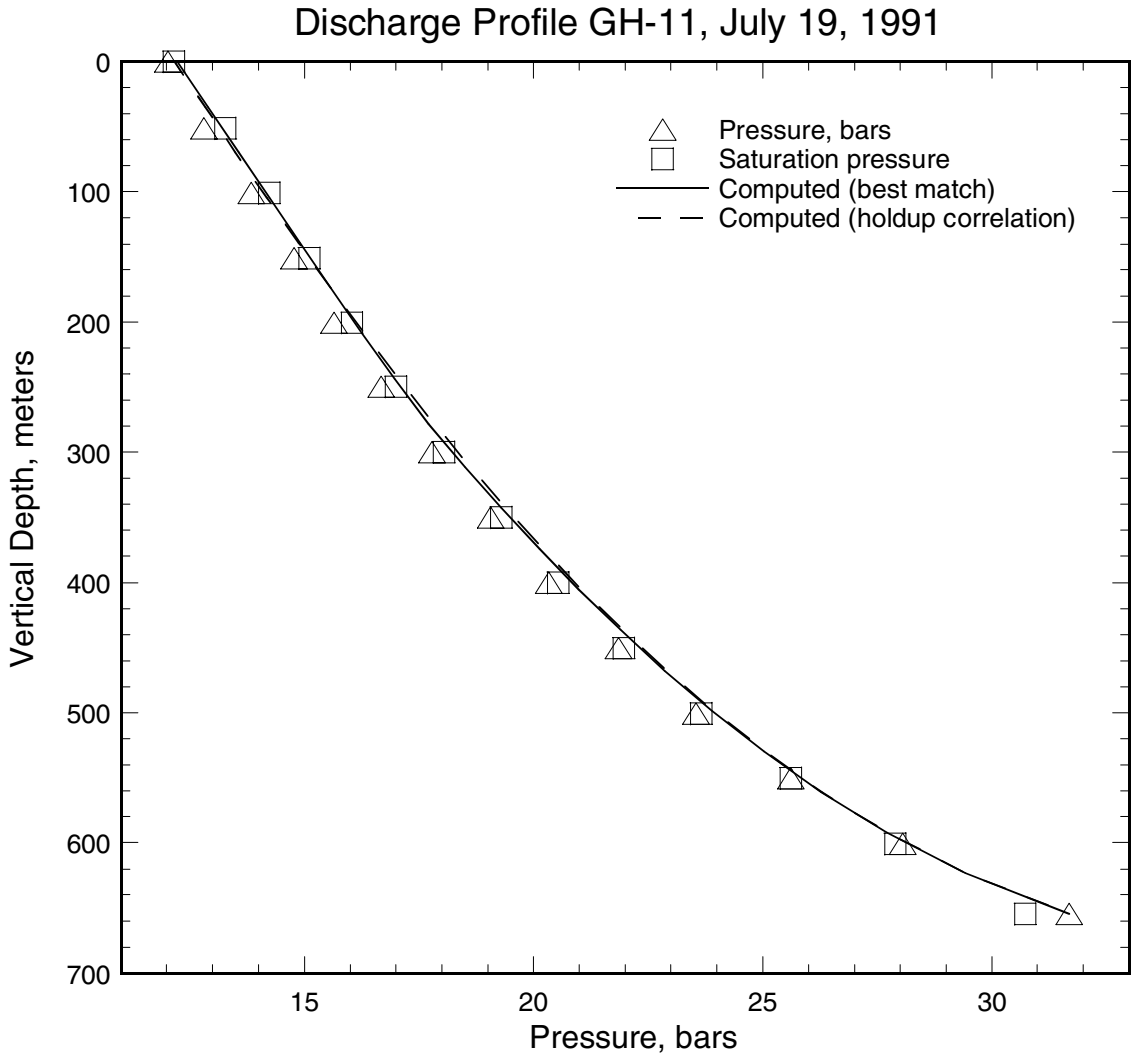

Figure C.39. Pressure profile (triangles) recorded in well GH-11 on July 19, 1991. The squares indicate saturation pressure corresponding to the local measured temperature. The solid line is the computed pressure profile using an adjustable holdup correlation (see Section 2 for details). The computed pressure profile using the correlation(s) for *K(Z)* developed in Section 3 is shown as a dashed line.

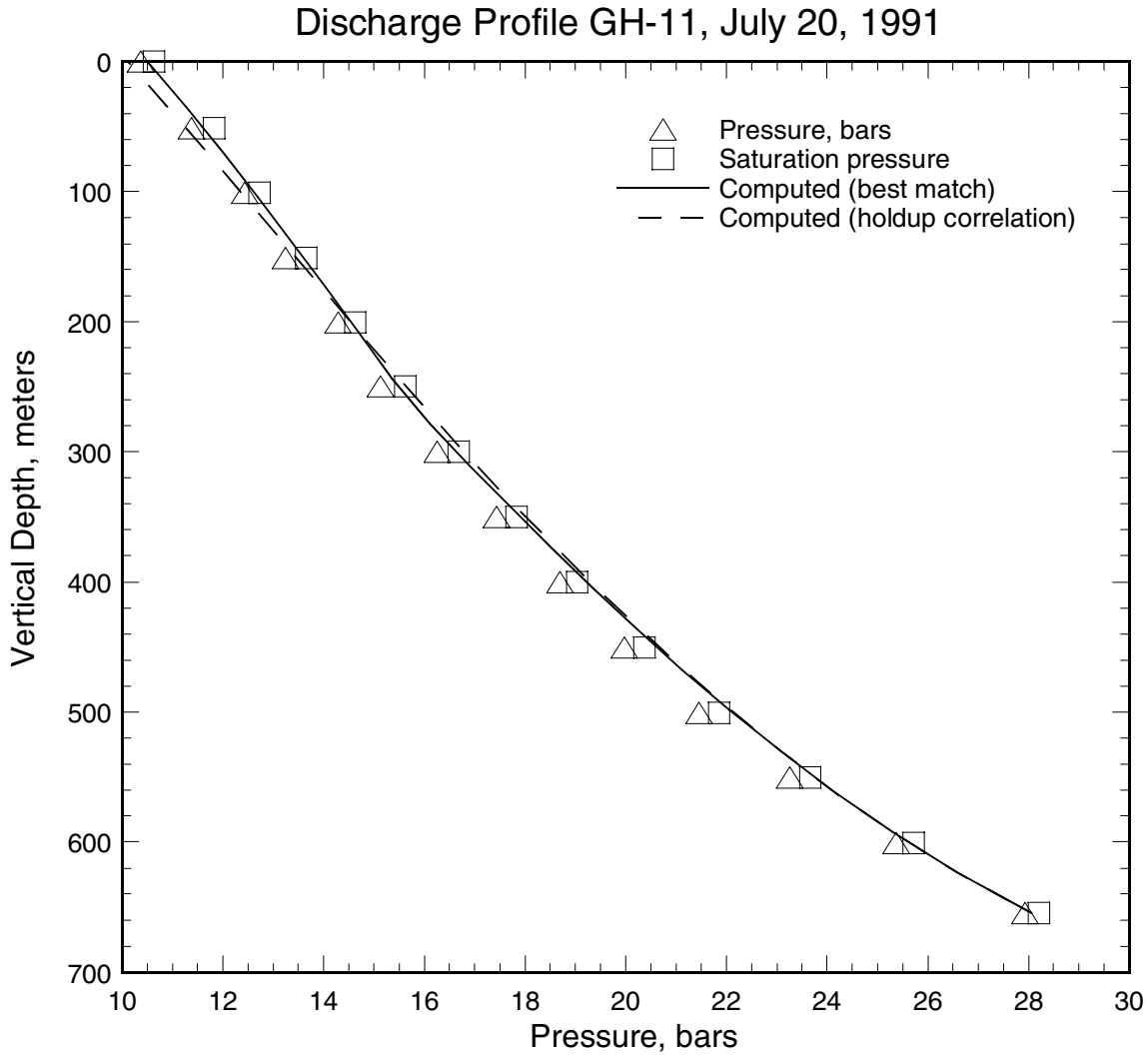

Figure C.40. Pressure profile (triangles) recorded in well GH-11 on July 20, 1991. The squares indicate saturation pressure corresponding to the local measured temperature. The solid line is the computed pressure profile using an adjustable holdup correlation (see Section 2 for details). The computed pressure profile using the correlation(s) for *K(Z)* developed in Section 3 is shown as a dashed line.

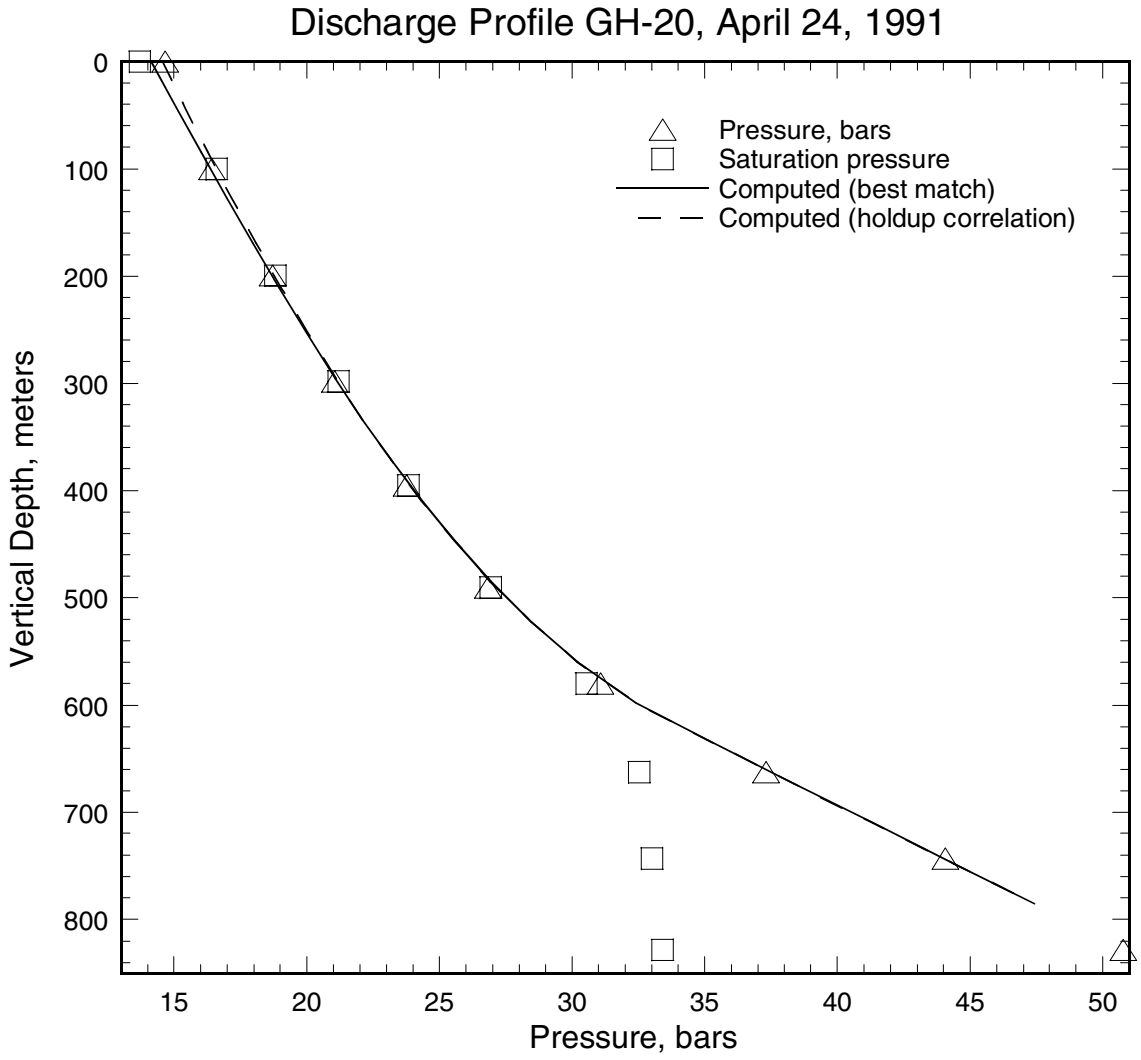

Figure C.41. Pressure profile (triangles) recorded in well GH-20 on April 24, 1991. The squares indicate saturation pressure corresponding to the local measured temperature. The solid line is the computed pressure profile using an adjustable holdup correlation (see Section 2 for details). The computed pressure profile using the correlation(s) for *K(Z)* developed in Section 3 is shown as a dashed line.

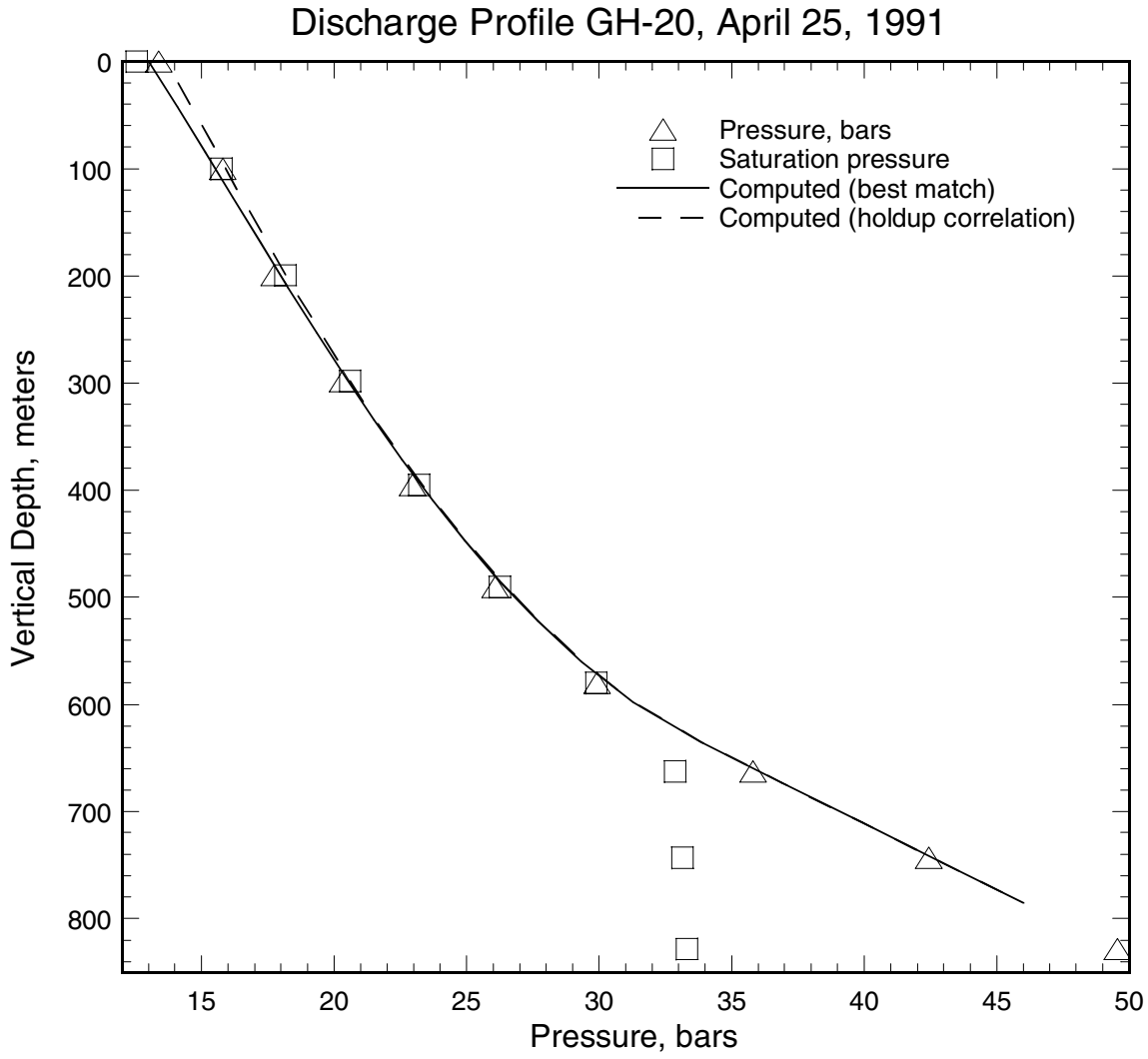

Figure C.42. Pressure profile (triangles) recorded in well GH-20 on April 25, 1991. The squares indicate saturation pressure corresponding to the local measured temperature. The solid line is the computed pressure profile using an adjustable holdup correlation (see Section 2 for details). The computed pressure profile using the correlation(s) for *K(Z)* developed in Section 3 is shown as a dashed line.

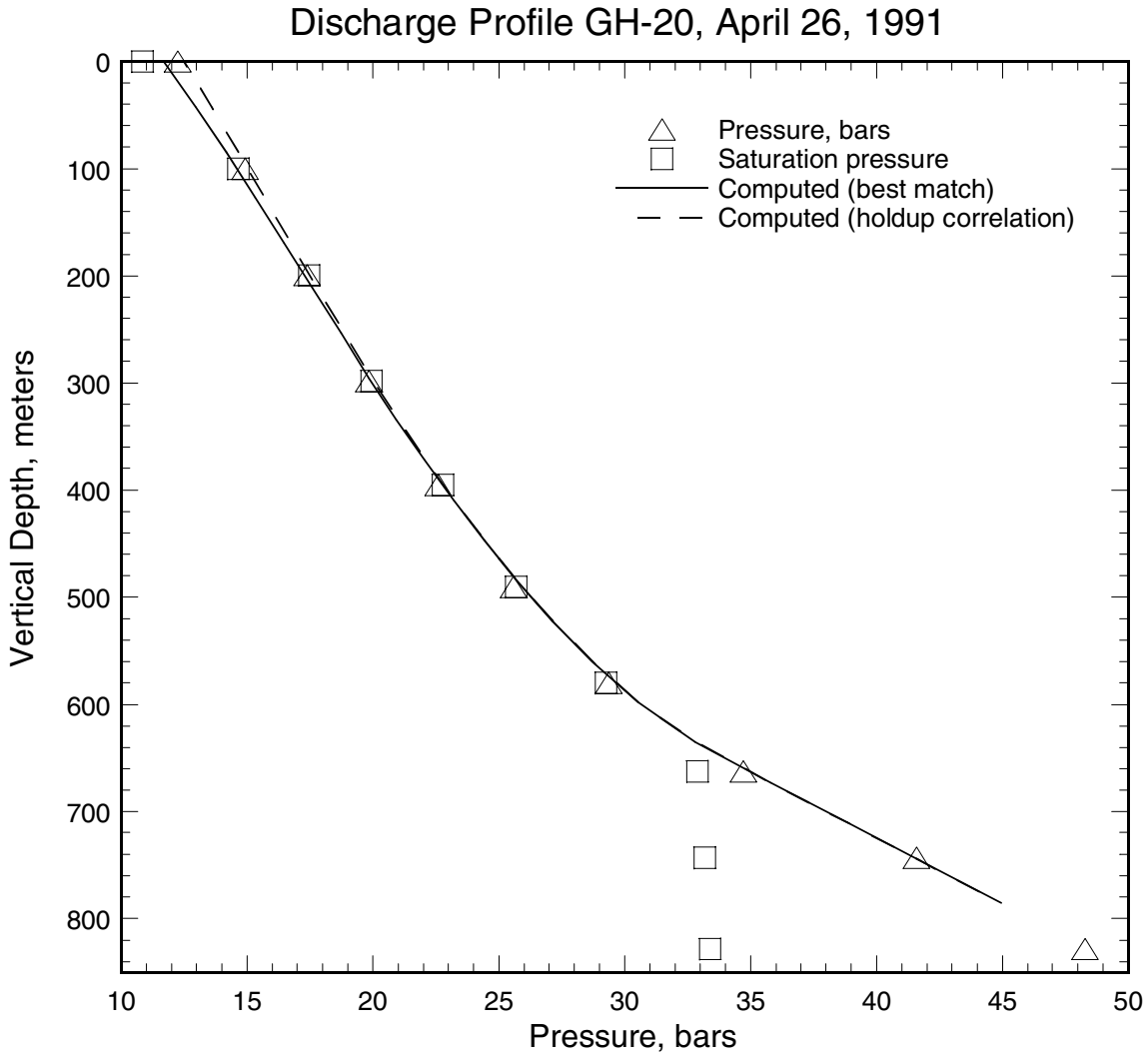

Figure C.43. Pressure profile (triangles) recorded in well GH-20 on April 26, 1991. The squares indicate saturation pressure corresponding to the local measured temperature. The solid line is the computed pressure profile using an adjustable holdup correlation (see Section 2 for details). The computed pressure profile using the correlation(s) for *K(Z)* developed in Section 3 is shown as a dashed line.

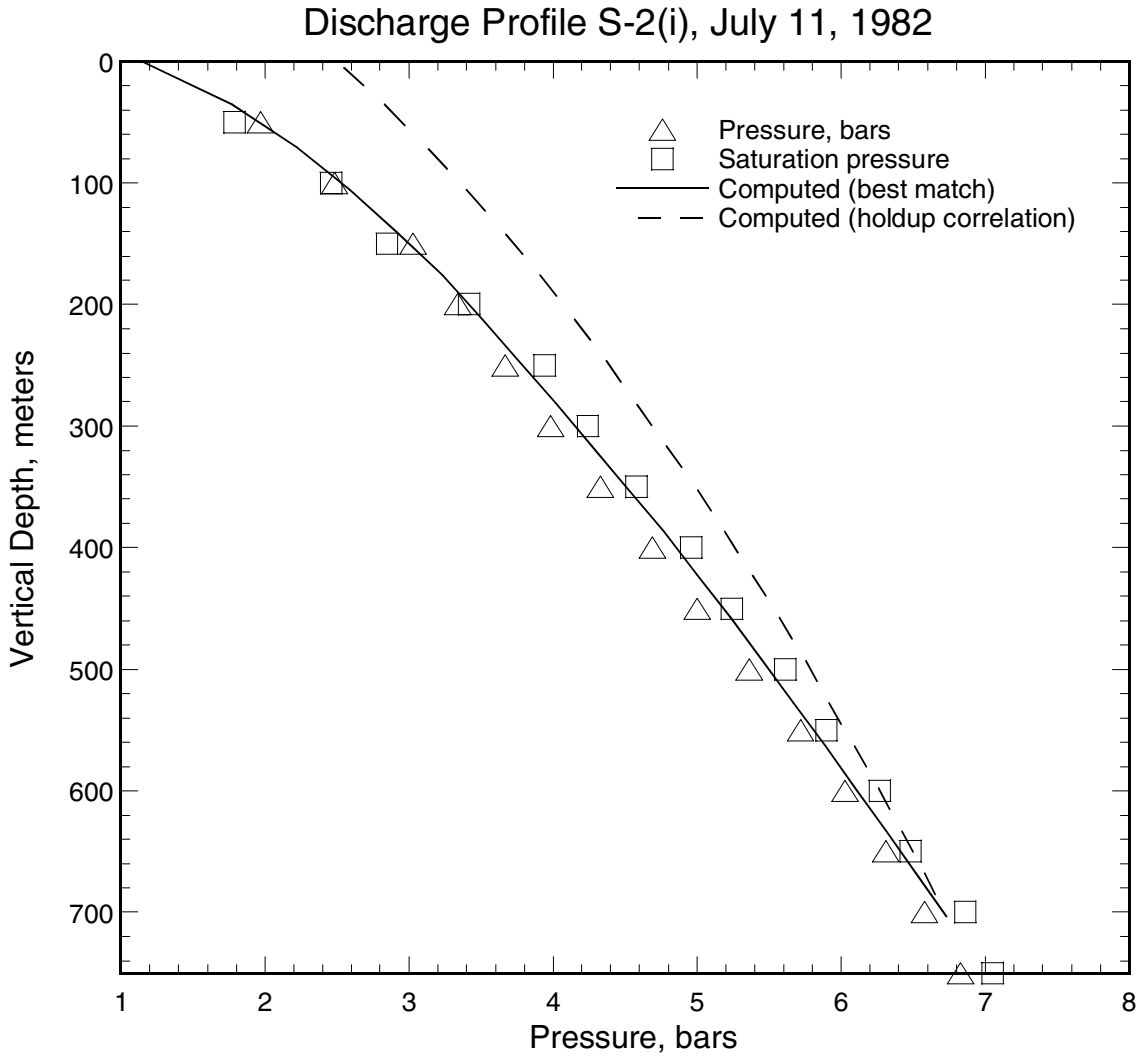

Figure C.44. Pressure profile (triangles) recorded in discharging well S-2(i). The squares indicate saturation pressure corresponding to the local measured temperature. The solid line is the computed pressure profile using an adjustable holdup correlation (see Section 2 for details). The computed pressure profile using the correlation(s) for *K(Z)* developed in Section 3 is shown as a dashed line.

APPENDIX D: SIMULATION OF SPINNER DATA

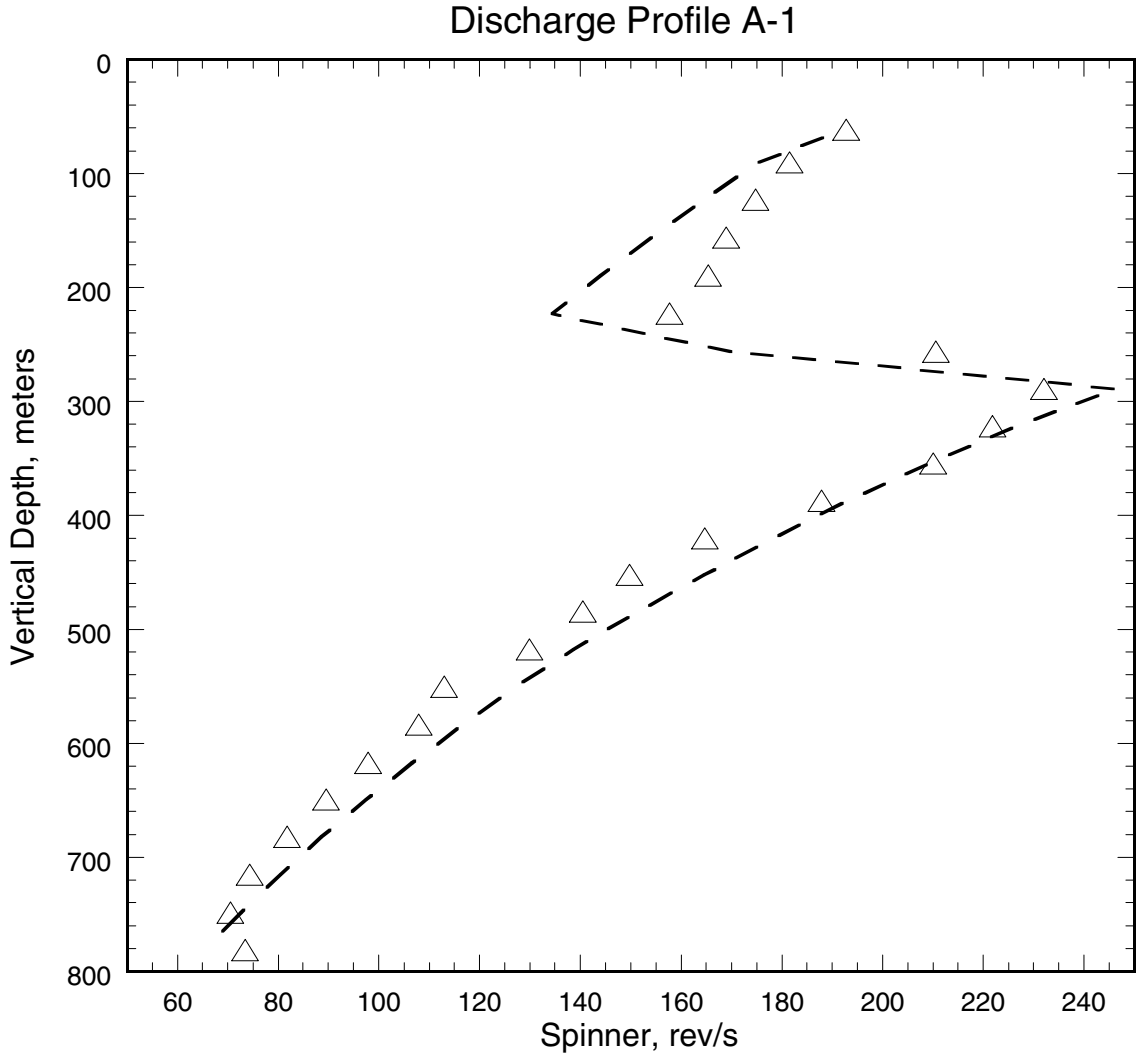

Figure D.1. Comparison of the smoothed spinner response (triangles) with the computed spinner response (dashed line) for well A-1.

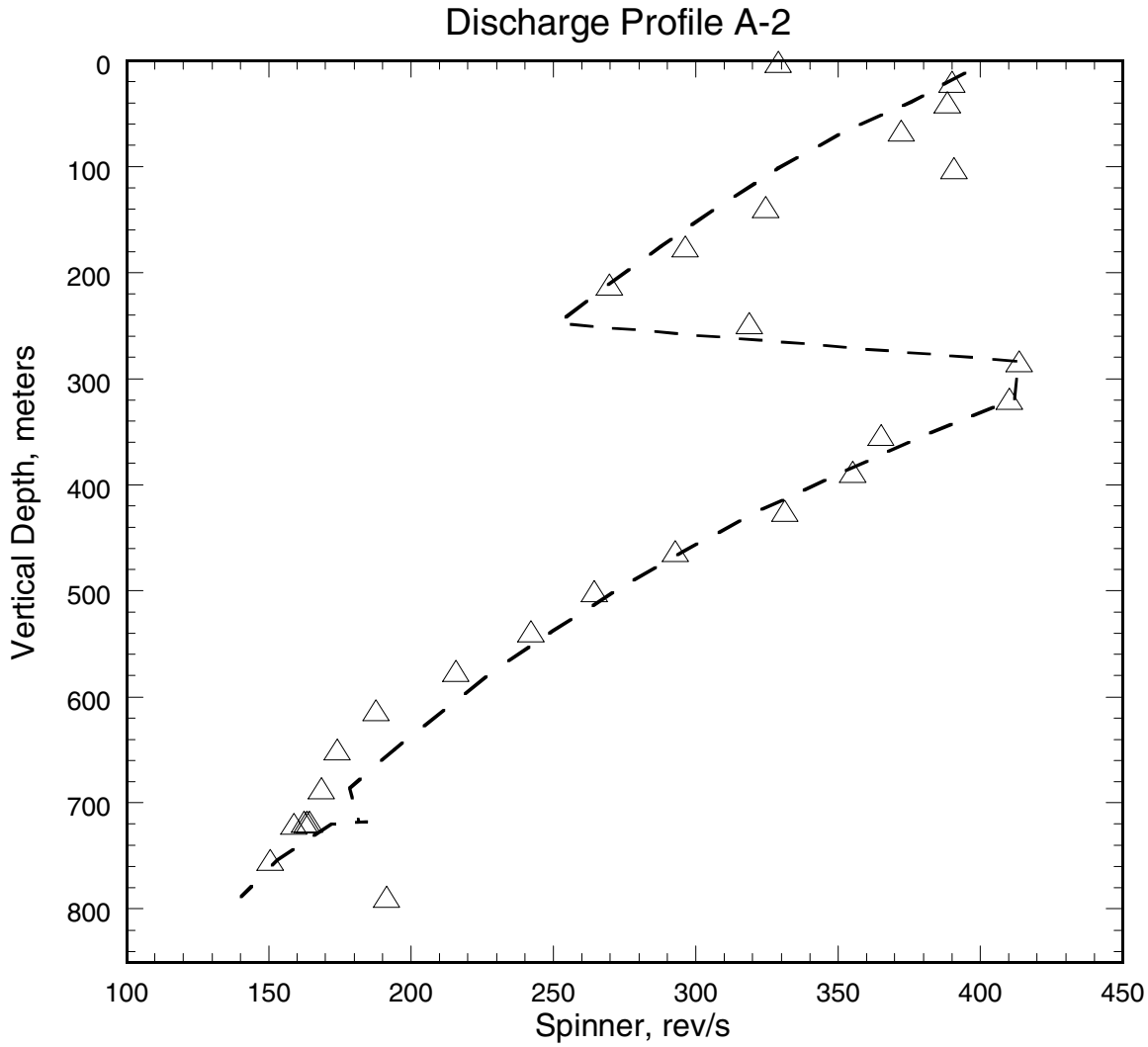

Figure D.2. Comparison of the smoothed spinner response (triangles) with the computed spinner response (dashed line) for well A-2.

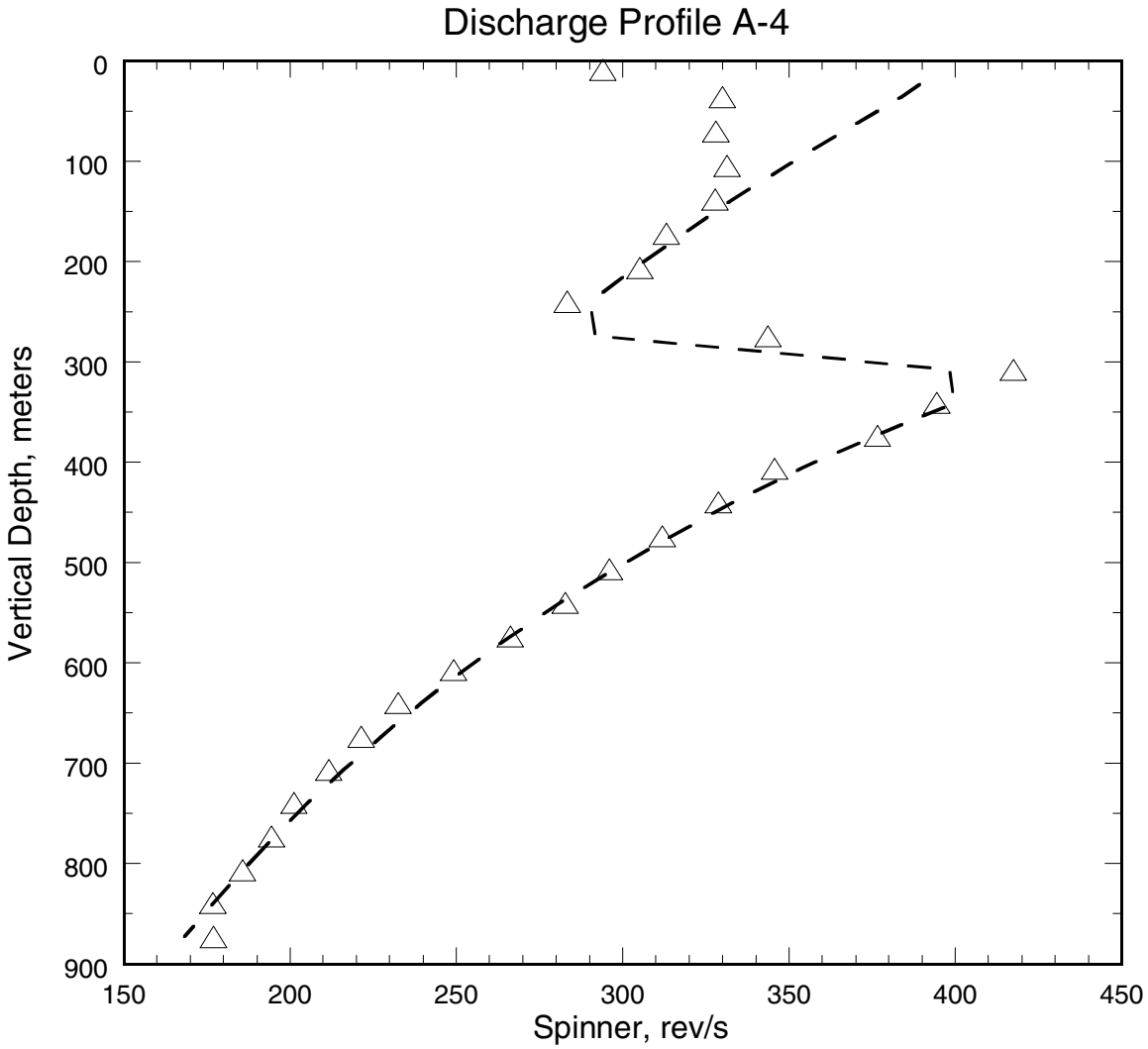

Figure D.3. Comparison of the smoothed spinner response (triangles) with the computed spinner response (dashed line) for well A-4.

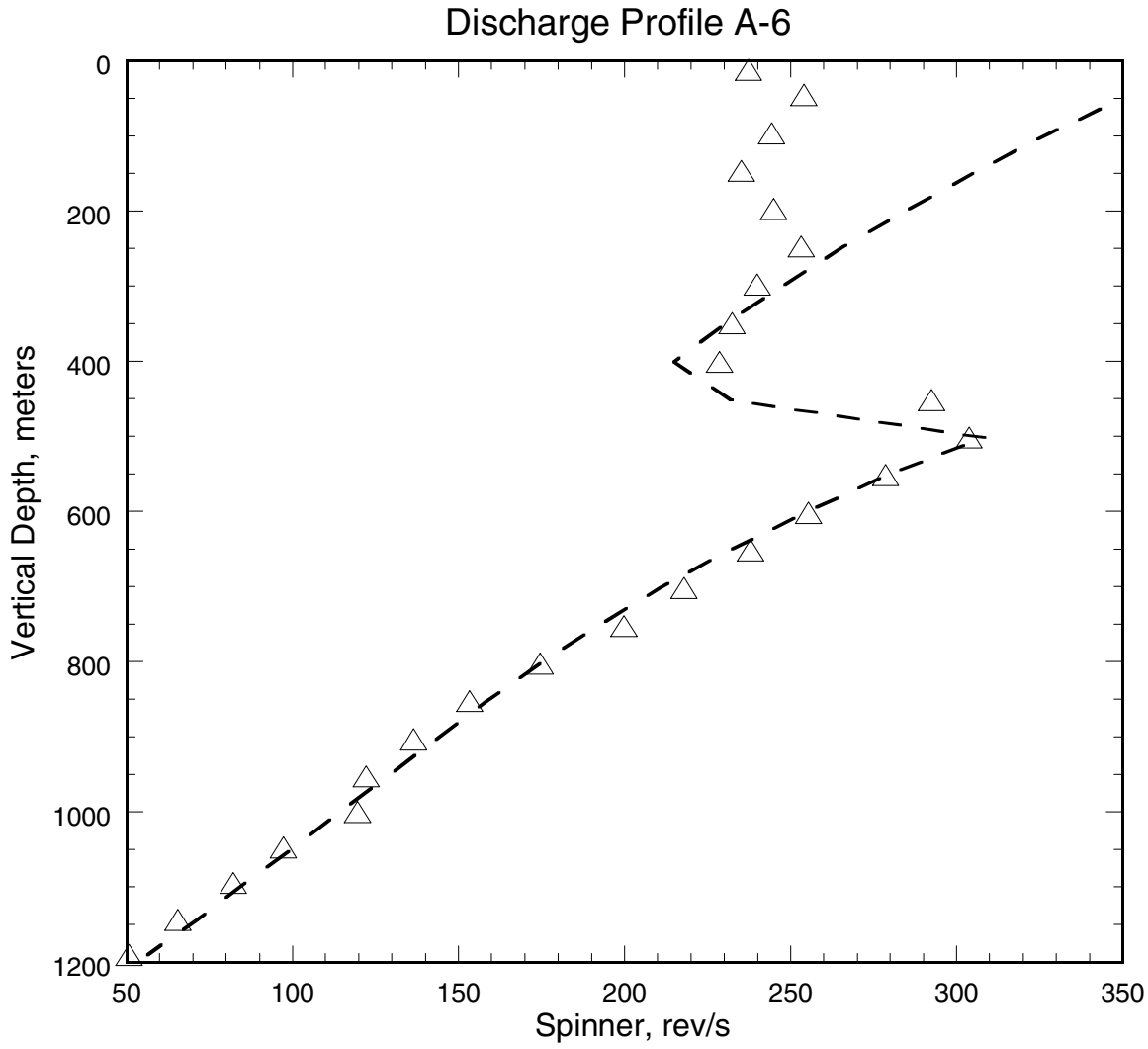

Figure D.4. Comparison of the smoothed spinner response (triangles) with the computed spinner response (dashed line) for well A-6.

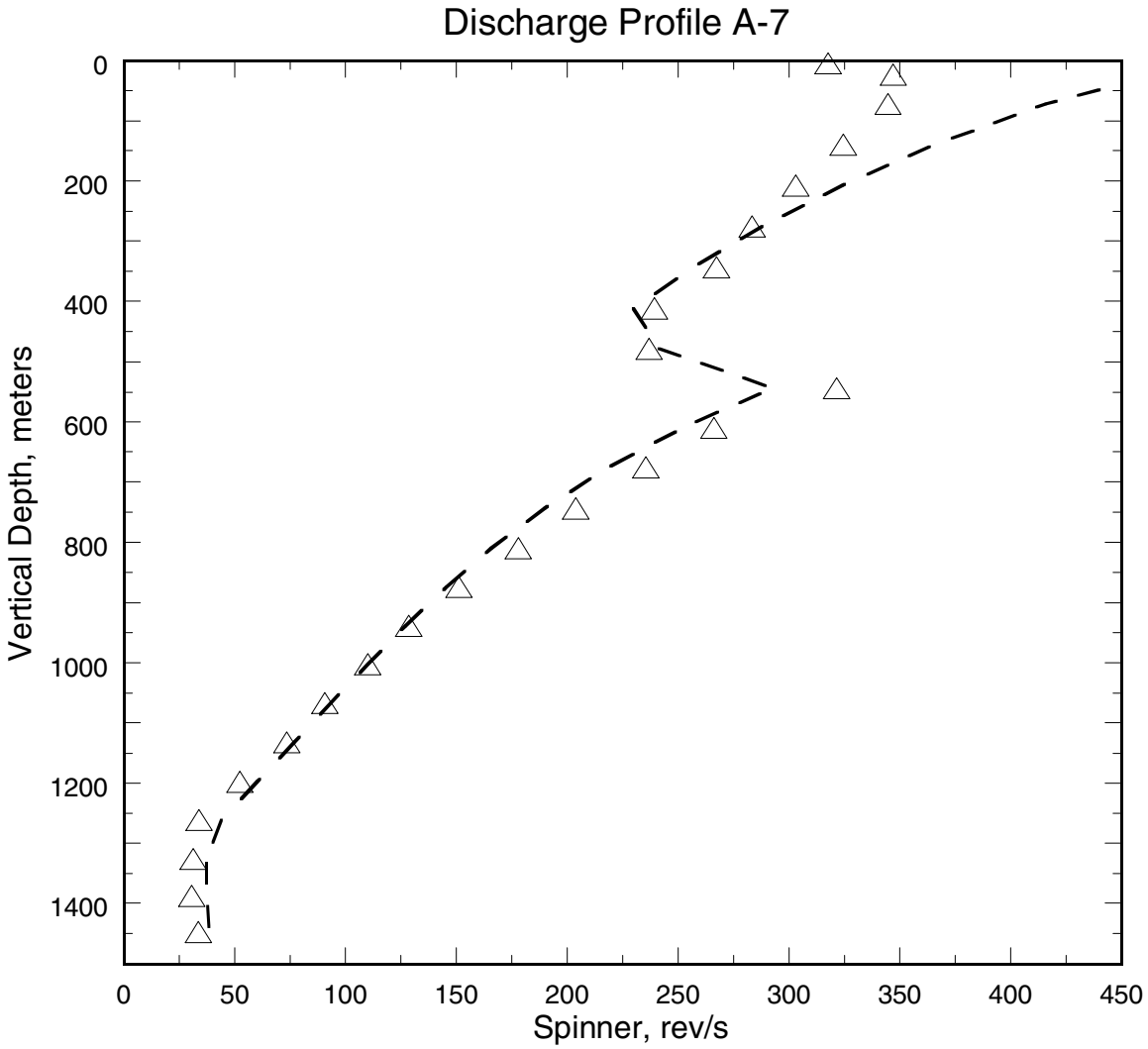

Figure D.5. Comparison of the smoothed spinner response (triangles) with the computed spinner response (dashed line) for well A-7.

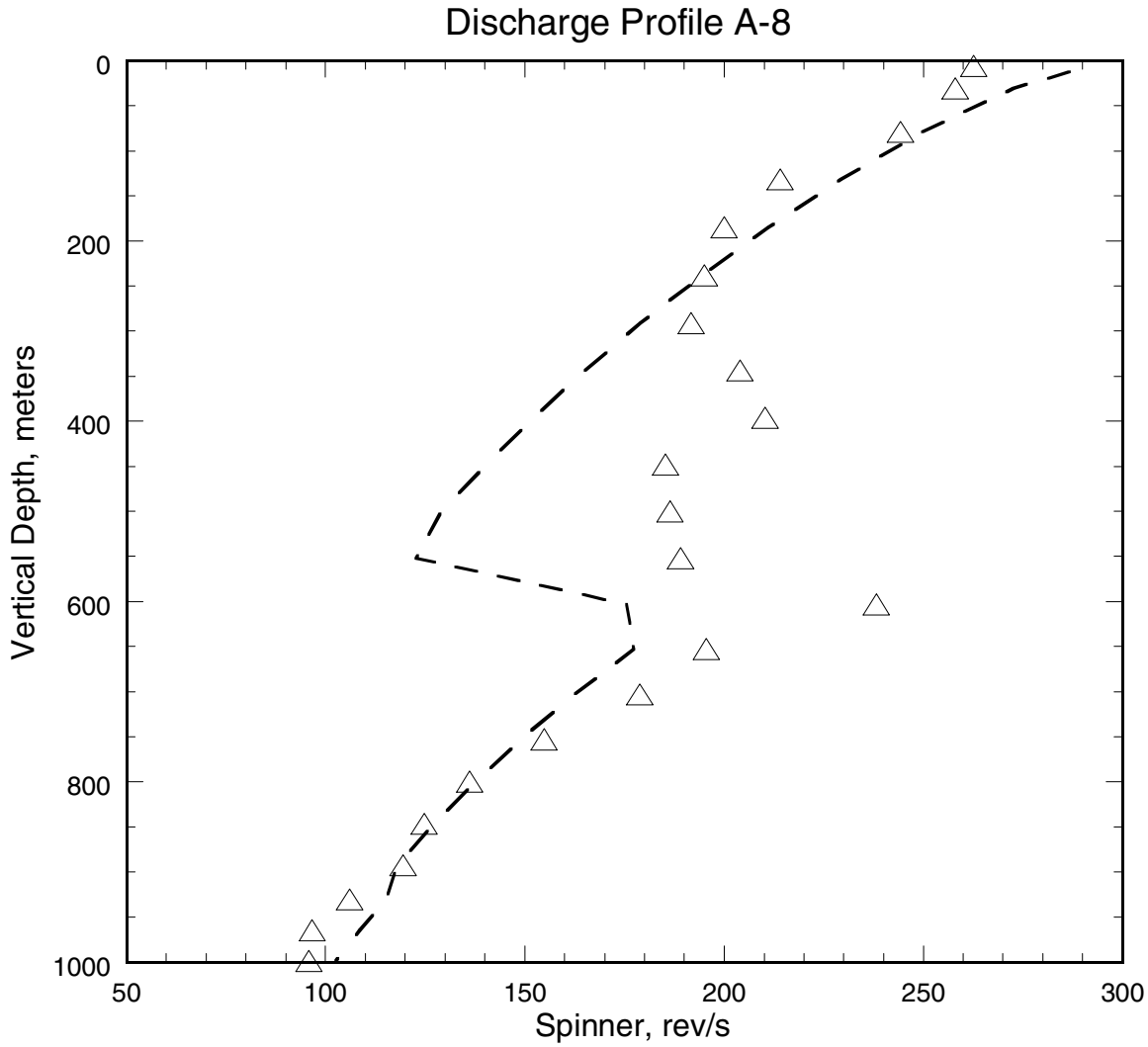

Figure D.6. Comparison of the smoothed spinner response (triangles) with the computed spinner response (dashed line) for well A-8.

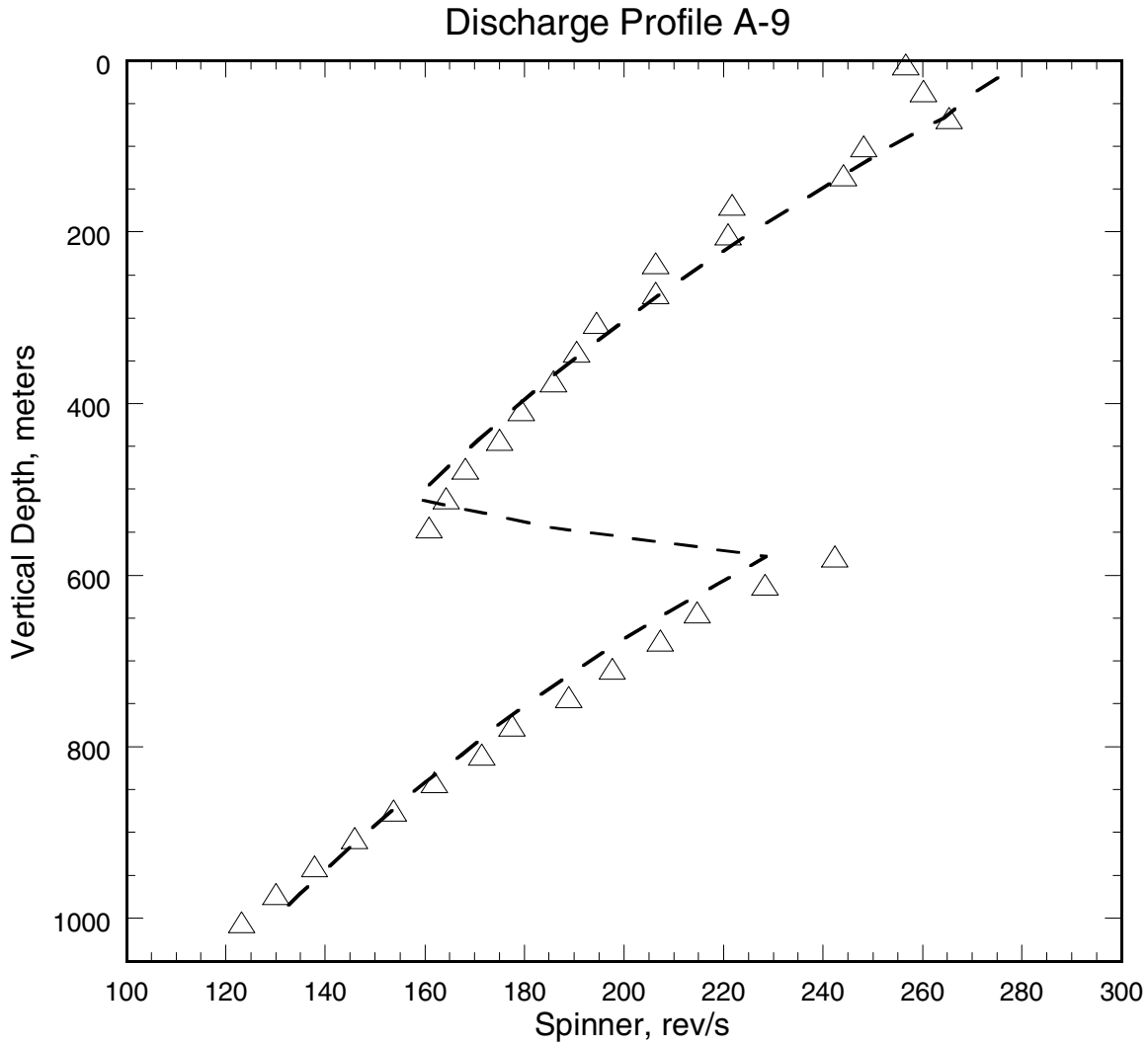

Figure D.7. Comparison of the smoothed spinner response (triangles) with the computed spinner response (dashed line) for well A-9.

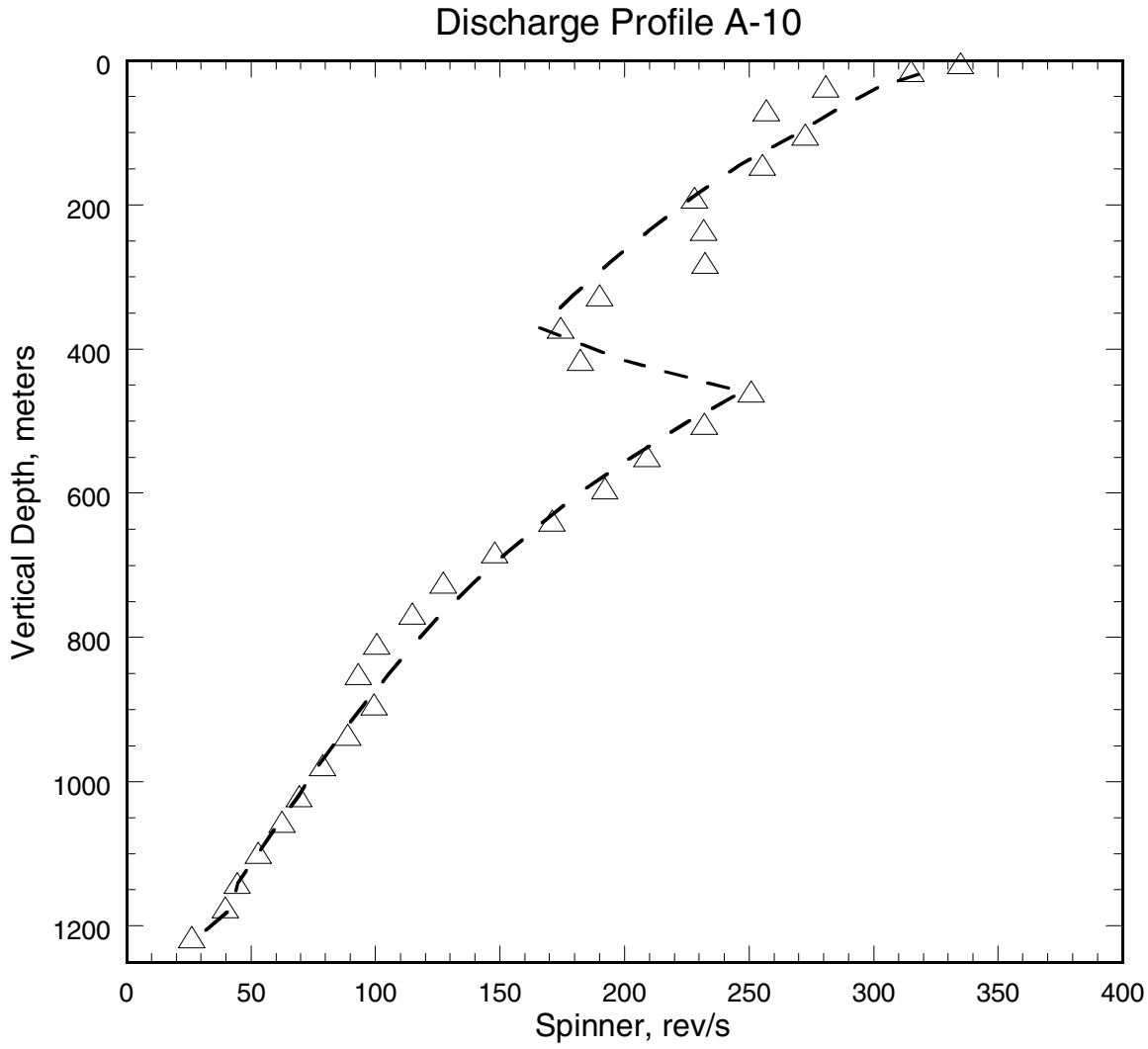

Figure D.8. Comparison of the smoothed spinner response (triangles) with the computed spinner response (dashed line) for well A-10.

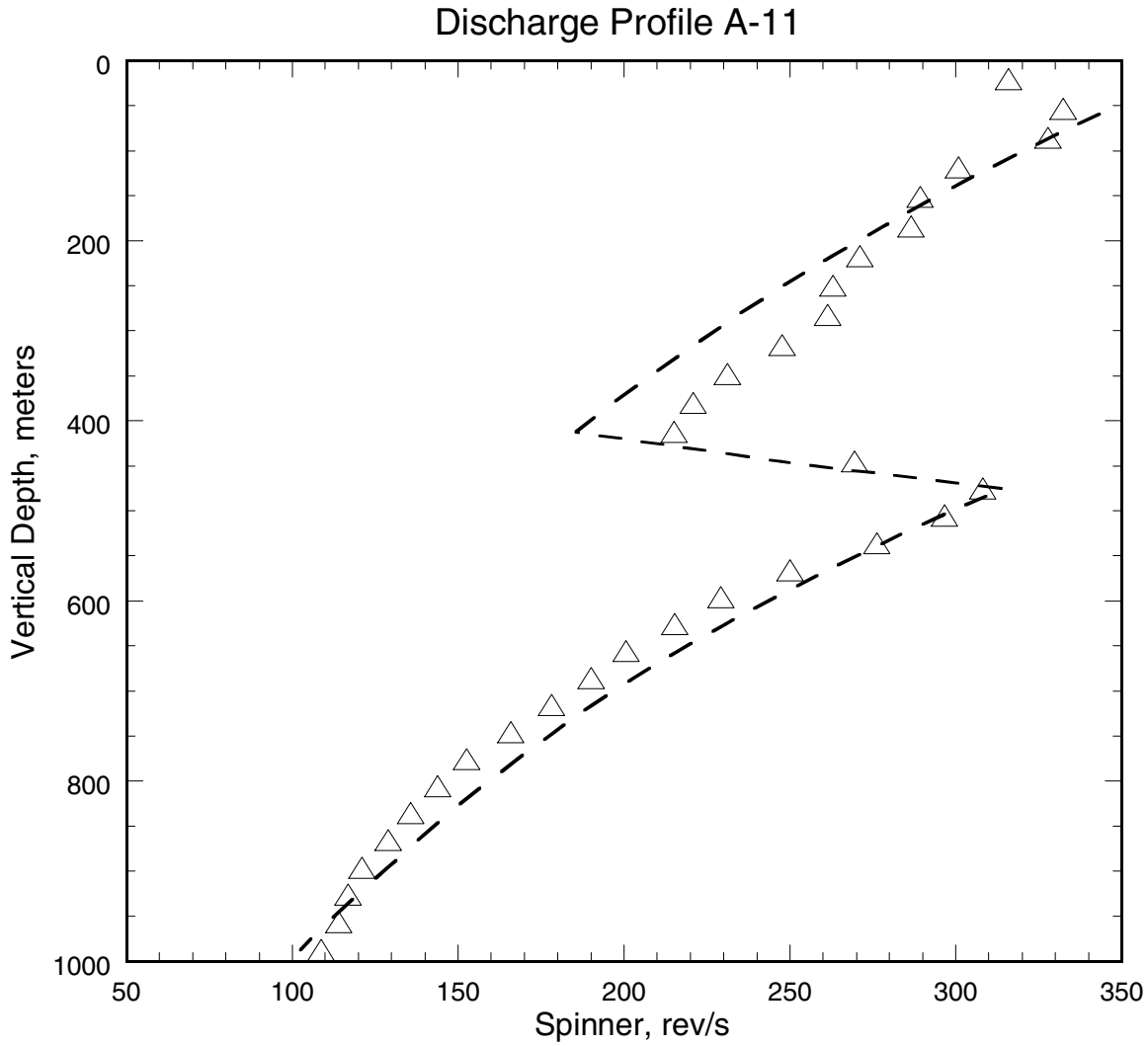

Figure D.9. Comparison of the smoothed spinner response (triangles) with the computed spinner response (dashed line) for well A-11.

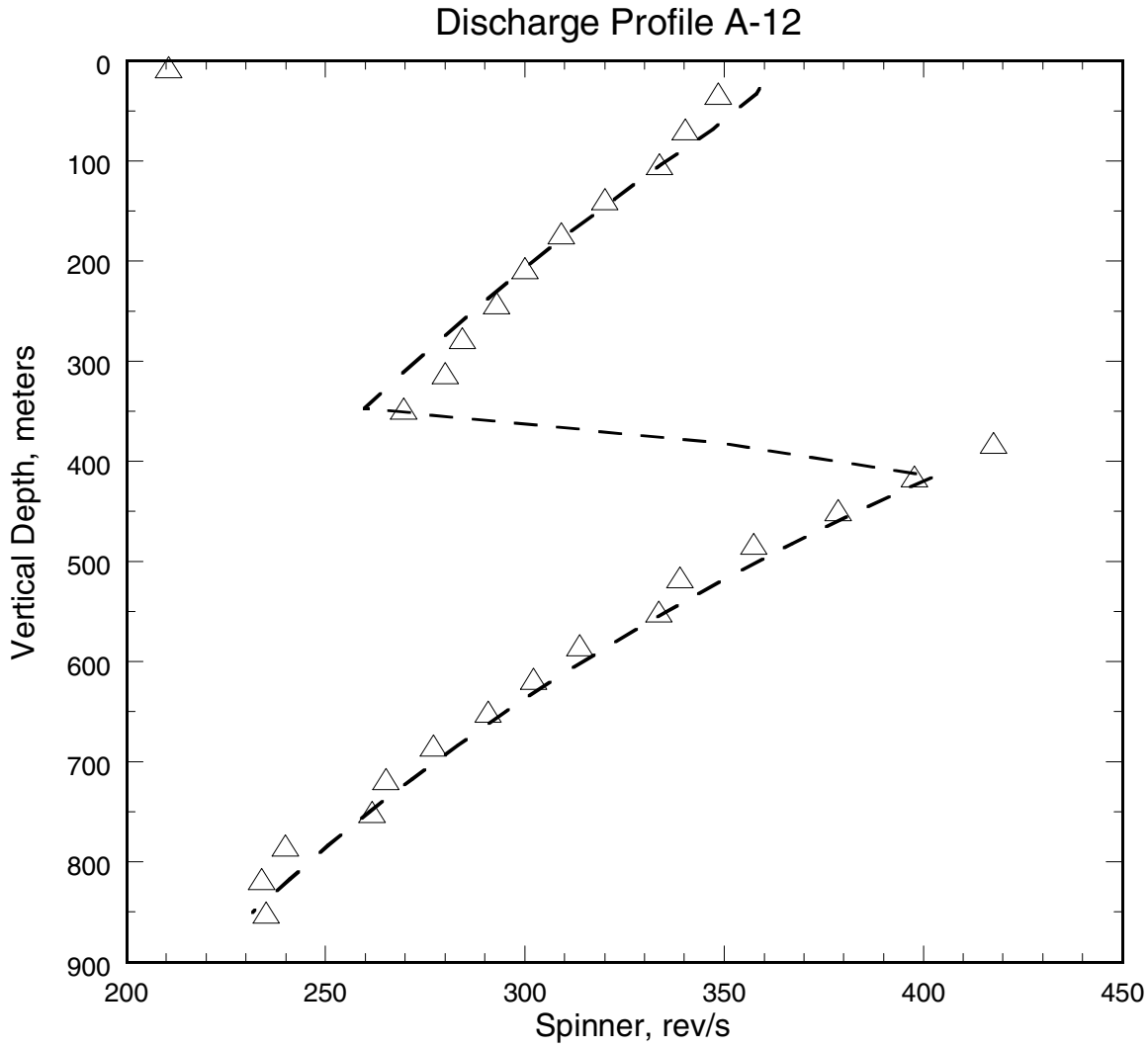

Figure D.10. Comparison of the smoothed spinner response (triangles) with the computed spinner response (dashed line) for well A-12.

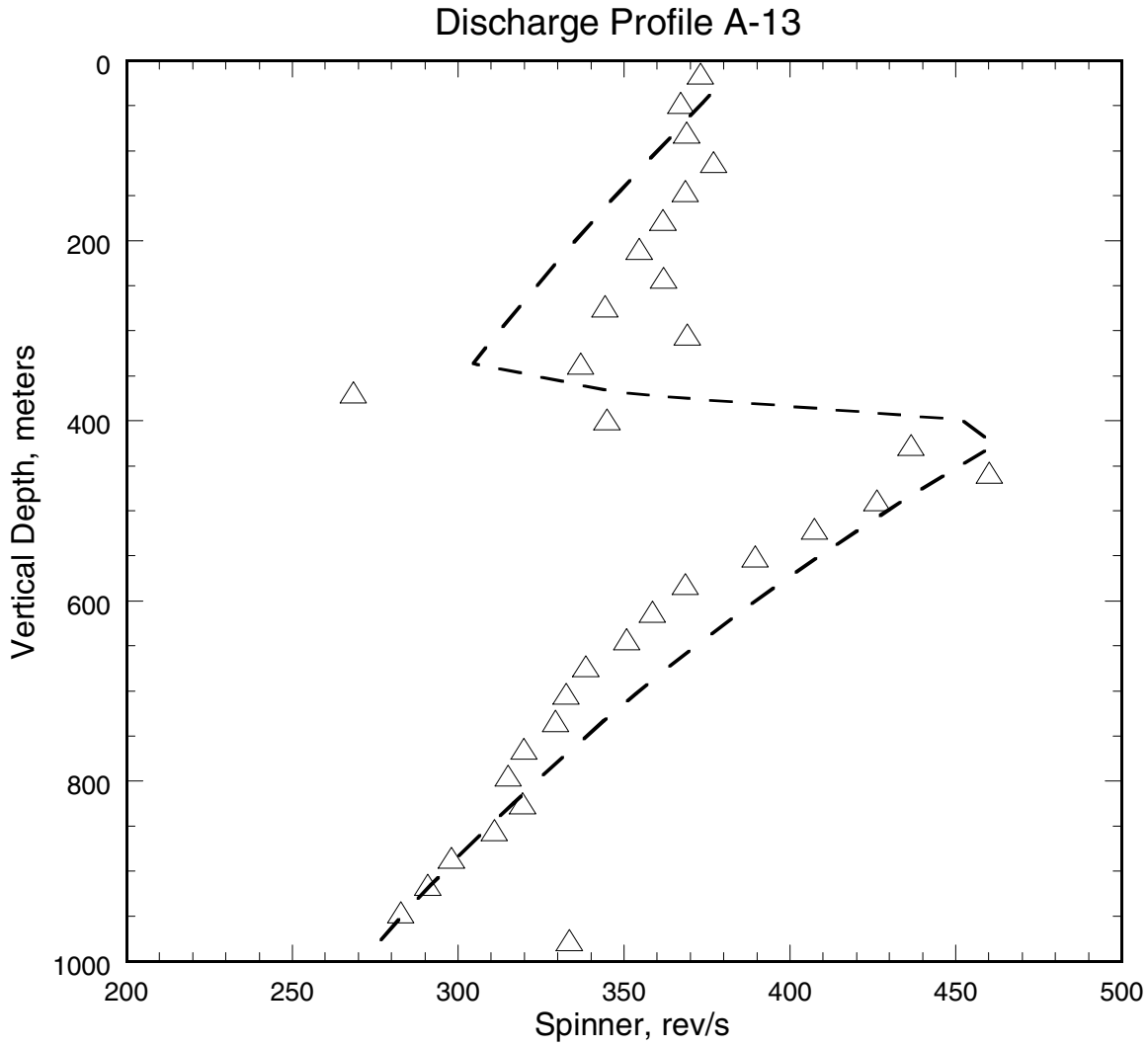

Figure D.11. Comparison of the smoothed spinner response (triangles) with the computed spinner response (dashed line) for well A-13.

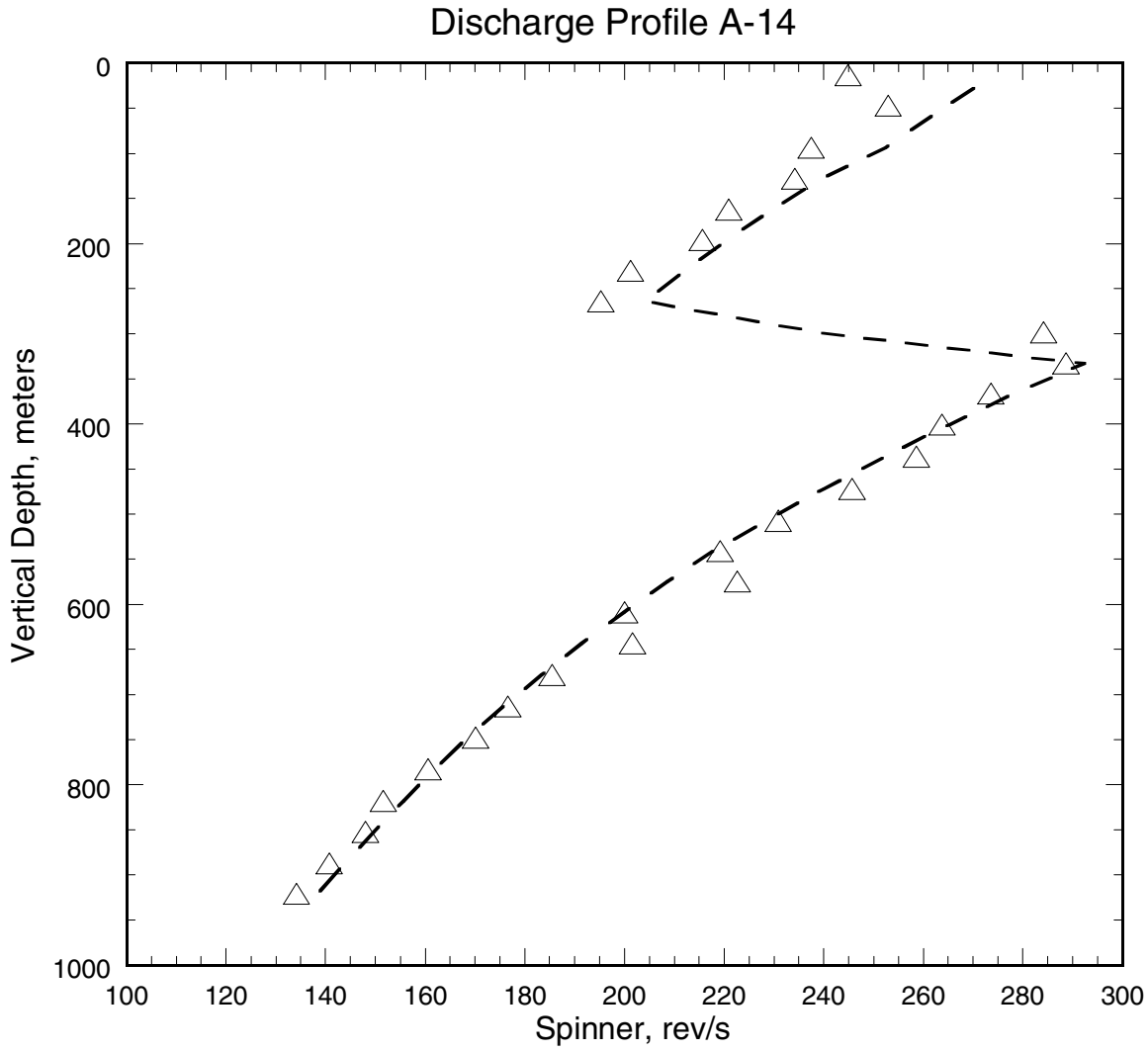

Figure D.12. Comparison of the smoothed spinner response (triangles) with the computed spinner response (dashed line) for well A-14.

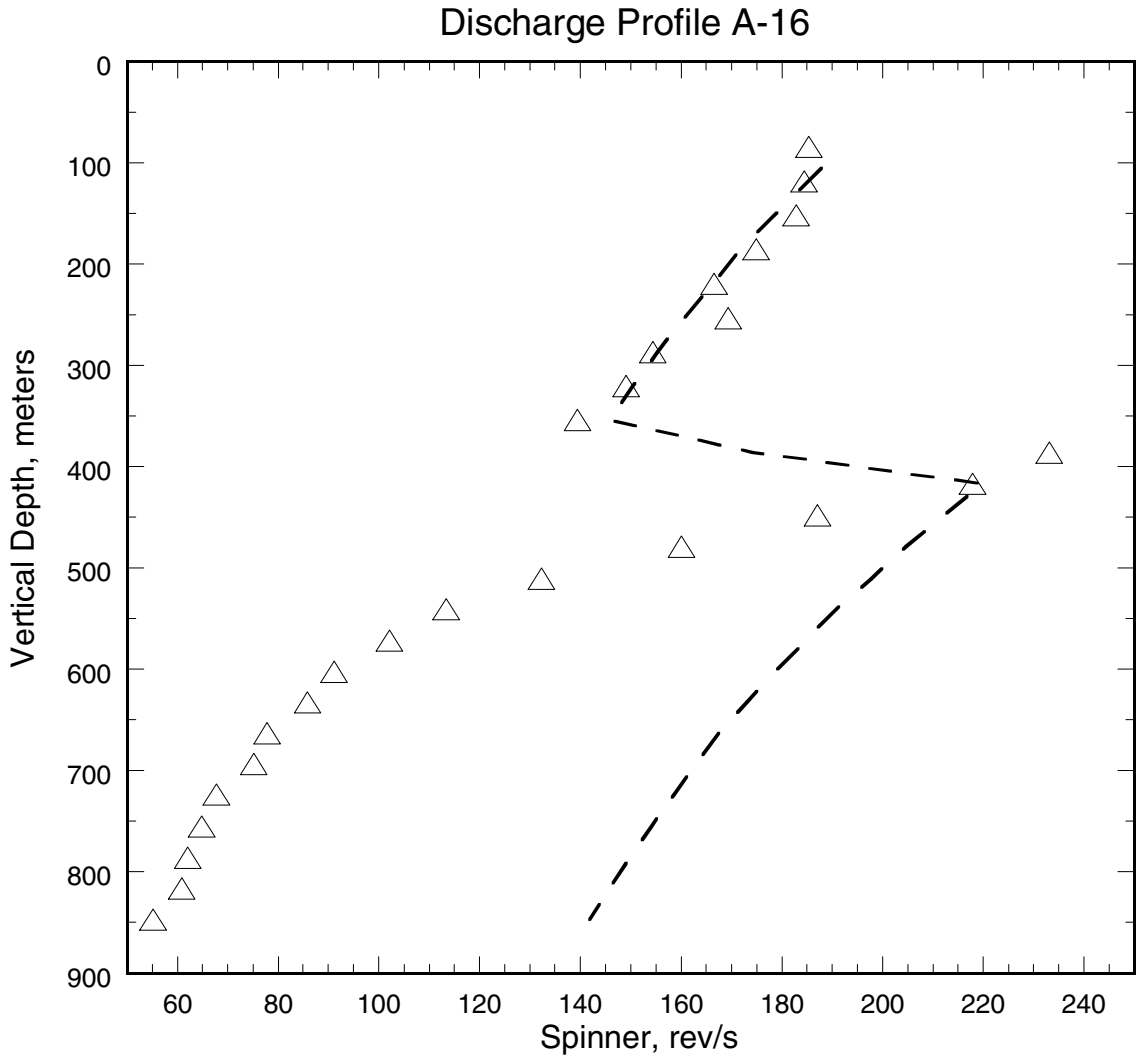

Figure D.13. Comparison of the smoothed spinner response (triangles) with the computed spinner response (dashed line) for well A-16.

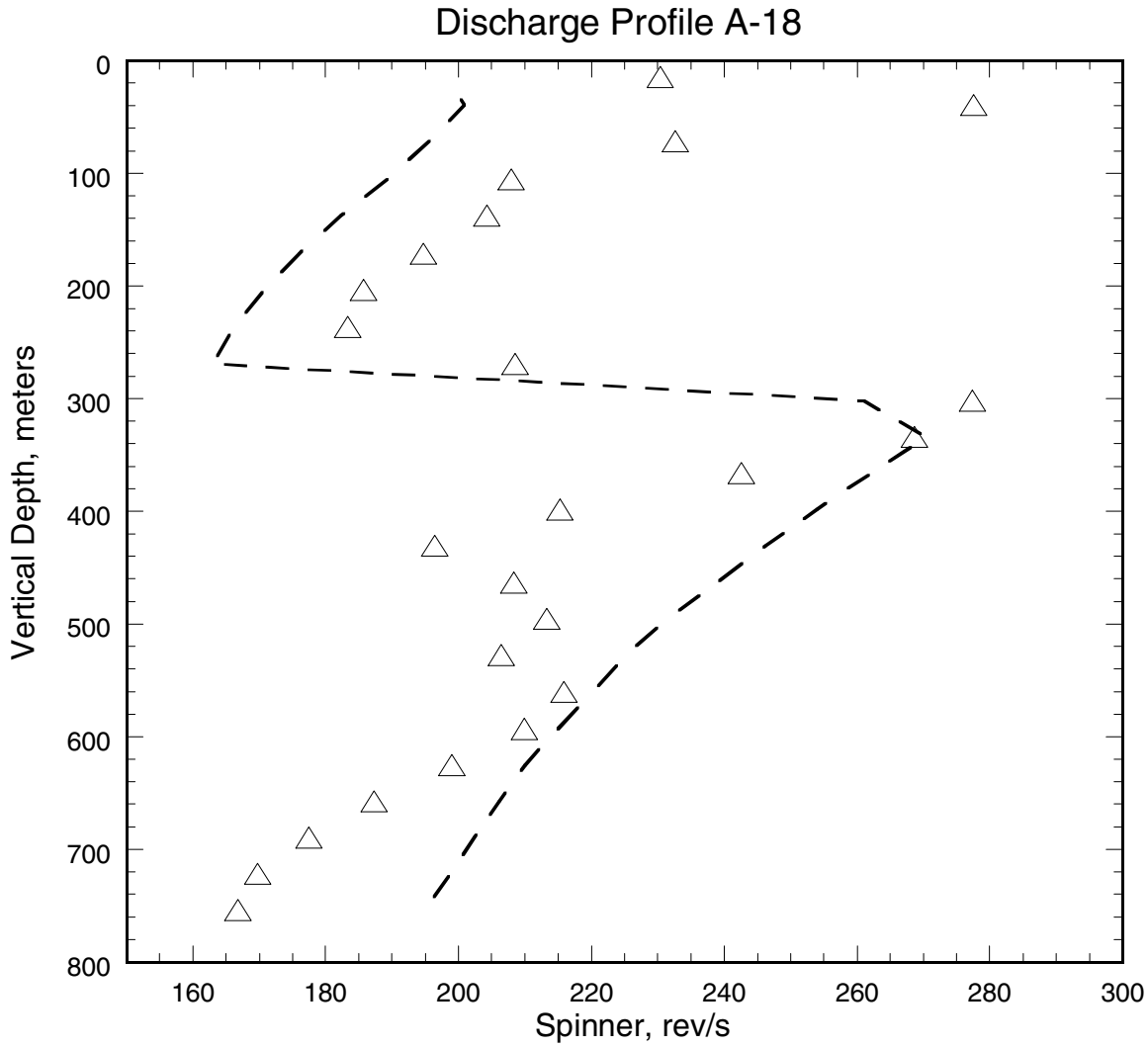

Figure D.14. Comparison of the smoothed spinner response (triangles) with the computed spinner response (dashed line) for well A-18.

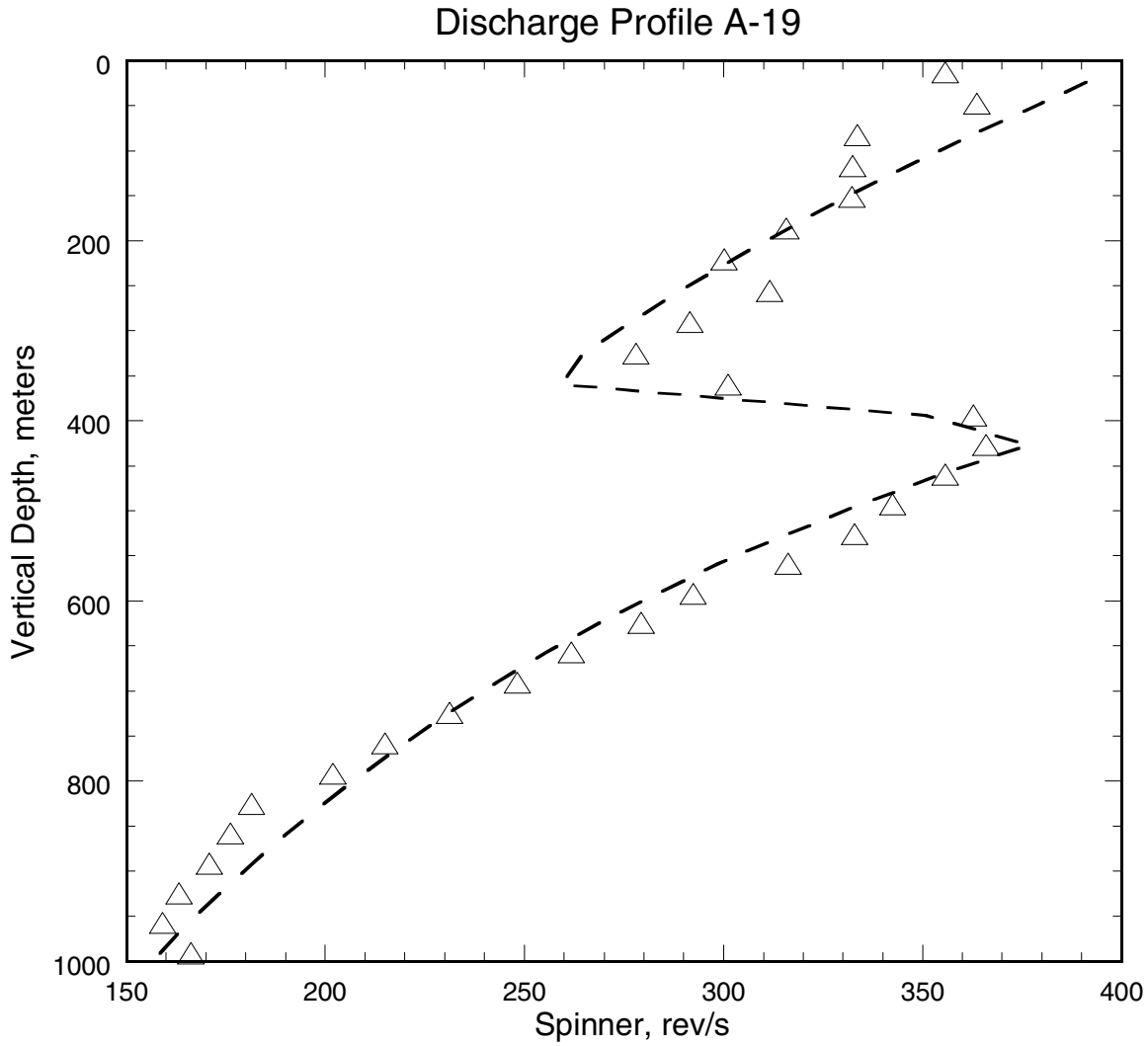

Figure D.15. Comparison of the smoothed spinner response (triangles) with the computed spinner response (dashed line) for well A-19.

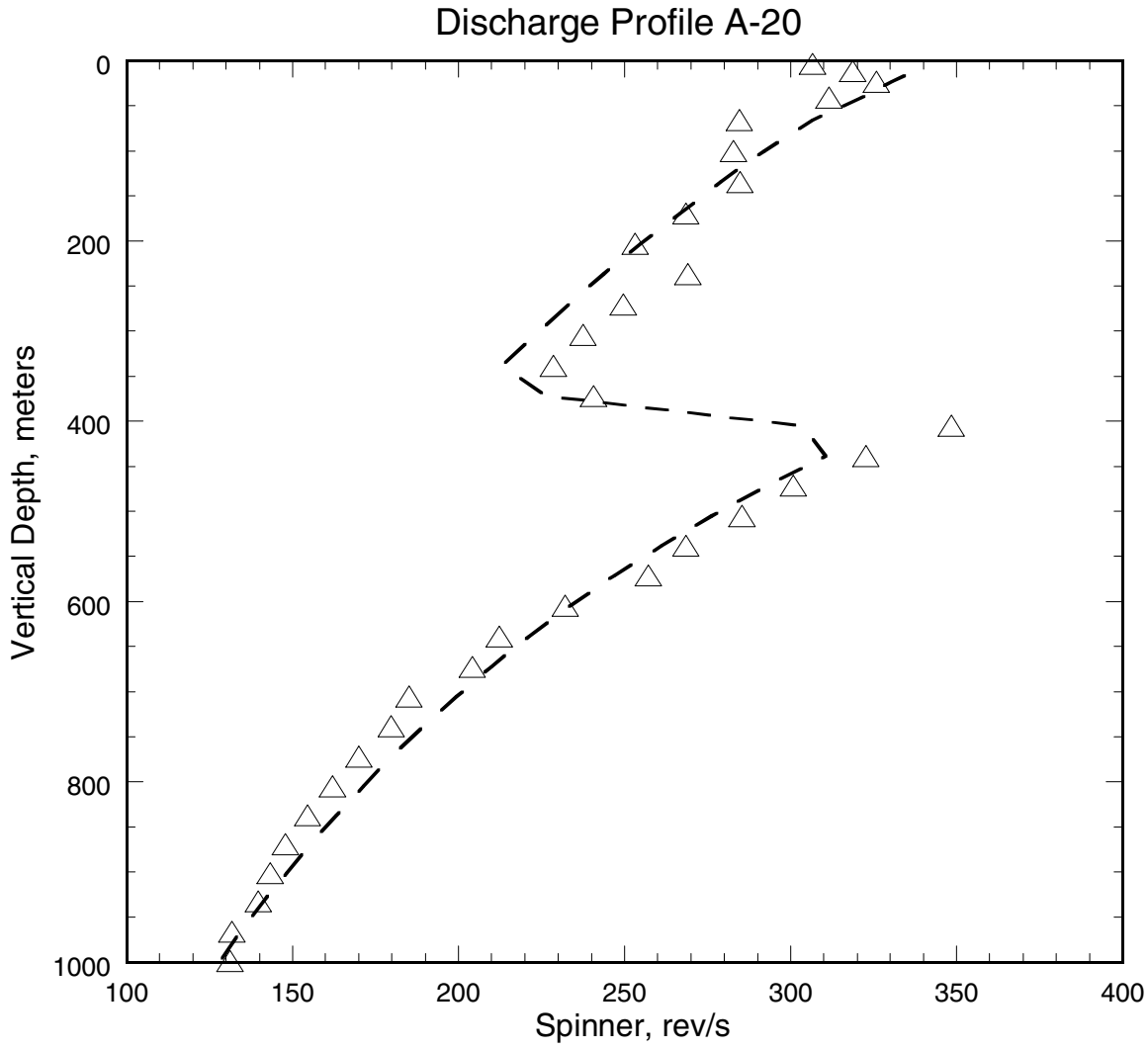

Figure D.16. Comparison of the smoothed spinner response (triangles) with the computed spinner response (dashed line) for well A-20.

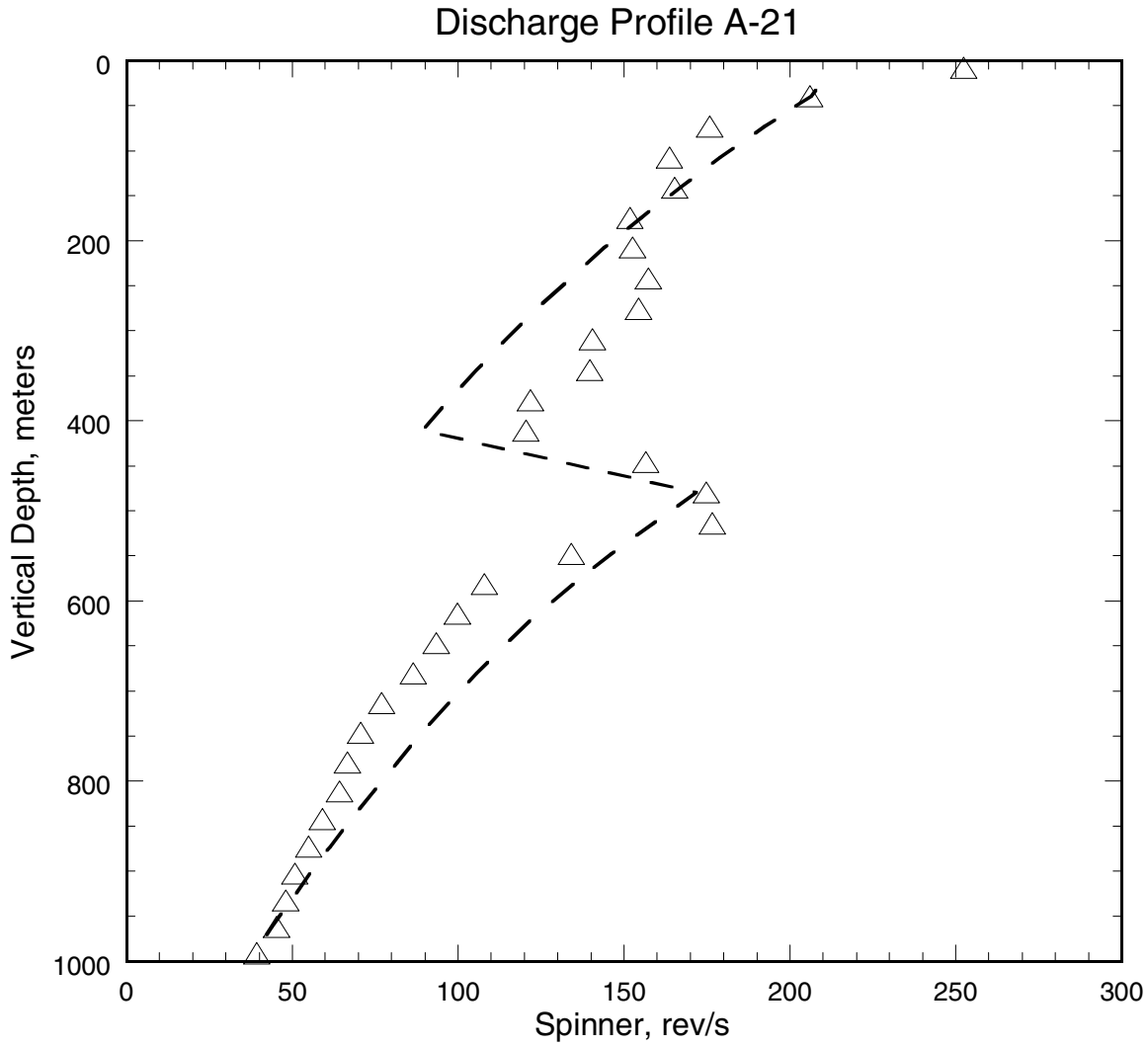

Figure D.17. Comparison of the smoothed spinner response (triangles) with the computed spinner response (dashed line) for well A-21.

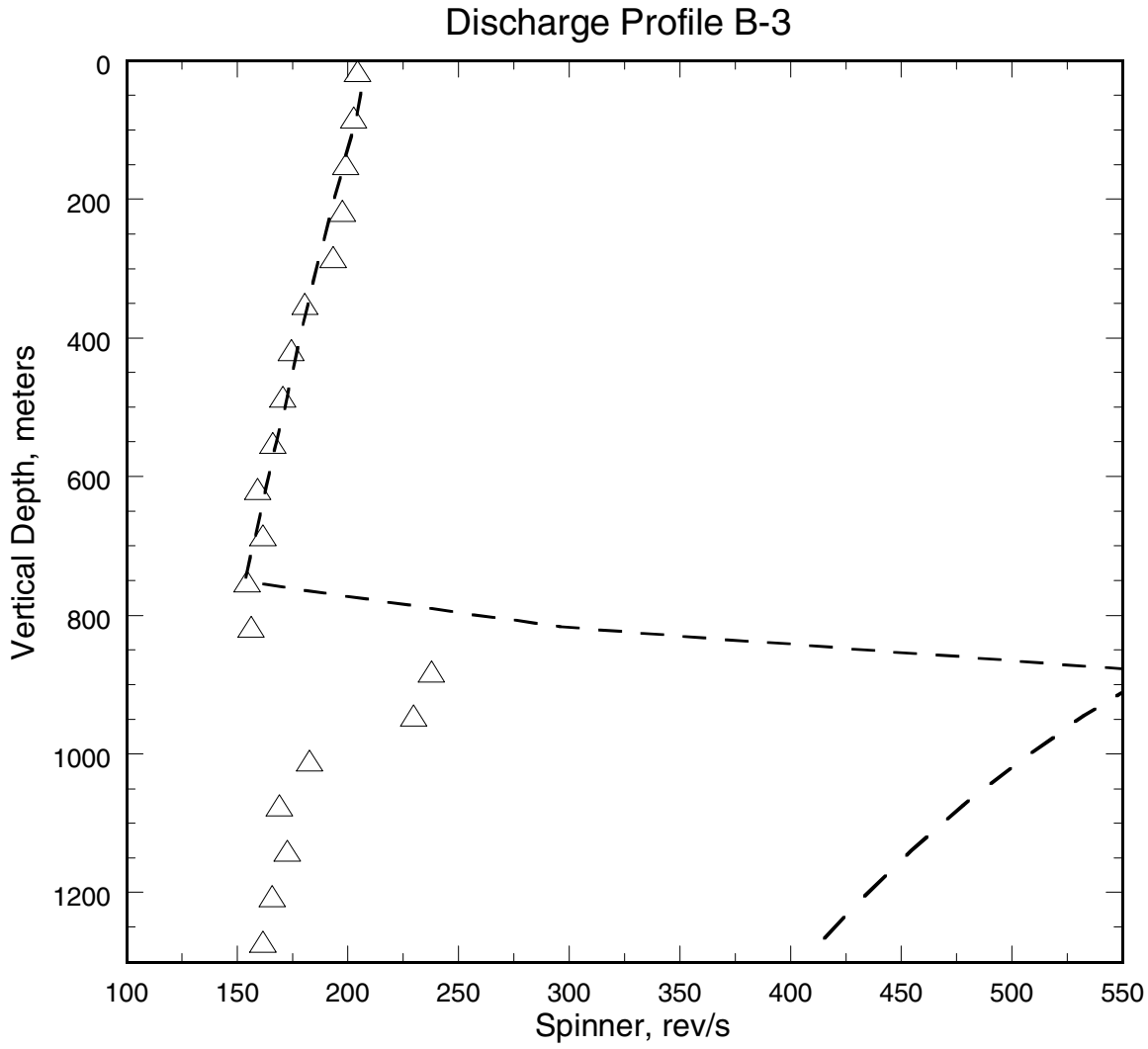

Figure D.18. Comparison of the smoothed spinner response (triangles) with the computed spinner response (dashed line) for well B-3.

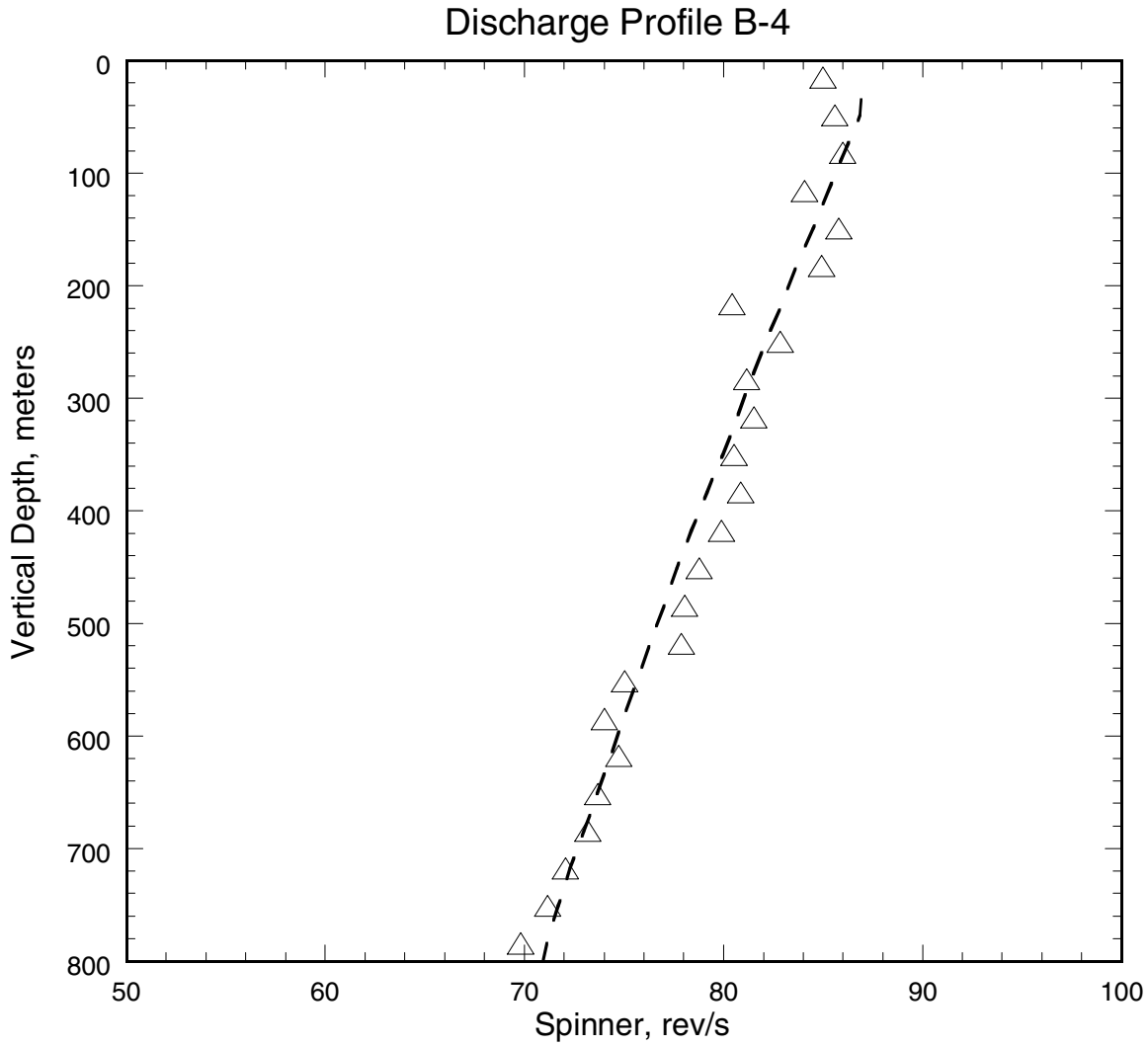

Figure D.19. Comparison of the smoothed spinner response (triangles) with the computed spinner response (dashed line) for well B-4.

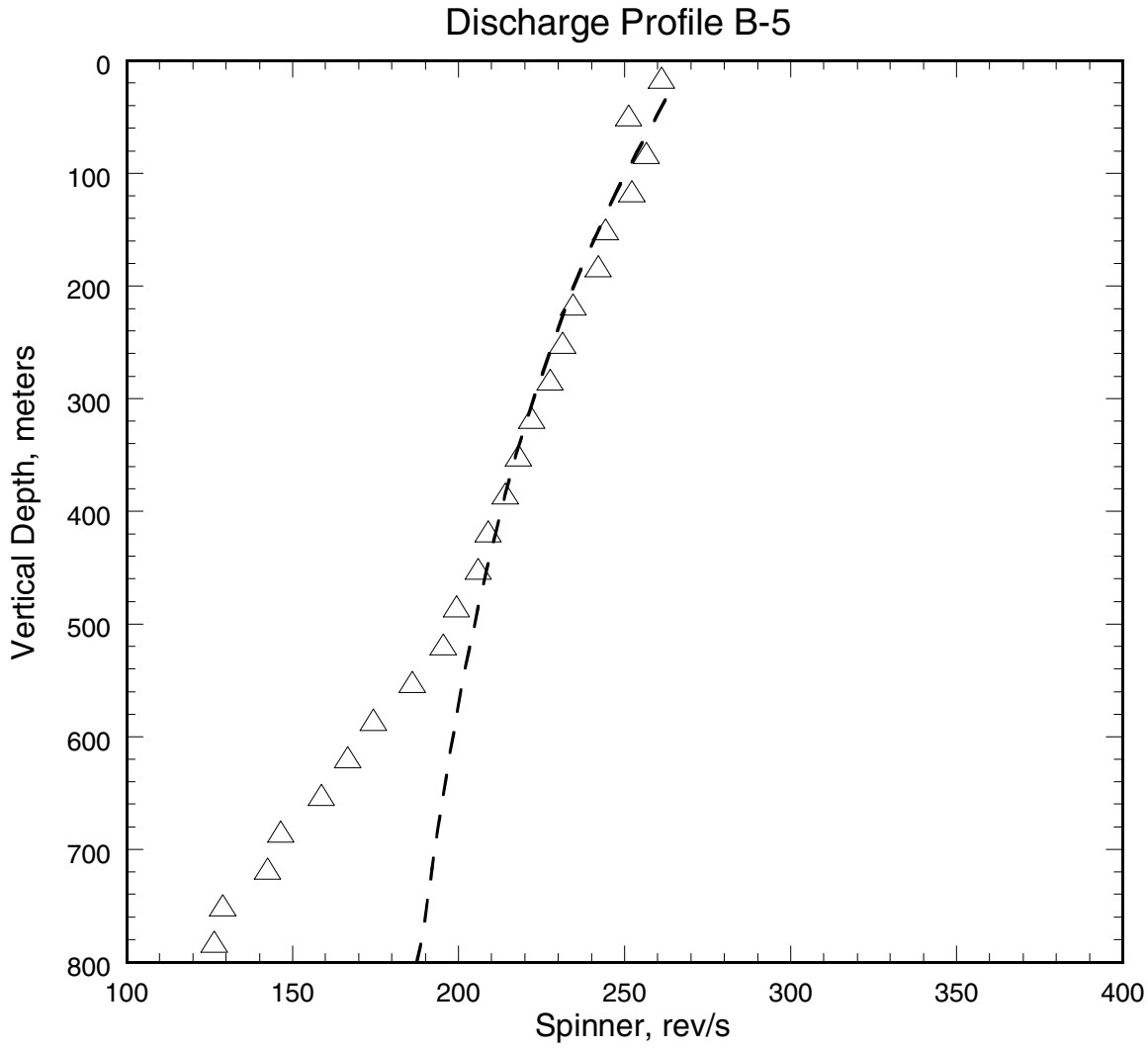

Figure D.20. Comparison of the smoothed spinner response (triangles) with the computed spinner response (dashed line) for well B-5.

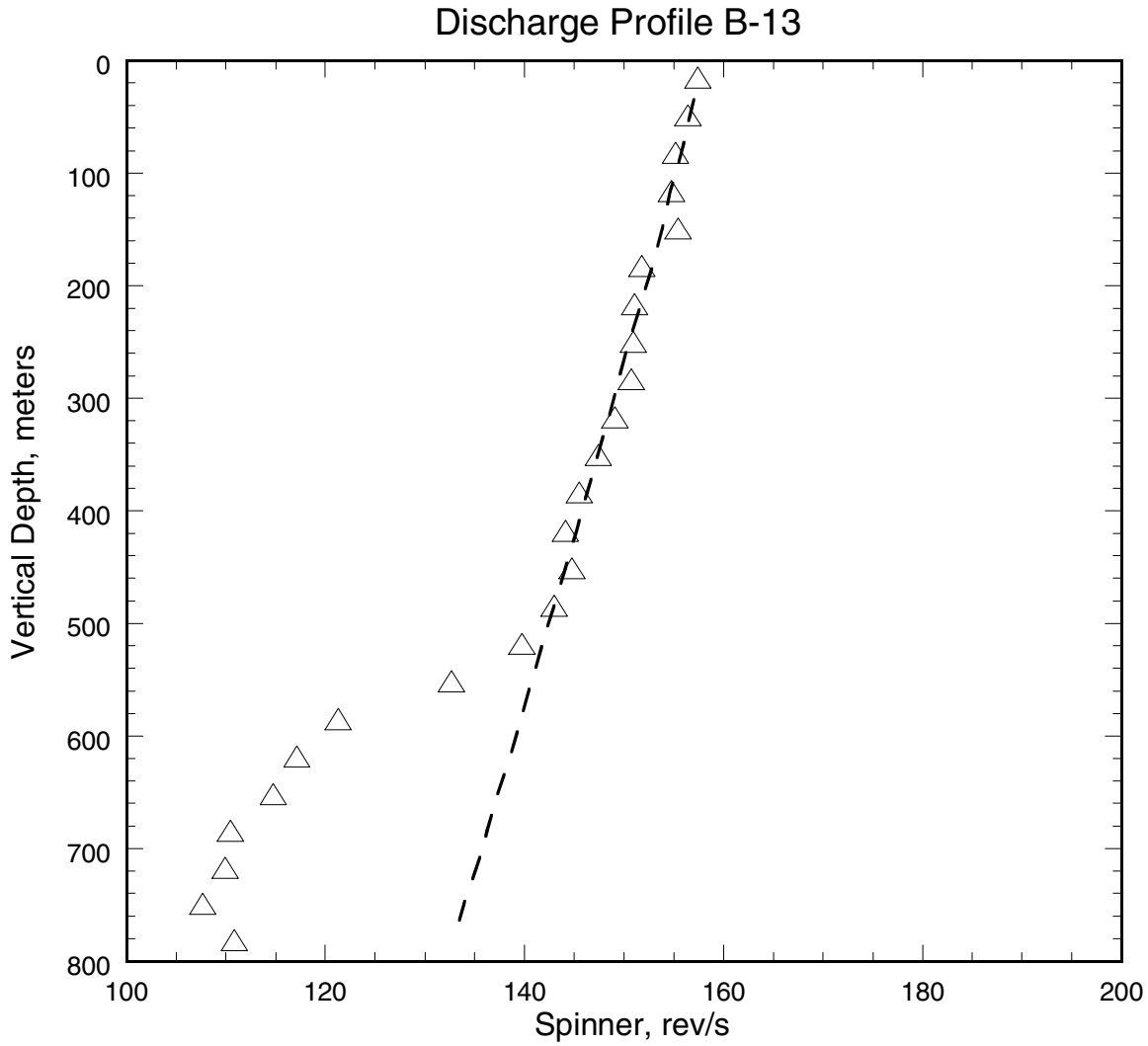

Figure D.21. Comparison of the smoothed spinner response (triangles) with the computed spinner response (dashed line) for well B-13.

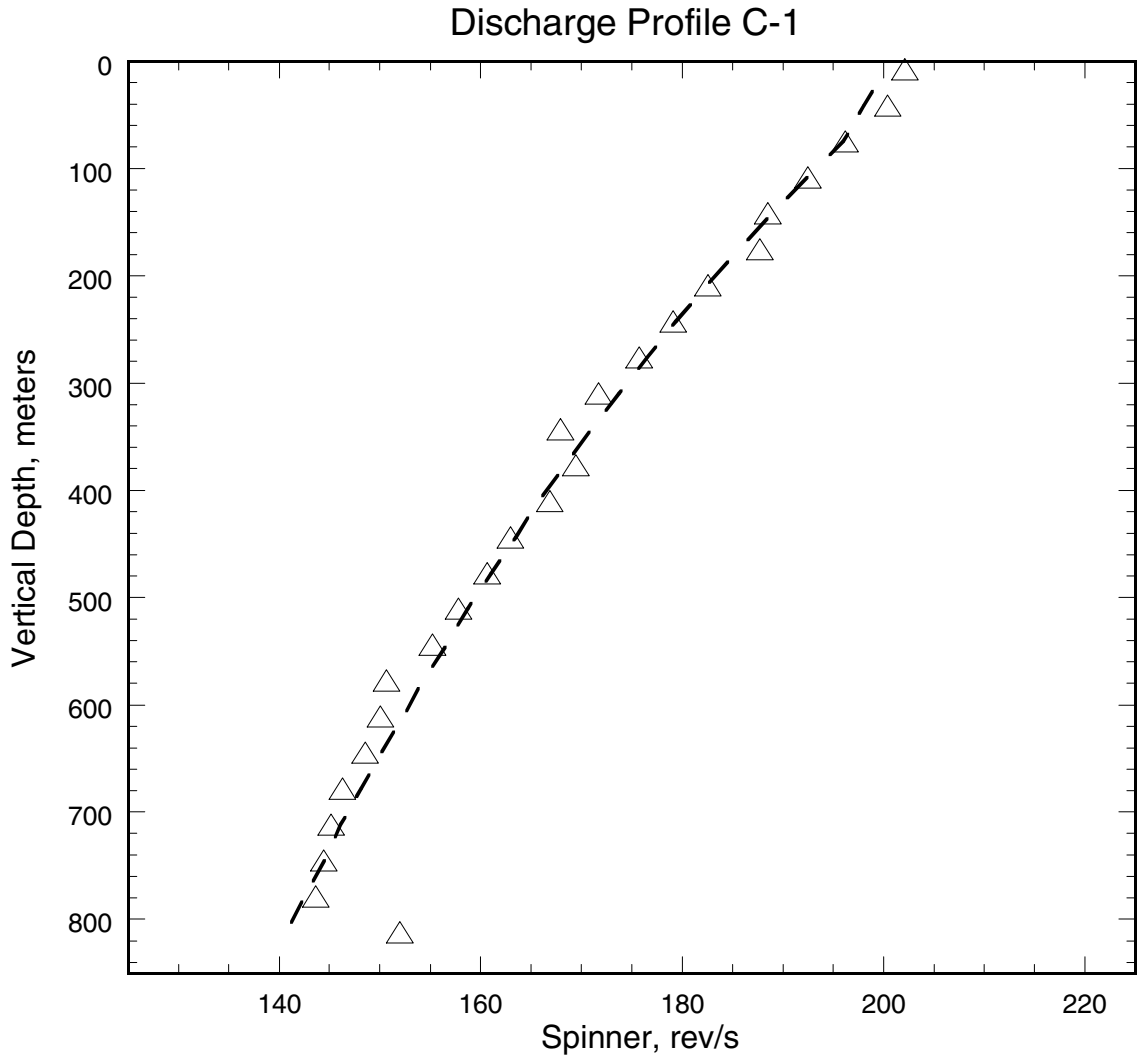

Figure D.22. Comparison of the smoothed spinner response (triangles) with the computed spinner response (dashed line) for well C-1.

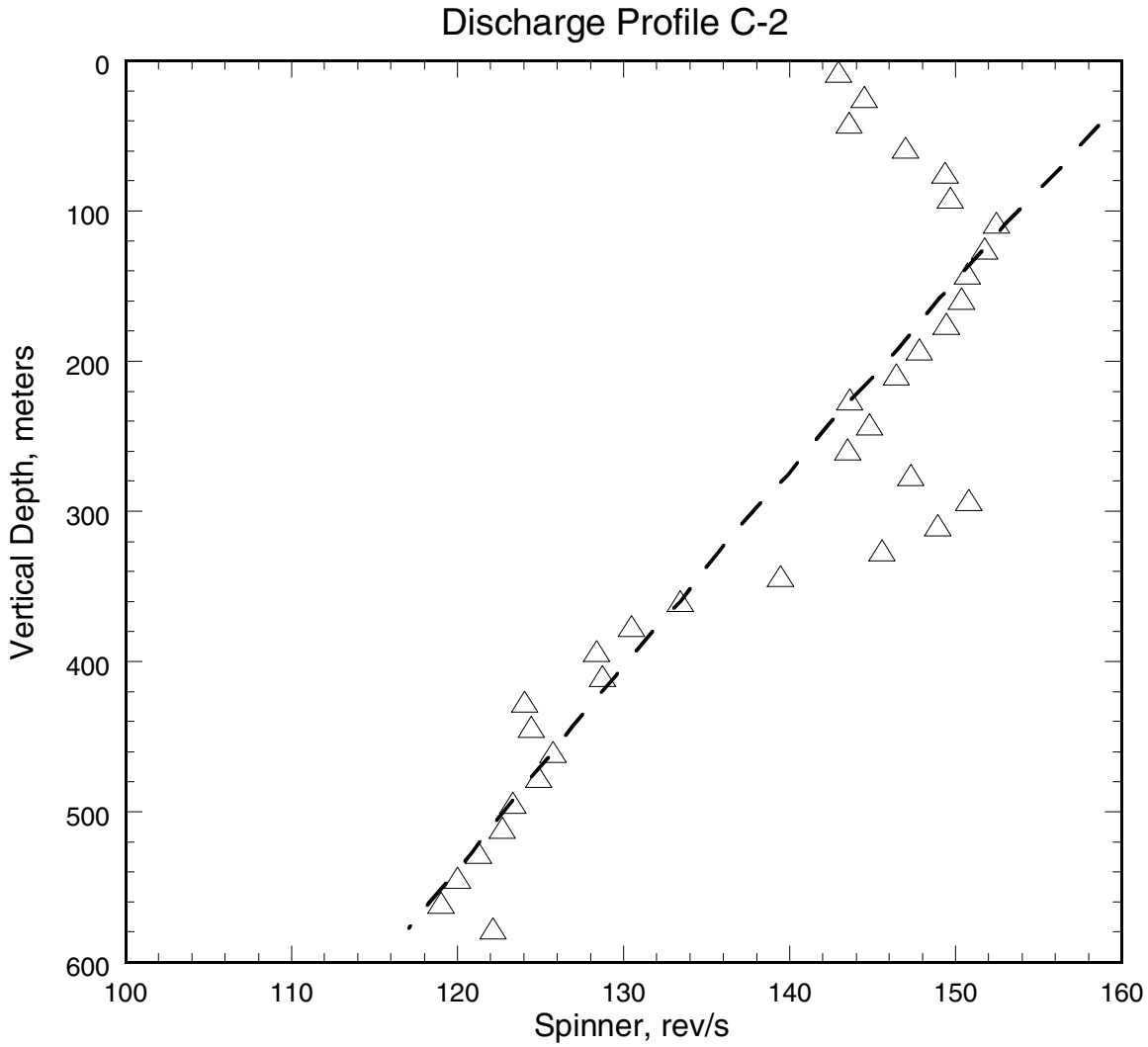

Figure D.23. Comparison of the smoothed spinner response (triangles) with the computed spinner response (dashed line) for well C-2.

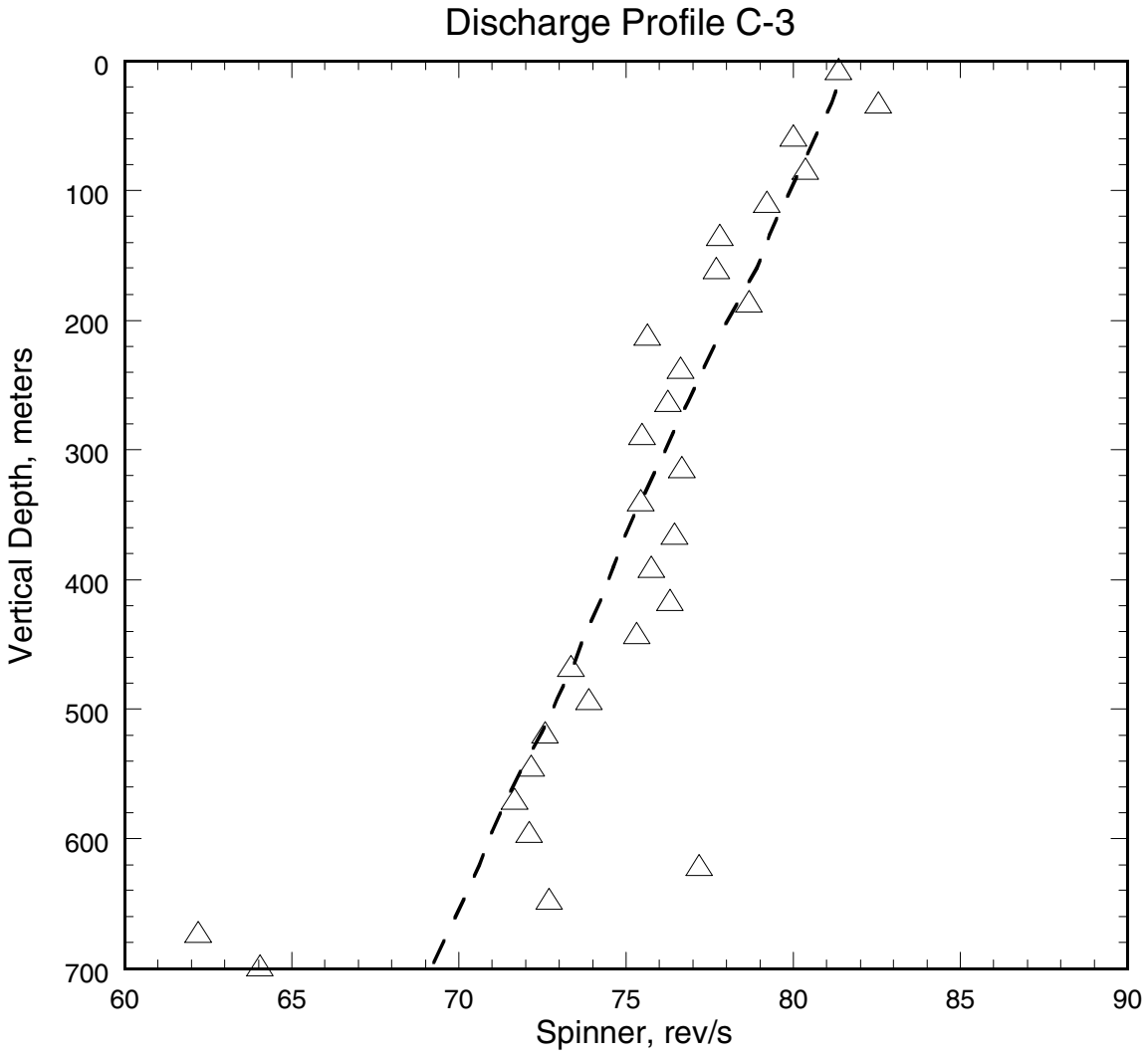

Figure D.24. Comparison of the smoothed spinner response (triangles) with the computed spinner response (dashed line) for well C-3.

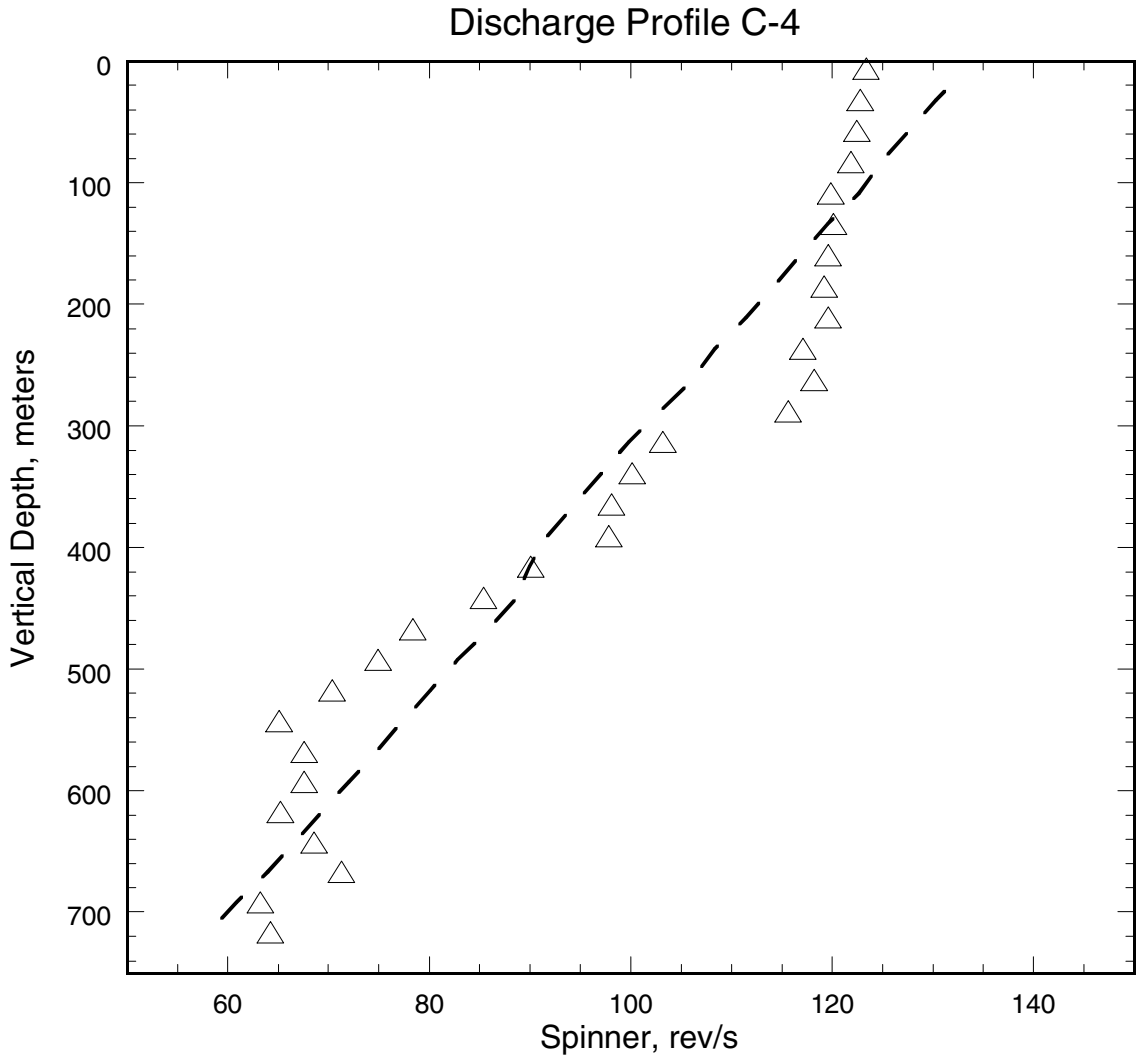

Figure D.25. Comparison of the smoothed spinner response (triangles) with the computed spinner response (dashed line) for well C-4.

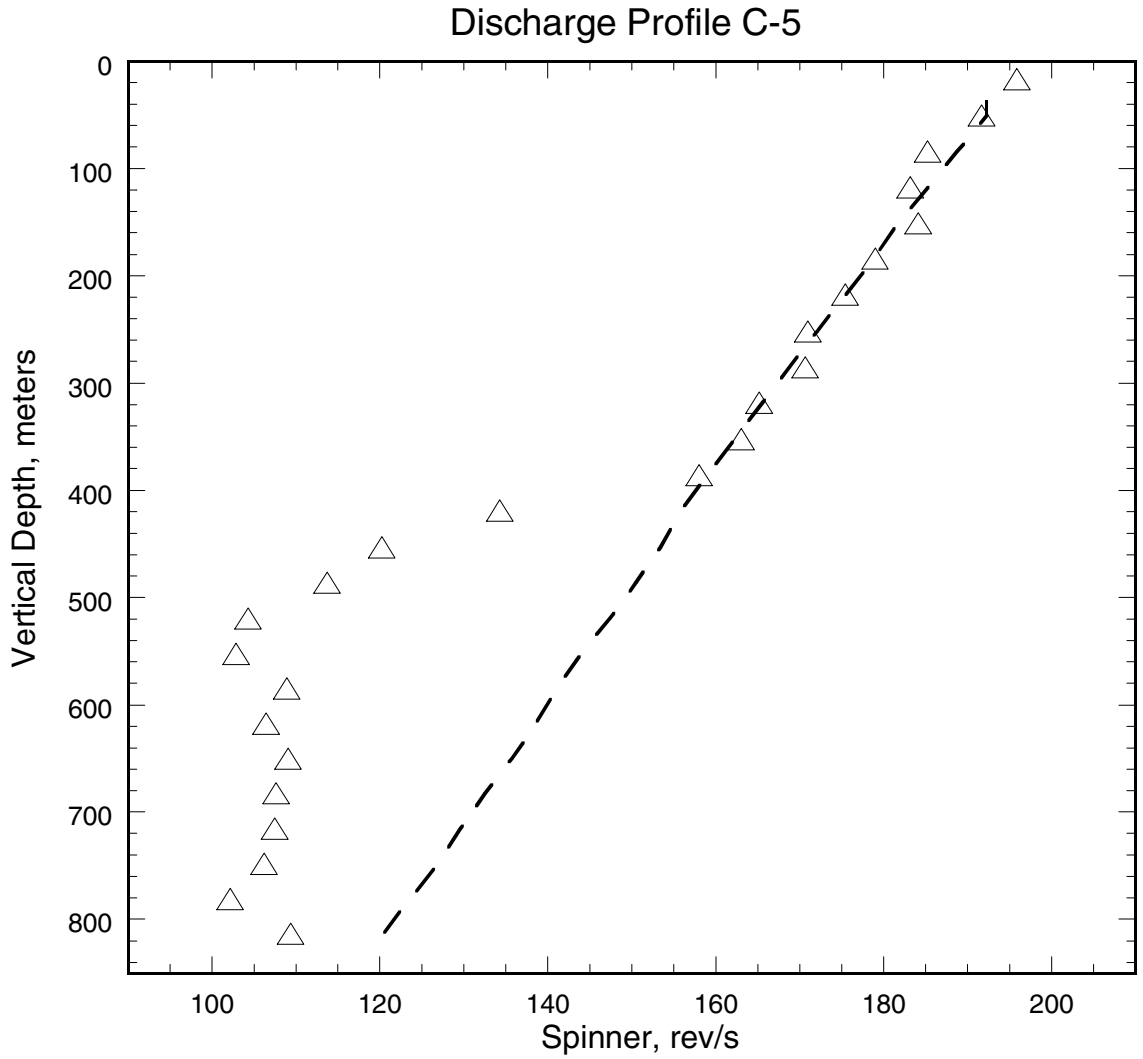

Figure D.26. Comparison of the smoothed spinner response (triangles) with the computed spinner response (dashed line) for well C-5.

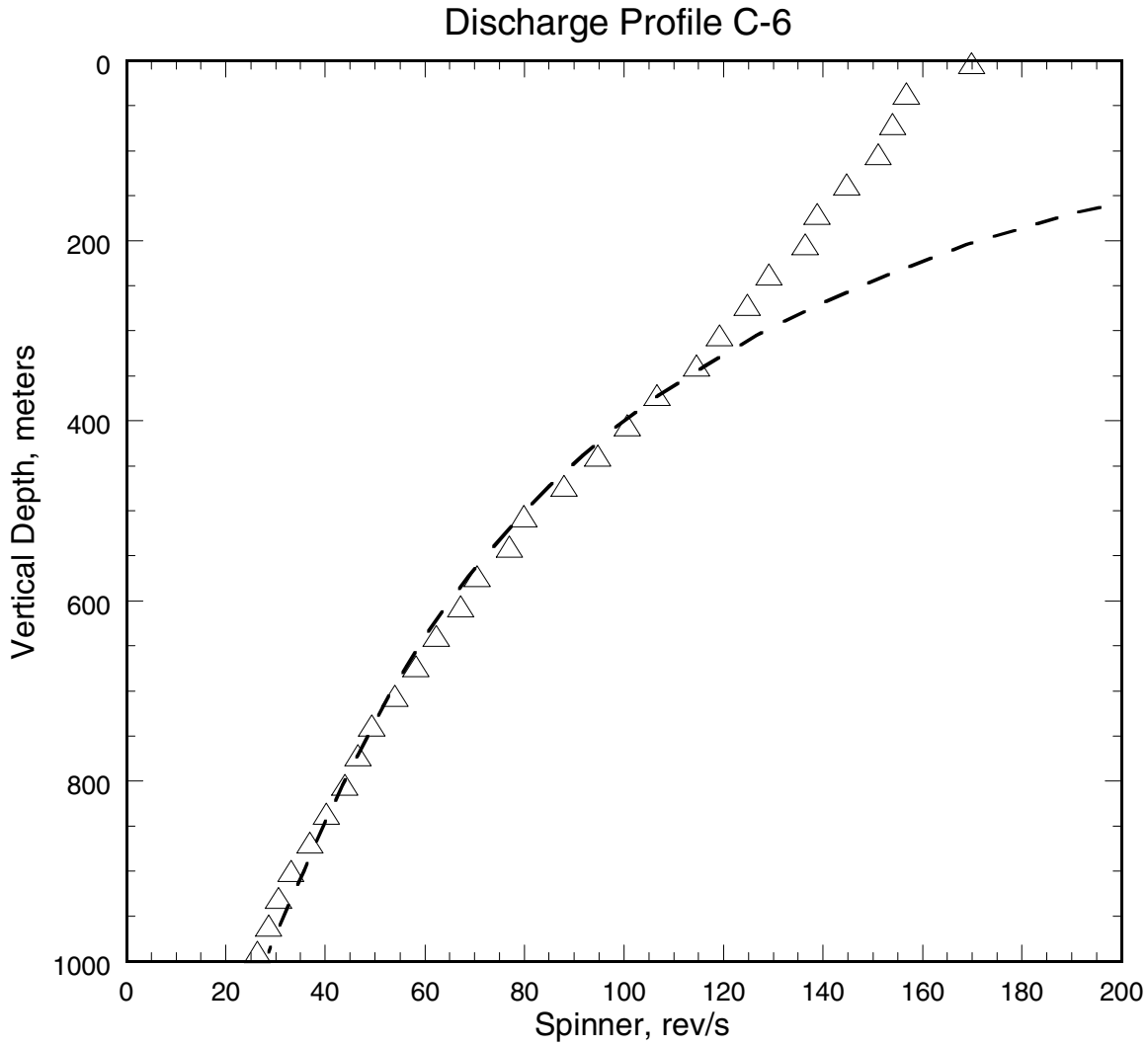

Figure D.27. Comparison of the smoothed spinner response (triangles) with the computed spinner response (dashed line) for well C-6.

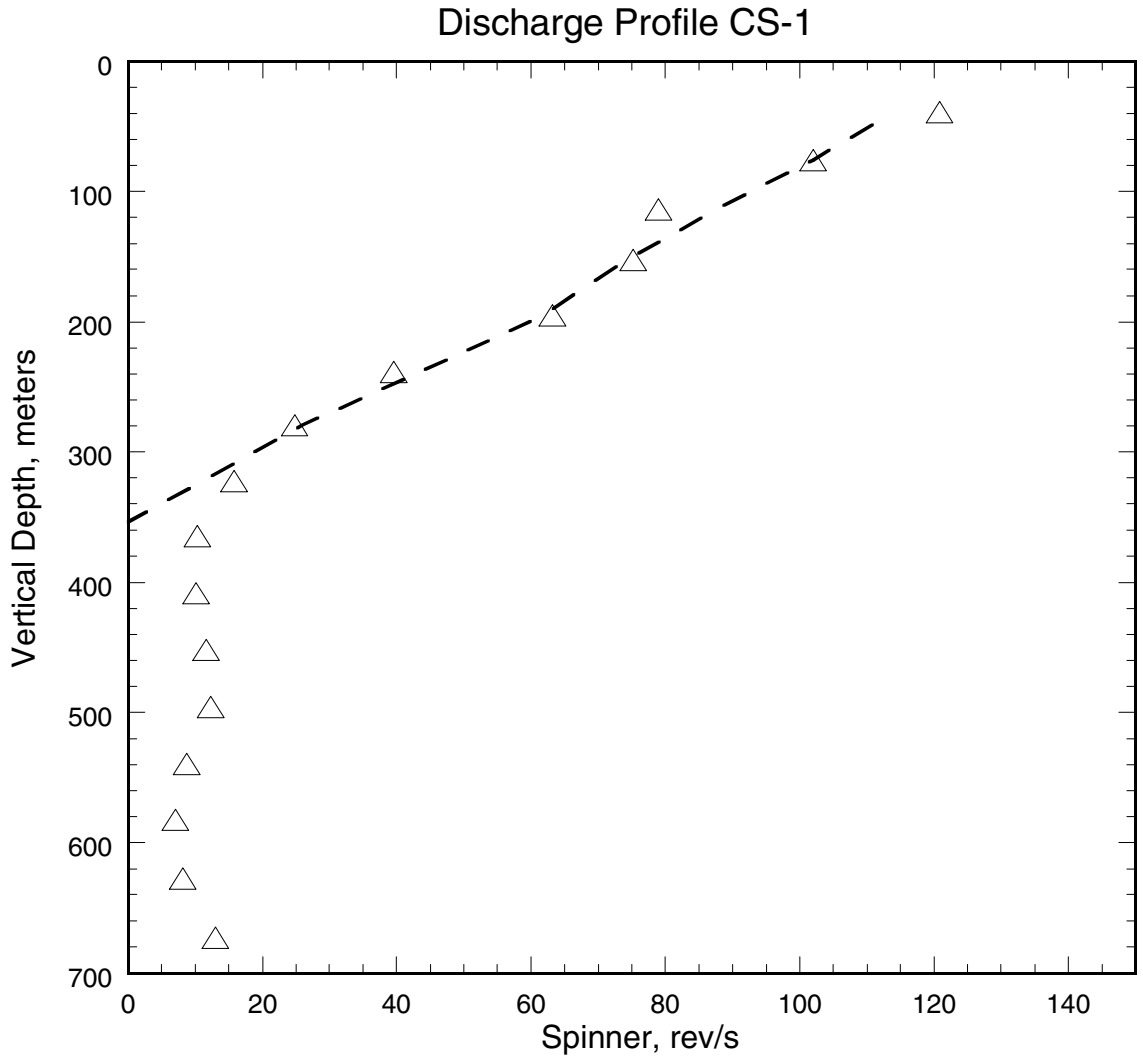

Figure D.28. Comparison of the smoothed spinner response (triangles) with the computed spinner response (dashed line) for well CS-1.

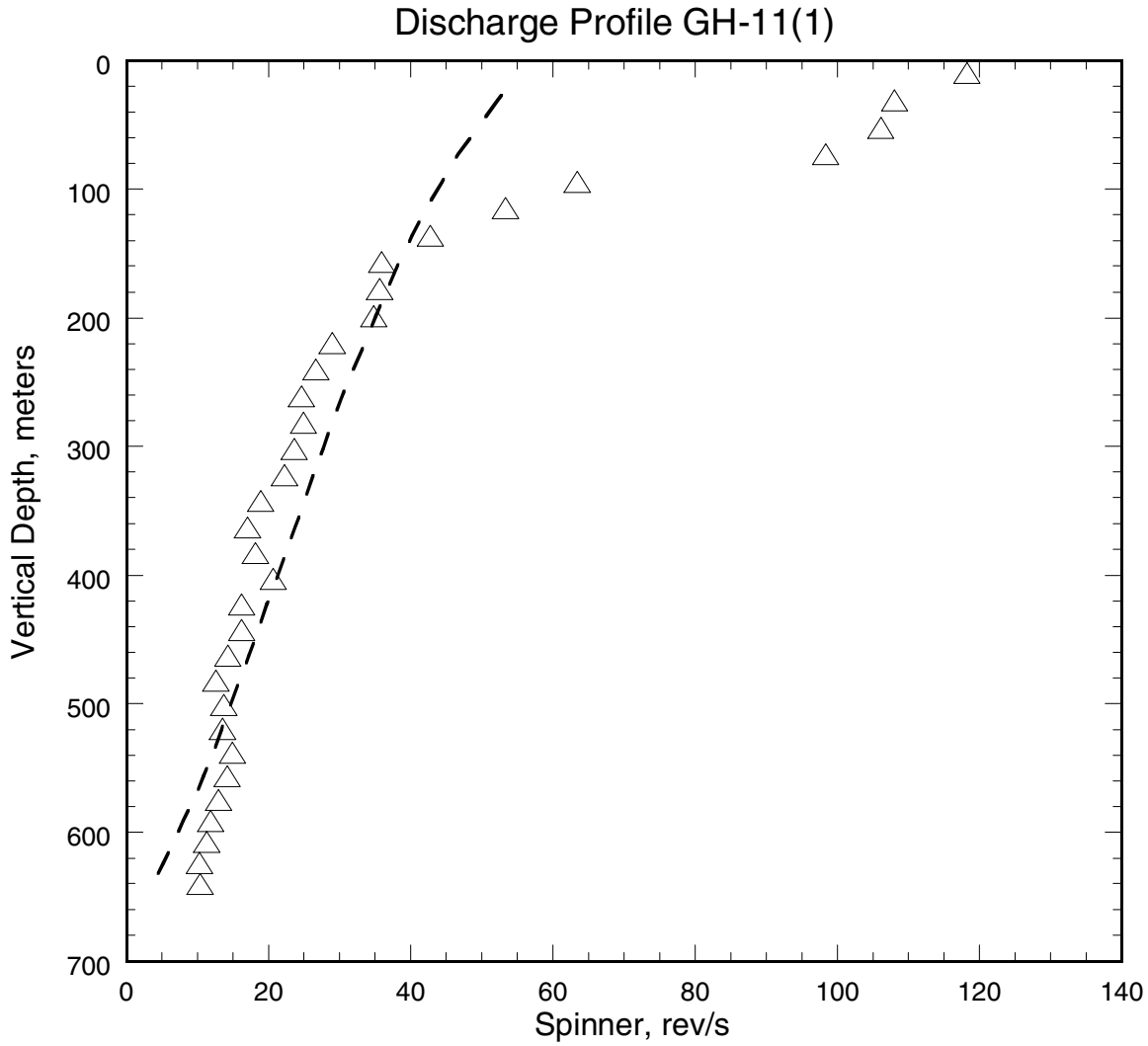

Figure D.29. Comparison of the smoothed spinner response (triangles) recorded on July 19, 1991, with the computed spinner response (dashed line) for well GH-11.

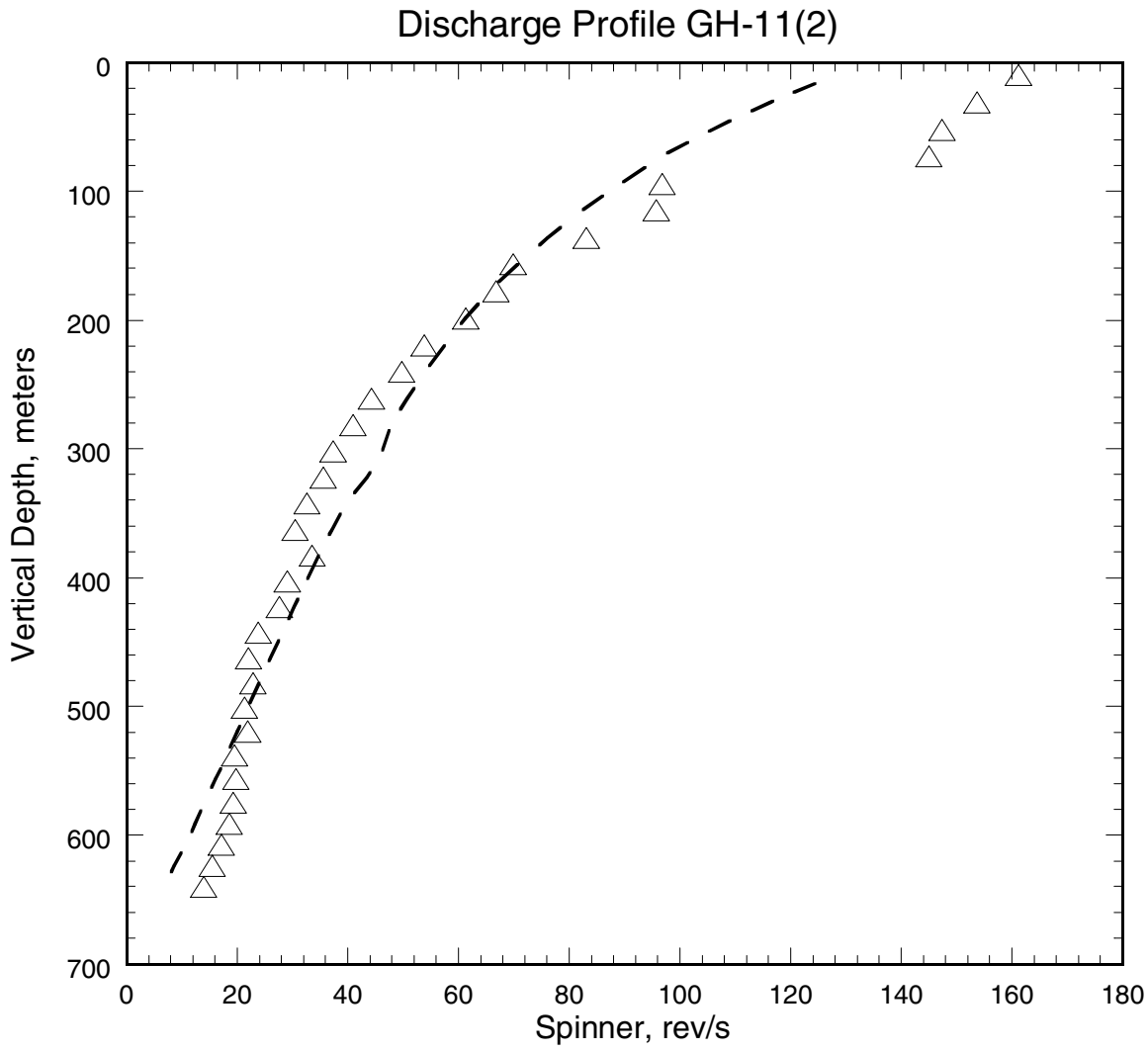

Figure D.30. Comparison of the smoothed spinner response (symbols) recorded on July 20, 1991, with the computed spinner response (solid line) for well GH-11.

APPENDIX E: FORTRAN SUBROUTINES USED FOR COMPUTING FLOW PARAMETER *K* AND ITS DERIVATIVE WITH RESPECT TO FLOWING QUALITY

E.1 SUBROUTINE HLDFN1

```
subroutine HLDFN1(z, hmk, dhmkdz)

implicit double precision (a-h, o-z)

fx(x) = 1d0 - exp((z0 - x)/d2)
fxp(x) = (1d0 - fx(x))/d2
flin(x) = h1 + (x - z1)*(h2 - h1)/(z2 - z1)
fq(x) = ((c3*x + c2)*x + c1)*x + c0
fqp(x) = (3*c3*x + 2*c2)*x + c1

z0 = 1.4890052379545d0
d2 = 0.28102355946805d0
z1 = 2d0 - 0.02d0
z2 = 2.5d0 - 0.02d0
h1 = 0.85d0
h2 = 0.965d0
x1 = 2.35d0
x2 = 3d0
c0 = -3.16290261d0
c1 =  4.05475208d0
c2 = -1.32255807d0
c3 =  0.14433505d0
dflin = (h2 - h1)/(z2 - z1)

if (z .lt. x1) then
    hmk = flin(z)
    dhmkdz = dflin
elseif (z .lt. x2) then
    hmk = fq(z)
    dhmkdz = fqp(z)
else
    hmk = fx(z)
    dhmkdz = fxp(z)
endif
end
```

E.2 SUBROUTINE HLDFN2

```
subroutine HLDFN2(z, hmk, dhmkdz)

implicit double precision (a-h, o-z)

fx(x) = 1d0 - a*exp(-b*x)
fxp(x) = (1d0 - fx(x))*b
flin(x) = cf1 + cf1p*(x - x1)
fq(x) = ((c3*x + c2)*x + c1)*x + c0
fqp(x) = (3*c3*x + 2*c2)*x + c1

x1 =   1.12
x2 =   1.3

c0 =   -7.83576510
c1 =   19.75133183
c2 =  -14.82676152
c3 =    3.73126886

    ! use fq to determin fx and flin
cf1 = fq(x1)
cf1p = fqp(x1)
cf2 = fq(x2)
cf2p = fqp(x2)
b = cf2p/(1d0 - cf2)
a = (1d0 - cf2)*exp(b*x2)

if (z .lt. x1) then
    hmk = flin(z)
    dhmkdz = cf1p
elseif (z .lt. x2) then
    hmk = fq(z)
    dhmkdz = fqp(z)
else
    hmk = fx(z)
    dhmkdz = fxp(z)
endif

end
```

E.3 SUBROUTINE HOLDFK

```
      Subroutine HOLDFK (FLOW,AREA,DIAM,RHOL,RHOG,VISL,VISG,GRAV,SRFT,
     1                   QS,QF,
     1                         XK,DXKDQF)
C
C
C     PROGRAM TO CALCULATE STEADY TWO-PHASE FLUID UPFLOW IN A WELLBORE
C
C
      IMPLICIT DOUBLE PRECISION (A-H, O-Z)
C
C     Input:
C     FLOW = mass flow rate, kg/s
C     AREA = cross-section area, m**2
C     DIAM = diameter, m
C     RHOL = liquid density, kg/m**3
C     RHOG = gas density, kg/m**3
C     VISL = liquid viscosity, Pa-s
C     VISG = gas viscosity, Pa-s
C     GRAV = positive gravity acceleration, m/s**2
C     SRFT = surface tension, pa-m
C     QS   = static steam quality
C     QF   = flowing steam quality
C
C     Output:
C     XK      (dimensionless "K" function)
C     DXKDQF  (derivative of "K" w.r.t. "QF")
C
      DATA PI / 3.141592653589793D+00 /
C
      DATA ALPHA1 /+0.0388887/
      DATA BETA1  /0.0065170/
      DATA GAMMA1 /-0.0002960/
      DATA OMEGA1 /-1.0d-1/
      DATA ALPHA2 /-9.546812d-03/
      DATA BETA2  /9.759590d-03/
      DATA GAMMA2 /-1.498680d-04/
      DATA OMEGA2 /-1.0d-1/
C
      DATA FLUX1 /687.d+0/
      DATA FLUX2 /650.d+0/

C
C     "Epslon" is the minimum value of (1 - QF)/(1 - QS)
      DATA EPSLON / 1.D-02 /
C
C     CALCULATE FLUX (Mass discharge per unit cross-sectional area)
      FLUX = FLOW/AREA
C
C     Calculate "y" and its derivative w.r.t. QF
      DD1    = (1.D+00 - QF)*RHOG
      DD2    = QF*RHOL
      DDD    = DD1 + DD2
      Y      = DD1/DDD
      DYDQF  = -RHOL*RHOG/(DDD*DDD)
      OMY    = 1.D+00 - Y
```

```
C
C     Calculate liquid-phase saturation "SL"
      OMQS   = 1.D+00 - QS
      SL     = OMQS*RHOG
      SL     = SL / (SL + QS*RHOL)
      SG = 1.d+0 - SL
C
C     Calculate "rhoNS"
      RN     = RHOL*SL + RHOG*SG
C
C     Calculate "visNS"
      VN     = VISL*SL + VISG*SG
C
C     Calculate Reynolds #
      CR     = (4.D+00*FLOW) / (PI*DIAM)
      RE     = CR / VN
C
C     Calculate Froude #
      RN2    = RN*RN
      FOA2   = FLOW/AREA
      FOA2   = FOA2*FOA2
      CF     = FOA2/(GRAV*DIAM)
      FR     = CF/RN2
C
C     High Flux correlation (HLDFN1)
      IF (FLUX .LE. FLUX2) GO TO 51
C     Calculate "Z" parameter and derivative w.r.t. QF
      F1     = RE**ALPHA1
      F2     = FR**BETA1
      F3     = Y **GAMMA1
      F4     = SL**OMEGA1
      DF3DQF = GAMMA1*F3* DYDQF/Y
      F124   = F1*F2*F4
      Z      = F124*F3
      DZDQF  = F124*DF3DQF
C
C     Calculate "K" and its derivative w.r.t. QF
      CALL HLDFN1 (Z, XK,DXKDZ)
      DXKDQF = DXKDZ*DZDQF
      XK1=XK
      DXKD1=DXKDQF
      IF (FLUX.GE.FLUX1) GO TO 52


C     Low Flux Correlation (HLDFN2)
C     Calculate "Z" parameter and derivative w.r.t. QF
   51 CONTINUE
      F1     = RE**ALPHA2
      F2     = FR**BETA2
      F3     = Y **GAMMA2
      F4     = SL**OMEGA2
      DF3DQF = GAMMA2*F3* DYDQF/Y
      F124   = F1*F2*F4
      Z      = F124*F3
      DZDQF  = F124*DF3DQF
C
C     Calculate "K" and its derivative w.r.t. QF
      CALL HLDFN2 (Z, XK,DXKDZ)
      DXKDQF = DXKDZ*DZDQF
      XK2=XK
      DXKD2=DXKDQF
      IF (FLUX.LE.FLUX2) GO TO 52
C
```

```
C     Transition zone
      CONST1 =   (FLUX1 - FLUX)/(FLUX1-FLUX2)
      CONST = -CONST1 +  1. D+0
      XK = XK1 *CONST + XK2 * CONST1
      DXKDQF = DXKD1 *CONST + DXKD2 * CONST1

C
C     Enforce "epslon" limitation
   52 CONTINUE
      XX1    = 1.D+00 - EPSLON*OMQS
      XKSTAR = QS*(EPSLON*OMQS*RHOG + XX1*RHOL) /
     1            (XX1*(OMQS*RHOG + QS*RHOL))
C
      IF (XK .GT. XKSTAR) RETURN
C
      XK     = XKSTAR
      DXKDQF = 0.D+00
      RETURN
C
      END
```